University of Alberta Library
0 1620 2667138 6

89-168

Ex Libris
Universitatis
Albertaensis

THE UNIVERSITY OF ALBERTA

RELEASE FORM

NAME OF AUTHOR LOK YAN

TITLE OF THESIS PROPAGATION OF FRICTIONALLY-DECAYING BAROTROPIC MODONS OVER FINITE-AMPLITUDE TOPOGRAPHY

DEGREE FOR WHICH THESIS WAS PRESENTED MASTER OF SCIENCE

YEAR THIS DEGREE GRANTED SPRING, 1989

Permission is hereby granted to THE UNIVERSITY OF ALBERTA LIBRARY to reproduce single copies of this thesis and to lend or sell such copies for private, scholarly or scientific research purposes only.

The author reserves other publication rights, and neither the thesis nor extensive extracts from it may be printed or otherwise reproduced without the author's written permission.

[redacted]

DATED ...Nov. 23... 1988

THE UNIVERSITY OF ALBERTA

FACULTY OF GRADUATE STUDIES AND RESEARCH

The undersigned certify that they have read, and recommend to the Faculty of Graduate Studies and Research, for acceptance, a thesis entitled PROPAGATION OF FRICTIONALLY-DECAYING BAROTROPIC MODONS OVER FINITE-AMPLITUDE TOPOGRAPHY submitted by LOK YAN in partial fulfilment of the requirements for the degree of MASTER OF SCIENCE in METEOROLOGY.

[redacted]

Date.....

Abstract

An analytical asymptotic theory is developed which describes the propagation of the finite-amplitude solitary Rossby wave called a *modon* under the combined effects of weak frictional dissipation and finite-amplitude but slowly-varying topography. The asymptotic theory developed here explicitly assumes that the modon undergoes an adiabatic deformation governed by globally-averaged energy and enstrophy balances. The theory presented therefore unifies and extends the accurate frictional dissipation theory developed by Swaters and Flierl (1988) and the topographic theory by Swaters(1986b). The results of the unified theory predict that the topographic forcing has an influence on the rate of the frictional dissipation.

Acknowledgements

The author would like to thank Dr. G.E. Swaters for his initiation of this project, his careful review and invaluable suggestions. Special thanks are extended to Drs. K. Haines and K. Miyakoda for permission to reproduce some figures. Preparation of this thesis was supported in part by a Science Subvention from the Atmospheric Environment Service of Canada and by Operating Research Grants from the Natural Science and Engineering Research Council of Canada awarded to Dr. G.E. Swaters.

Table of Contents

Chapter		Page
1.	Introduction	1
2.	The Shallow-water potential vorticity equation	8
3.	The Asymptotic Solution for the forced Modon	14
	3.1 The leading-order Modon solution	16
4.	Derivation of the Transport Equations	23
5.	The Steady-State Solution	30
6.	The Inviscid and Viscous Topographic Solution	34
	6.1 The ridge topography	34
	6.2 The Valley Topography	55
	6.3 The Shelf topography	68
7.	Conclusions	82
Bibliography		85
Appendix: Derivation of the nonlinear hyperbolic equation (A.6)		89

List of Figures

Page

Fig.1a. The widespread record coldness over North America for January 1977. 2

Fig.1b. Height contours of the 500-mb surface for 15 February, 1983. 2

Fig.2. Geometry of the inviscid shallow-water model used in this thesis. 9

Fig.3. The vorticity, $q(=\zeta)$, and the streamfunction,ψ, scatter diagram. 18

Fig.4. Contour plot of a barotropic modon with $a=c=1.0$ and $\kappa=3.9226$. 21

Fig.4d. Three dimensional plot of streamfunction with $a=c=1.0$ and $\kappa=3.9226$. 22

Fig.5 Depth of fluid $H(X)$ and ridge topography. 38

Fig.6a Comparison between the exact nonlinear and linearized steady-state topographically-modulated modon radius. 39

Fig.6b Comparison between the exact nonlinear and linearized steady-state topographically-modulated modon speed 40

Fig.6c Comparison between the exact nonlinear and linearized steady-state topographically-modulated modon wavenumber. 41

Fig.6d plots of the normalized average energy and enstrophy. 42

Fig.7. Comparison between the linear solutions for the vorticity and the exact nonlinear solutions determined in this thesis. 43

Fig.8. Sequences of plots of the vorticity as the modon propagates towards the ridge. 44

Fig.9. Plot of slow space $X(T)$ vs. T. 45

Fig.10. Plot of the modon speed $c(X)$ vs. X with τ changing from 0.01 to 0.03 to 0.05 in the ridge. 46

Fig.11a. Plots of the exact nonlinear steady-state frictionally- and topographically-modulated arrival time. 47

Fig.11b. Plots of the exact nonlinear steady-state frictionally- and topographically-modulated modon speed. 48

Fig.11c. Plots of the exact nonlinear steady-state frictionally- and topographically-modulated modon radius. 49

Fig.11d. Plots of the exact nonlinear steady-state frictionally- and topographically-modulated modon wavenumber. 50

Page

Fig.11e. Plots of the exact nonlinear steady-state frictionally- and topographically-modulated energy. 51

Fig.11f. Plots of the exact nonlinear steady-state frictionally- and topographically-modulated enstrophy. 52

Fig.11g. Plots of the exact nonlinear steady-state frictionally- and topographically-modulated vorticity. 53

Fig.11h. Plots of the exact nonlinear steady-state frictionally- and topographically-modulated streamfunction. 54

Fig.12 Depth of fluid $H(X)$ and valley topography. 56

Fig.13a Comparison between modon radius when the modon propagates towards a ridge and a valley. 57

Fig.13b Comparison between modon speed when the modon propagates towards a ridge and a valley. 58

Fig.13c Comparison between modon wavenumber when the modon propagates towards a ridge and a valley. 59

Fig.14a. Plots of the exact nonlinear steady-state frictionally- and topographically-modulated arrival time. 60

Fig.14b. Plots of the exact nonlinear steady-state frictionally- and topographically-modulated modon speed. 61

Fig.14c. Plots of the exact nonlinear steady-state frictionally- and topographically-modulated modon radius. 62

Fig.14d. Plots of the exact nonlinear steady-state frictionally- and topographically-modulated modon wavenumber. 63

Fig.14e. Plots of the exact nonlinear steady-state frictionally- and topographically-modulated energy. 64

Fig.14f. Plots of the exact nonlinear steady-state frictionally- and topographically-modulated enstrophy. 65

Fig.14g. Plots of the exact nonlinear steady-state frictionally- and topographically-modulated vorticity. 66

Fig.14h. Plots of the exact nonlinear steady-state frictionally- and topographically-modulated streamfunction. 67

Fig.15 Depth of fluid $H(X)$ and shelf topography. 69

Fig.16a Plot of the exact nonlinear steady-state topographically-modulated modon radius. 70

Page

Fig.16b Plot of the exact nonlinear steady-state topographically-modulated modon speed. 71

Fig.16c Plot of the exact nonlinear steady-state topographically-modulated modon wavenumber. 72

Fig.16d Plot of the exact nonlinear steady-state topographically-modulated energy and enstrophy. 73

Fig.17a. Plots of the exact nonlinear steady-state frictionally- and topographically-modulated arrival time. 74

Fig.17b. Plots of the exact nonlinear steady-state frictionally- and topographically-modulated modon speed. 75

Fig.17c. Plots of the exact nonlinear steady-state frictionally- and topographically-modulated modon radius. 76

Fig.17d. Plots of the exact nonlinear steady-state frictionally- and topographically-modulated modon wavenumber. 77

Fig.17e. Plots of the exact nonlinear steady-state frictionally- and topographically-modulated energy. 78

Fig.17f. Plots of the exact nonlinear steady-state frictionally- and topographically-modulated enstrophy. 79

Fig.17g. Plots of the exact nonlinear steady-state frictionally- and topographically-modulated vorticity. 80

Fig.17h. Plots of the exact nonlinear steady-state frictionally- and topographically-modulated streamfunction. 81

1. Introduction

One of the most noticeable large-scale disruptions of the ambient westerlies in the midlatitude Northern Hemisphere is the formation of "blocks". Atmospheric blocking is a large-amplitude synoptic-scale phenomenon which splits the ambient mean westerlies into two distinct meridional flows with one heading northward and other southward, and thereby "blocking" the predominantly zonal synoptic wind. Blocking can occur either as a ridge pattern (see Fig.1a) or as a dipole pressure pattern (see Fig.1b) or in some other pattern. A *dipole* block takes the form of a meridionally aligned vortex pair with the anticyclone north of the cyclone. The horizontal length scales and approximate vertical deflections of the geopotentials of this system are typically of the order of 2,000 km and 0.1 km, respectively. The *ridge* block takes the form of a blocking high which diverts the mean westerlies northward. There are three major geographical regions where blocking or persistent anomalies frequently occur: over the North Pacific extending westward to south of the Aleutians, over the eastern North Atlantic extending to the southeast of Greenland, and over the northern Soviet Union extending northeastward to the Arctic Ocean (Rex,1950a,b; Austin,1980; Dole and Gordon,1983). Blocking does occur in the southern hemisphere, but is less well documented there (Shukla and Mo,1983; Frederiken,1984; Trenberth and Mo,1985; Mo et al.,1987). The understanding of this phenomenon is very important in determining regional weather patterns. It is, in fact, acknowledged that if the range of reliable weather prediction is to be extended to, say, 10-15 days, it will be cruical to understand the behaviour of persistent anomalous flows (e.g., blocks) (Benzi et al.,1986).

The anomalous regional weather that may be associated with atmospheric blocking can be quite severe. For example, the extremely cold winter occuring in North America in January 1977 (Miyakoda et al.,1983), and the "1976 European Drought"(Green,1977; Illari,1984) have been identified as being associated with blocks. The synoptic circulation over North America during the 1977 winter was dominated by a persistent, large-scale ridge over Alaska, resulting in unusually high temperatures on the west coast of North America but record cold temperatures over the continental interior (see Fig.1a). Over Europe, the westerly flow was

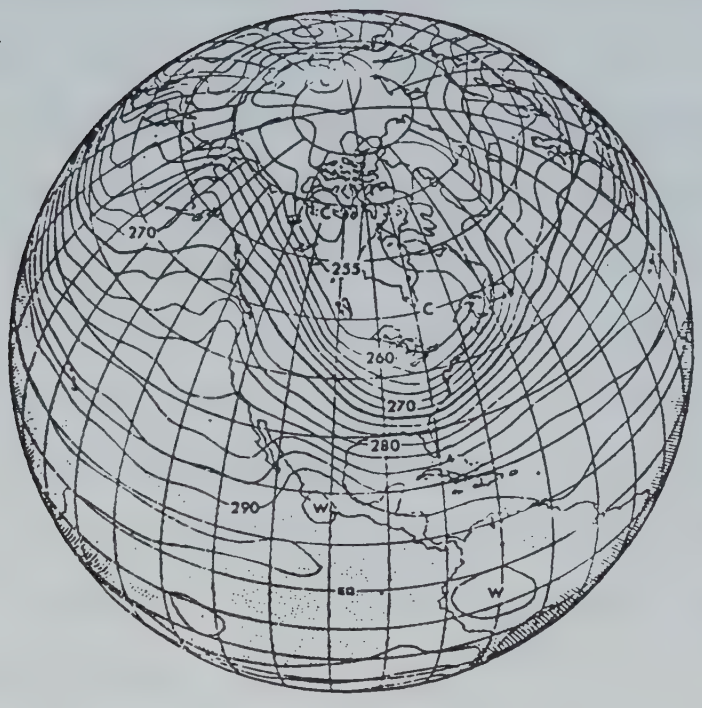

Fig.1a. The widespread record coldness over North America for January 1977 is shown by a 10-30 day mean temperature map at the 850 mb level. The observed temperature shown is for the last 20 days of a one-month forecast. The contour interval is 2.5 K where K is degree Kelvin (courtesy of Miyakoda et al.,1983).

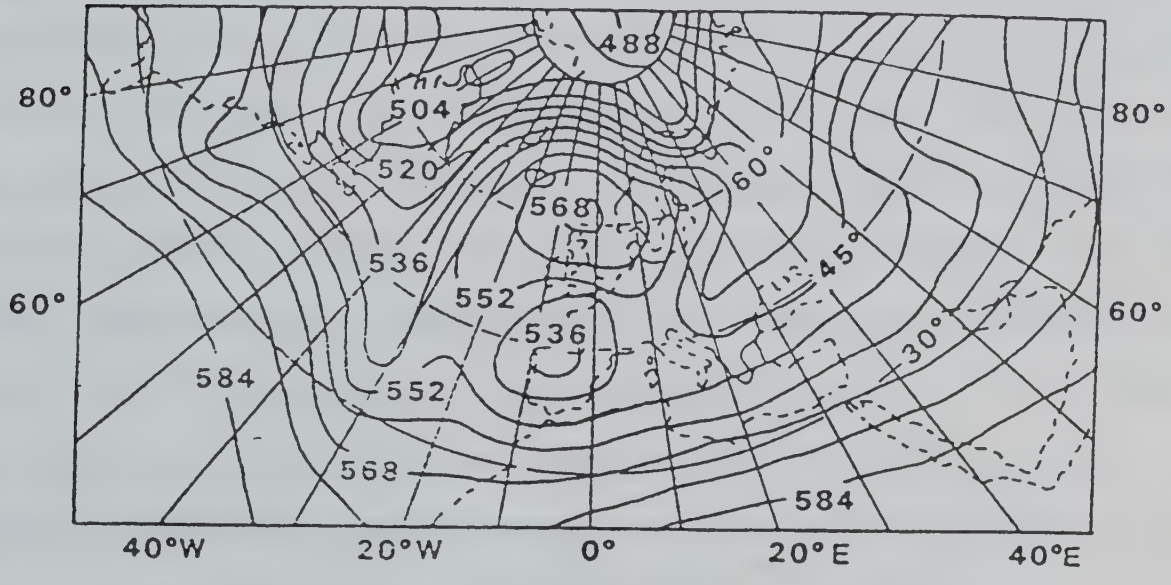

Fig.1b. Height contours of the 500-mb surface for 15 February, 1983. The contour interval is 8 dm. The shape of this dipole-vortex configuration resembles to that of the modon solution moving westward (courtesy of Haines and Marshall, 1987).

split into a dipole configuration and remained blocked for three months, resulting in hot and dry weather in the region of the anticyclone and persistent rain in the cyclonic region (see a similar pattern in Fig.1b).

There is still no unified and generally accepted theory for the formation, maintenance and breakdown of blocks. A comprehensive review of present blocking theories is given by Benzi et al.(1986). Briefly, they are divided into "global" and "local" theories. Examples of global theories include Egger(1978) who has suggested that blocking may occur due to planetary wave-wave interactions. Tung and Lindzen(1979) have suggested that blocks may occur as a result of the linear resonance of planetary-scale waves with surface forcing, i.e., continental elevation or land-sea differential heating. Charney and DeVore(1979) and Wiin-Nielsen(1979) have suggested that the atmosphere may exhibit multiple equilibria of which one may be the blocking state.

McWilliams(1980) proposed a local theory, suggesting that atmospheric blocks can be produced by internal dynamics alone due to a balance between nonlinear and dispersive effects, i.e., a free inertial mode. Warn and Brasnett(1983) showed that under certain conditions Rossby solitons governed by the Korteweg-de Vries equation could be simultaneously amplified and stalled by topography, i.e., a transition to a regional blocking-like configuration. Recently, further evidence supporting the "local" point of view has been provided by Dole and Gordon(1983) and Pierrehumbert and Malguzzi(1984). Dole and Gordon showed statistically that synoptic observations of blocking reveal a local character. Pierrehumbert and Malguzzi showed that a high amplitude equilibrium state (identified with a blocking event) can be maintained by a local nonlinear resonance phenomenon. As well, Shutts(1983) also demonstrated that dipole blocking patterns can be created by an eddy in a weak, uniform westerly flow. Haines and Marshall(1987) have shown that the anomalous transfer of potential vorticity induced by the straining of eddies in a diffluent flow is able to sustain the dipole block. McWilliams(1980) and Haines and Marshall(1987) have suggested that the *modon* (Stern,1975; Larichev and Reznik,1976; Flierl et al., 1980) is a useful prototype model for some dipole blocking events.

The modon is an exact, finite-amplitude, steadily-travelling, dipole vortex solution of the quasi-geostrophic and shallow-water potential vorticity equations. The essential characteristics of the modon solution can be summarized as follows (Flierl,1987):

1. The nonlinearity in the solitary vortices holds the eddy pair together.
2. The streamlines "inside" the modon are closed and so the fluid is trapped; hence the modon is capable of transporting or isolating a significant volume of fluid.
3. The potential vorticity varies linearly with the streamfunction, but the relationship is not an analytic function. Consequently, the gradient of the potential vorticity is discontinuous.
4. The modon wavenumber depends on the modon speed and the radius via a dispersion relation.
5. The modon translation speed generally lies outside the range of the linear Rossby wave phase speeds.

The striking resemblance of the equivalent barotropic modon of McWilliams(1980) to some Atlantic blocking configurations suggests that modon can be considered as a prototype model of some atmospheric blocking events (see Fig.1b and Fig.4c). It is therefore important to understand the fundamental dynamical properties of these solitary waves such as their generation, maintenance and deformation due to external forcing.

Among the three processes, Flierl(1987) points out that the generation mechanism is the least well understood. Mied and Lindemann(1982) have suggested that modongenesis in the ocean may occur from the interaction between baroclinic eddies. McWilliams(1983) numerically demonstrated that a modon can be generated by monopole collision. Aref and Siggia(1980) have shown theoretically that a jet can break up into dipolar structures. Basdevant et al.(1984) have provided some experimental evidence for this type of instability. Flierl et al.(1983) performed laboratory experiments, showing that additional vortices may also be generated during the process of modongenesis. Boyd(1985) has suggested that atmospheric forcing of the equatorial ocean associated with an El Niño event could generate a

modon. Although modongenesis seems to be a very complicated process, and a lot of work remains to be done, the mathematical construction of the modon solution is now relatively complete. The modon has been shown to exist both in westerly and easterly background flows and in spherical as well as Cartesian geometry (Verkley,1984; Tribbia,1984; Verkley,1987).

With regard to the maintenance of modons, Shutts(1983) has shown numerically that the action of barotropic eddies, through their averaged Reynolds stresses, can reinforce blocking flow patterns. Pierrehumbert and Malguzzi(1984) suggest that localized weak forcing may lead to local multiple equilibria, with the high-amplitude state being a modon maintained against dissipation by the forcing due to air-sea temperature contrasts. Haines and Marshall(1987) conclude that the anomalous transfer of potential vorticity induced by the straining of synoptic systems propagating in a diffluent jet can maintain the modon against dissipation. Makino et al.(1981) and McWilliams and Zabusky(1982) numerically simulated head-on and overtaking collisions between modons and showed that the modons may interact elastically and recover their initial shapes at the end of the collisions. McWilliams and Zabusky also investigated inelastic collisions, showing that two modons may undergo a fusion process in an overtaking collision, while fission may result from a head-on collision.

The linear stability of westward-travelling modons has been proven analytically by Laedke and Spatschek(1985). Swaters(1986a) established sufficient conditions characterizing the neutral modes in the linear instability problem for equivalent-barotropic modons. Swenson(1986b) showed that the modon-with-rider configuration (Flierl et al., 1980) is unstable. In the presence of weak, linear, north-south current shear, numerical simulations of a propagating modon have been shown to be stable (Swenson,1986a). McWilliams et al.(1981) demonstrated numerically that the eastward-travelling modon is resistant to perturbations of small-but-finite amplitude, but may be destroyed by perturbations of large amplitude.

McWilliams et al.(1981) also numerically simulated the frictional dissipation of a barotropic modon. Their solution showed that the dissipation, at least in the early stages, occurs adiabatically (i.e. essentially "shape" perserving) with the amplitude and the translation speed of the modon monotonically decreasing. Eventually, as the amplitude

becomes very small, Rossby wave dispersion dominates and the modon "breaks" up. Swaters(1985) and Swaters and Flierl(1988) have shown that the Ekman frictional decay of a barotropic modon can be accurately described by a multiple-scales asymptotic theory in which the modon parameters (i.e., the translation speed, radius and modon wavenumber) temporally adjust while preserving globally-integrated energy and enstrophy.

Swaters(1986b) developed a multiple-scales asymptotic theory to describe the interaction of a barotropic modon with finite-amplitude topography that has slowly-varying horizontal gradients relative to the modon radius. The theory was based on the shallow-water equations. The principal idea behind the theory was that for relatively weak topographic forcing, the modon would adjust itself adiabatically according to the conservation of vorticity, energy and enstrophy. The final product in the theory was a set of nonlinear hyperbolic equations which described the evolution of the modon parameters. He showed that when the modon propagates over slowly varying topography corresponding to a region of shallower (deeper) fluid, the modon radius increases (decreases), the translation speed decreases (increases) and the modon wavenumber decreases (increases). Based on a simple linear approximation, Swaters concluded that there was also a corresponding amplification (diminishing) of the extrema in the streamfunction and vorticity fields. However, as we shall show in Chapter 6, this last conclusion is incorrect. In fact there is a corresponding diminishing (amplification) of the extrema in the streamfunction and vorticity fields. The error is due to the truncation in the linear approximation. Finally, we should point out that Carnevale et al.(1988) recently have numerically shown that if the modon is forced by a strong topographic perturbation, the dipole-vortex configuration which comprises the modon may undergo a fission-like process in which the modon bifurcates into two essentially independent, oppositely-signed vortices.

The principal objective of this thesis is to blend the frictional dissipation theory of Swaters and Flierl(1988) and the topographic modulation theory of Swaters(1986b) into one unified theoretical description of an orographically-forced *and* frictionally-damped barotropic modon. The theory is constructed from the nonlinear rigid-lid shallow-water equations

including the effects of finite-amplitude topography and Rayleigh damping. The assumed Rayleigh damping term is a crude but analytically tractable model for the vortex stretching that results from the "pumping" and "suction" of an Ekman boundary layer (i.e., the leading order vertical velocity at the "top" of an Ekman boundary layer is proportional to the geostrophic vorticity of the atmosphere "above" the Ekman boundary layer (Pedlosky,1987)).

The outline of this thesis is as follows. In Chapter 2, we review the derivation of the potential vorticity equation for a homogeneous, incompressible, hydrostatic atmosphere on a β-plane including a Rayleigh damping term and topography. In Chapter 3, we present the asymptotic solution for the topographically-forced and frictionally-damped modon. In Chapter 4, the transport equations describing the evolution of the modon parameters are derived. These equations are derived assuming that the modon is adiabatically deforming according to leading-order globally-averaged energy and enstrophy balances. The term "adiabatic deformation" is in this context meant to imply that throughout the deformation the non-analytic vorticity/streamfunction relationship and modon dispersion relation that defines these solitary Rossby waves are being continuously maintained. In Chapter 5, we construct the steady-state transport equations. In Chapter 6, we examine the inviscid limit of the transport equations and compare the exact nonlinear solutions that we can obtain with the linear topographic solutions presented by Swaters(1986b). Also, we describe the predictions of our transport equations in the steady-state approximation for different topographic configurations and the values of the damping coefficient. The thesis is summarized and conclusions are presented in Chapter 7.

2. The Shallow-water potential vorticity equation

In order to focus attention on the frictional and topographic problem, we reduce the model of the atmosphere to a very simple form: we assume that the atmosphere can be modelled as a homogeneous, hydrostatic and incompressible fluid on an infinite β-plane. Therefore, the governing *dimensional* equations of the flow are the shallow-water equations given in the form (Pedlosky,1987,Chap3):

$$u_t + uu_x + vu_y - fv = - p_x/\rho - \tau^* u, \tag{2.1a}$$

$$v_t + uv_x + vv_y + fu = - p_y/\rho - \tau^* v, \tag{2.1b}$$

$$p_z = - \rho g, \tag{2.1c}$$

$$u_x + v_y + w_z = 0, \tag{2.1d}$$

where u, v, w and x, y, z are the zonal, meridional and vertical velocities and coordinates, respectively; t is time, p is the pressure, ρ is the constant density, g is the acceleration due to gravity and f is the Coriolis parameter given by $f=f_0+\beta y$. Subscripts denote the partial derivatives. Equations (2.1a) and (2.1b) are the zonal and meridional momentum equations, respectively; (2.1c) is the hydrostatic equation and (2.1d) expresses conservation of mass (see Fig.2 for the geometry of the flow). The parameter τ^* is the dimensional damping coefficient and has the unit of 1/sec.

Integrating the hydrostatic equation (2.1c) with respect to z and using the boundary condition at the top of the atmosphere (i.e., $z = h_0 + \eta(x,y,t)$) $p=0$ implies

$$p(x,y,t) = - \rho g\,(z - h_0) + \rho g\,\eta(x,y,t). \tag{2.2}$$

Differentiating (2.2) with respect to x and y and then substituting into (2.1a) and (2.1b) respectively, we obtain

$$u_t + uu_x + vu_y - fv = - g\eta_x - \tau^* u, \tag{2.3a}$$

$$v_t + uv_x + vv_y + fu = - g\eta_y - \tau^* v. \tag{2.3b}$$

The advantage of (2.3) over (2.1) is that the pressure has been formally eliminated from the

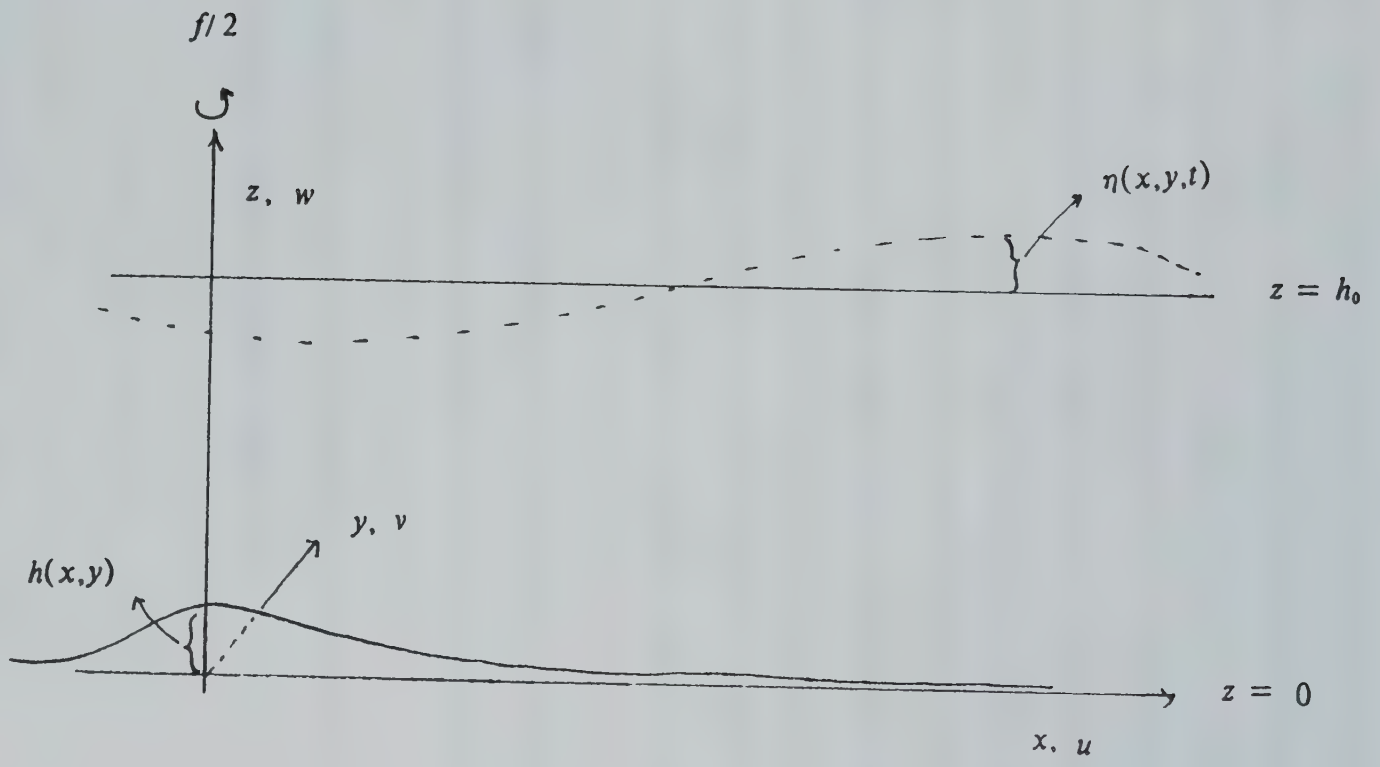

Fig.2. Geometry of the inviscid shallow-water model used in this thesis.

governing equations.

Note that in (2.1a) and (2.1b) the effects of friction have been modelled very crudely with a linear Rayleigh damping term. This type of formulation for the friction has certain advantages and disadvantages. The disadvantage is that the horizontal wind field will *not* explicitly contain a boundary layer near the earth's surface and therefore the appropriate boundary condition for the flow on the topography is that the normal velocity vanish there (i.e., *inviscid* boundary conditions). The advantage is that the frictional damping term in the yet-to-be derived leading-order vorticity equation will be proportional to the geostrophic vorticity. This is precisely the situation which occurs in quasi-geostrophic shallow-water theory when the effects of a surface Ekman boundary layer are incorporated into the quasigeostrophic potential vorticity equation (see Pedlosky,1987). In fact, this is the correct way to interpret the model (2.1). These equations will approximately describe the large-scale dynamics of a barotropic atmosphere with finite-amplitude topography under the influence of a thin Ekman boundary layer adjacent to the earth's surface. The net effect of the Ekman boundary layer on the synoptic scale dynamics is parameterized in the Rayleigh dissipation terms.

At the bottom of the atmosphere, i.e., $z = h(x,y)$, there can be no normal flow through the topography. Stated mathematically, this condition is written as follows

$$\hat{\mathbf{n}} \cdot \mathbf{u} = 0, \tag{2.4a}$$

where $\hat{\mathbf{n}}$ is the normal unit vector on the topographic surface and $\mathbf{u}$ is the Eulerian fluid velocity vector. The unit normal on $z=h(x,y)$ is given by

$$\hat{\mathbf{n}} = (h_x, h_y, -1)/[\, h_x^{\,2} + h_y^{\,2} + 1]^{1/2}. \tag{2.4b}$$

It therefore follows from (2.4a) that

$$w = uh_x + vh_y, \tag{2.5a}$$

evaluated on $z=h(x,y)$.

At the top of the atmosphere, the appropriate boundary condition is that a particle on the free surface remains on the surface for all time, i.e.,

$$\frac{D}{Dt}(z - \eta) = 0, \tag{2.5b}$$

evaluated on $z=\eta(x,y,t)$ where $\frac{D}{Dt} = \partial_t + \mathbf{u}\cdot\nabla$, $\mathbf{u}\equiv(u,v,w)$ and $\nabla = (\partial_x, \partial_y, \partial_z)$. Equation (2.5b) simplifies to

$$w = \eta_t + u\eta_x + v\eta_y, \tag{2.5c}$$

evaluated on $z = h_0 + \eta(x,y,t)$.

These two boundary conditions allow one to explicitly eliminate the vertical velocity from the governing equations as follows. We integrate the continuity equation (2.1d) with respect to z from $z=h(x,y)$ to $z=h_0+\eta$ and substitute (2.5a) and (2.5c) in for the vertical velocity at $z=h$ and $z=h_0+\eta$, respectively, and assume that each component of the horizontal wind is independent of height. The resulting continuity equation can be put into the form

$$\eta_t + [\, u(\eta + h_0 - h)]_x + [\, v(\eta + h_0 - h)]_y = 0. \tag{2.6}$$

In order to compare the significance of the individual terms in the shallow-water equations (2.3) and (2.6), we nondimensionalize with the following scales:

$$\begin{aligned} (x,y) &= a_0(x',y'), \\ (u,v) &= c_0(u',v'), \\ (t) &= (a_0/c_0)(t'), \\ (\eta) &= (f_0 c_0 a_0/g)(\eta'), \\ (h) &= h_0(h'), \end{aligned} \tag{2.7}$$

where a_0 and c_0 are the initial modon radius and speed. Typical synoptic scales for the radius and speed might be 1000(100)km and 10(0.1)m/s, respectively, in the atmosphere(ocean) (Swaters,1985). The time is scaled advectively and the pressure is scaled geostrophically. The primed variables are nondimensional while the unprimed variables are dimensional.

Substituting (2.7) into the zonal momentum equation (2.3a) leads to

$$\frac{c_0}{f_0 a_0}[u'_{t'} + u'u'_{x'} + v'u'_{y'}] - (1 + \frac{\beta a_0}{f_0}y')v' = -\eta'_{x'} - (\tau^*/f_0)u'. \qquad (2.8)$$

For the sake of further clarity we introduce the following nondimensional parameters:

$$R_0 = \frac{c_0}{f_0 a_0} \text{ as a Rossby number,}$$

$$\delta^2 = \frac{\beta a_0^2}{c_0} \text{ as a planetary vorticity factor,}$$

$$f = 1/R_0 + \delta^2 y' \text{ as a nondimensional Coriolis parameter,}$$

where $f_0 = 2\Omega\sin\psi_0$ is the constant Coriolis parameter with ψ_0 as the reference latitude, and $\beta(=2\Omega\cos\psi_0/R)$ is the northward gradient in the Coriolis parameter with R the radius of the earth and Ω the magnitude of the rotation frequency of the earth.

Subsequently, (2.8) is written as follows (dropping the primes)

$$u_t + uu_x + vu_y - fv = -\eta_x/R_0 - (\tau^*/f_0R_0)u. \qquad (2.9)$$

Similarly the nondimensional meridional momentum equation (2.3b) and the continuity equation (2.6) can be written in the form

$$v_t + uv_x + vv_y + fu = -\eta_y/R_0 - (\tau^*/f_0R_0)v, \qquad (2.10)$$

and

$$R_0F\eta_t + [u(R_0F\eta + 1 - h)]_x + [v(R_0F\eta + 1 - h)]_y = 0, \qquad (2.11)$$

where $F(=a_0^2/R_*^2)$ is the rotational Froude number with $R_* = \sqrt{gh_0}/f$. The external Rossby radius of deformation, R_*, is a fundamental horizontal length scale which measures how horizontally extensive a structure must be for buoyancy effects to be as important as the Coriolis force in the generation of vorticity (Gill,sec.7.5,1982; Ghil,sec.3.1,1987). In the atmosphere for synoptic scales, R_* is much greater than a_0 and so F is very small. The effect of neglecting all terms of $O(R_0F)$ in (2.11) is equivalent to assuming that the upper surface is a rigid-lid. This approximation filters out the long gravity wave solutions. Defining $H(x,y) = 1 - h(x,y)$ as the nondimensional depth of the fluid, the nondimensional continuity equation

can be written in the form

$$(uH)_x + (vH)_y = 0. \tag{2.12}$$

Equations (2.9), (2.10) and (2.12) are the nondimensional version of the shallow-water equations we will use in this thesis.

The appropriate equation that describes the dynamics of the flow is the potential vorticity equation, which can be obtained by differentiating (2.9) and (2.10) with respect to y and x, respectively, and then subtracting (2.9) from (2.10). Defining $\zeta = v_x - u_y$ as the vertical component of the relative vorticity and substituting the continuity equation into the vorticity equation, we have an equation for the conservation of potential vorticity:

$$\frac{D}{Dt}\left(\frac{\zeta + f}{H}\right) = -(\tau^*/f_0R_0)\zeta/H, \tag{2.13}$$

where $\frac{D}{Dt} \equiv \partial_t + u\partial_x + v\partial_y$.

Equation (2.12) allows us to introduce the mass transport streamfunction ψ defined as

$$\psi_y = -Hu, \tag{2.14a}$$

$$\psi_x = +Hv. \tag{2.14b}$$

Substitution of (2.14) into (2.13) gives

$$\nabla\cdot(\nabla\psi_t/H) + J[\psi,(\nabla\cdot(\nabla\psi/H) + f)/H] = -(\tau^*/f_0R_0)\nabla\cdot(\nabla\psi/H), \tag{2.15}$$

where $J(A,B) \equiv A_xB_y - A_yB_x$ is the determinant of the Jacobian matrix between A and B with respect to x and y. This is the vorticity equation for the nonlinear rigid-lid shallow-water equations under an infinite β-plane approximation (Leblond and Mysak, 1978; sec.20), including the combined effects of topography and Rayleigh damping.

3. The Asymptotic Solution for the forced Modon

In this chapter we develop a multiple-scales asymptotic theory for describing the frictional *and* topographic modulation of a barotropic modon. This theory will unify the theories developed by Swaters(1986b) and Swaters and Flierl(1988) for the topographic and dissipation problems, respectively. We begin from the assumption that the horizontal gradients in the topography are small relative to those in the modon, i.e.,

$$H \equiv H(\epsilon x, \epsilon y), \tag{3.1a}$$

where

$$\epsilon = \frac{\text{modon radius}}{\text{typical horizontal length scale of the topography}}$$

under the assumption $0<\epsilon<<1$. In fact, in what follows we shall make the further simplification that the topography has only a zonal gradient, i.e.,

$$H \equiv H(\epsilon x). \tag{3.1b}$$

The form (3.1b) corresponds to a meridionally aligned topographic feature. We shall assume that the frictional dissipation is of the same order of magnitude as the topographic gradient. Thus we define a *nondimensional* O(1) damping coefficient τ via

$$\epsilon\tau \equiv \tau^{*}/(f_0 R_0). \tag{3.1c}$$

The variable ϵx in (3.1b) is called a slow variable while x is called a fast variable. According to multiple-scale theory (Orszag and Bender, 1978; chap7), the fast and slow variables can be formally treated as independent variables. Thus the streamfunction is explicitly written in the form

$$\psi = \psi(x,y,t;X,T),$$

where

$$X = \epsilon x,$$

$$T = \epsilon t.$$

We therefore allow the modon to evolve over a long time scale as well. The objective of the multiple-scales analysis is to derive transport equations describing the topographic and

frictional modulation of the modon as the result of satisfying solvability conditions associated with the first-order perturbation equations in an asymptotic expansion formally valid as $\epsilon \to 0^+$.

Following Swaters(1986b), the perturbation solution to the streamfunction in (2.15) can be written in the form

$$\psi = H(X)[\, A(X,T) + \psi^{(0)}(\xi,y;\, X,\, T) + \epsilon\, \psi^{(1)}(\xi,y;\, X,\, T) + \ldots\,], \tag{3.2}$$

with the associated Eulerian perturbation velocity field

$$u = u^{(0)}(\xi,y;\, X,T) + \epsilon\, u^{(1)}(\xi,y;\, X,T) + \ldots\,, \tag{3.3a}$$

$$v = v^{(0)}(\xi,y;\, X,,T) + \epsilon\, v^{(1)}(\xi,y;\, X,T) + \ldots\,, \tag{3.3b}$$

where ξ is a rapidly varying zonal phase variable given by

$$\xi = \frac{1}{\epsilon}\Theta(X,T),$$

whose derivatives are given by

$$\xi_t = -\, c(X,T)\, l(X,T), \tag{3.4a}$$

$$\xi_x = l(X,T). \tag{3.4b}$$

It follows from (3.4) that the following "conservation of crests" compatibility condition must hold:

$$l_T + (cl)_X = 0. \tag{3.5}$$

The parameters $l(X,T)$ and $c(X,T)$ are the slowly varying *zonal* wavenumber and modon translation speed, respectively. Note that there is no meridional dependence in the zonal phase variable. Swaters(1986b) has shown that this approximation is equivalent to assuming that the modon propagates only zonally. Even though this restriction is not realistic, it will help to give some insight into the essential features during the topographic interaction. A possible future extension of this theory would be to include two-dimensional effects.

With the above multiple scalings, the derivatives are rewritten

$$\partial_x \to l\partial_\xi + \epsilon\partial_X, \tag{3.6a}$$

$$\partial_y \to \partial_y, \tag{3.6b}$$

$$\partial_t \to -\, cl\partial_\xi + \epsilon\partial_T. \tag{3.6c}$$

It can be shown (Swaters,1986b) that substituting (3.2) into (2.15) with the transformations (3.6) and then collecting the leading order terms (i.e. the O(1) problem) yields

$$J[\psi^{(0)} + cy, \nabla^2\psi^{(0)} + \delta^2 y] = 0, \tag{3.7}$$

where $J[a,b] \equiv \frac{\partial(a,b)}{\partial(\xi,y)} \equiv l(a_\xi b_y - a_y b_\xi)$ and $\nabla = (l\partial_\xi, \partial_y)$.

3.1 The leading-order Modon solution

The general solution of (3.7) can be written in the form

$$\nabla^2\psi^{(0)} + \delta^2 y = \Phi(\psi^{(0)} + cy), \tag{3.8}$$

where Φ is an arbitary functional of the streaklines $(\psi^{(0)} + cy)$. We seek a solution which satisfies

$$|\psi^{(0)}| \to 0 \text{ as } r^2 = (\frac{\xi}{l})^2 + (y)^2 \to \infty. \tag{3.9}$$

It follows from (3.8) and (3.9) that for those streamlines which extend out to infinity that

$$\Phi(x) = \delta^2 x/c, \tag{3.10a}$$

where x is a general argument variable, and consequently that

$$\Phi(\psi^{(0)} + cy) = \delta^2(\psi^{(0)} + cy)/c. \tag{3.10b}$$

It therefore follows from (3.8) and (3.10b) that for those streamlines which extend out to infinity that

$$\nabla^2\psi^{(0)} - m^2\psi^{(0)} = 0, \tag{3.11a}$$

where

$$m^2 = \delta^2/c. \tag{3.11b}$$

The general solution to (3.11) which is bounded at infinity can be written in the form

$$\psi^{(0)}(r,\theta) = \Sigma K_n(mr)(C_{1_n}\sin n\theta + C_{2_n}\cos n\theta), \tag{3.12}$$

where Σ is a summation in which n is summed from 0 to ∞, and K_n is the modified Bessel function of order n and θ is defined through the relation

$$\tan\theta = ly/\xi,$$

and C_{1_n} and C_{2_n} are unknown constants to be determined from boundary conditions which will be specified later.

In order to have a solution of the form (3.12) we require that $m^2 > 0$. Since $\delta^2 > 0$, (3.11b) implies that

$$c(X,T) > 0. \tag{3.13}$$

This limitation on the speed of the modon solution distinguishes it from linear Rossby waves whose phase speeds are always negative (i.e. westward propagating). Larichev and Reznik (1976) pointed out that if a free surface is included in the model, c can be negative (i.e., the modon can move to the west as well) but even so it must travel faster than the fastest long Rossby waves. This characteristic that the β-plane modon translation speed will always lie outside the set of allowable linear β-plane Rossby wave speeds is typical of solitary wave models.

One of the characteristics of a modon solution (see the Introduction) is that Φ is not analytic because Φ will have multiple branches in the sense that (3.10a) is assumed to apply only in an exterior region (outside) of a circle of radius a. In the interior of the circle where the streamlines will not extend out to infinity, another branch of Φ applies. In the interior region we assume that Φ is linear, for simplicity, i.e.,

$$\nabla^2\psi^{(0)} + \delta^2 y = -\kappa^2(\psi^{(0)} + cy) \qquad r<a, \tag{3.14}$$

where the parameter κ is called the *modon* wavenumber. Recently, Haines and Marshall (1987) have shown (see Fig.3) that the functional relationship (3.14) is a very good model for some Atlantic dipole blocking events.

Rearranging (3.14), we obtain the equation

$$\nabla^2\psi^{(0)} + \kappa^2\psi^{(0)} = -(\kappa^2 c + \delta^2)y. \tag{3.15}$$

Therefore, the bounded interior solution can be put in the form

$$\psi^{(0)}(r,\theta) = \Sigma J_n(\kappa r)\,(C_{3_n}\sin n\theta + C_{4_n}\cos n\theta) - (\kappa^2 c + \delta^2) r\sin\theta/\kappa^2, \tag{3.16}$$

where n is summed from 0 to ∞, J_n is the Bessel function of order n and C_{3_n} and C_{4_n} are constants to be determined as follows.

The physical boundary conditions that we impose are that the velocity, pressure and absolute vorticity be continuous across the modon boundary $r=a$. If the absolute vorticity $(\nabla^2\psi^{(0)} + \delta^2 y)$ is continuous across $r=a$, it follows from (3.8), (3.10b) and (3.14) that

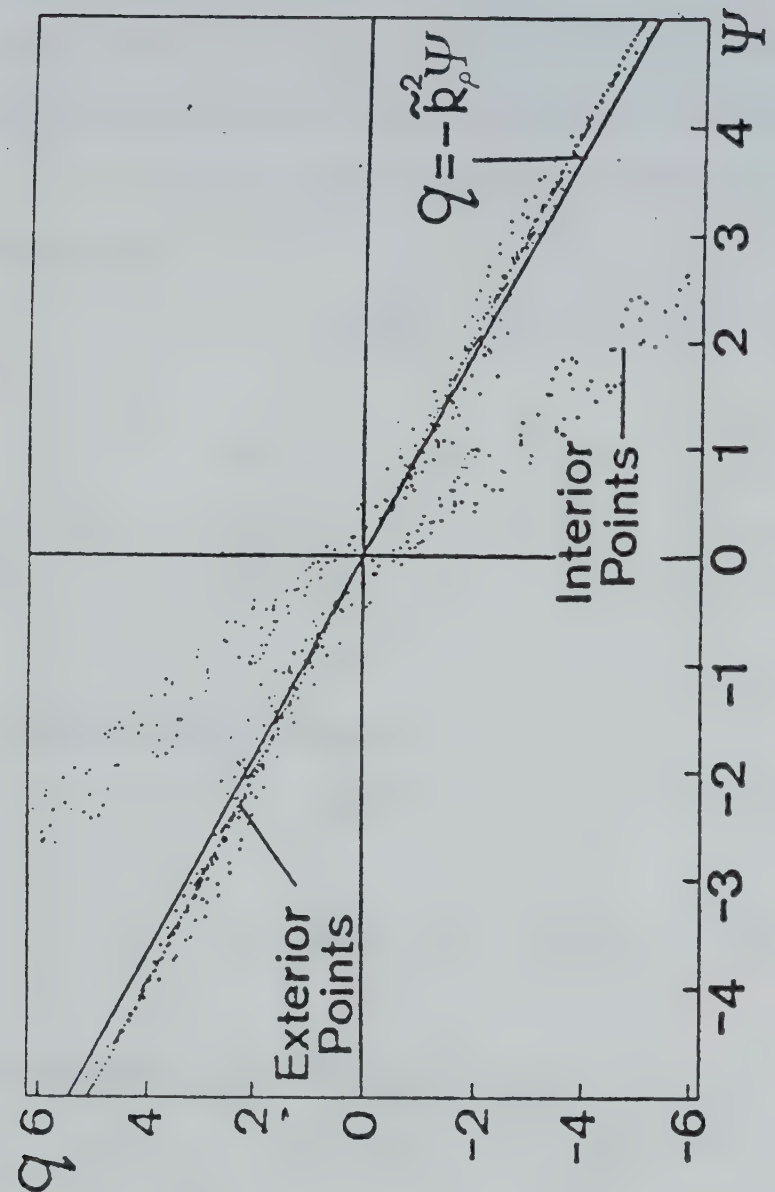

Fig.3. The vorticity, $q(=\zeta)$, and the streamfunction,ψ, scatter diagram, showing the distinctive linear relationship between the relative vorticity and the streamfunction for a modon solution (courtesy of Haines and Marshall,1987).

$$(\kappa^2+\delta^2/c)\,(\psi^{(0)} + cy) = 0,$$

on $r=a$. This can be satisfied only if

$$\psi^{(0)} + cy = 0, \tag{3.17}$$

on $r=a$. The physical interpretation of (3.17) is that the modon boundary forms a streakline in the co-moving reference frame. Therefore the modon interior traps fluid particles. Note that (3.17) and the form of the solutions (3.12) and (3.16) will imply that the normal velocity is continuous across the modon boundary. It follows from (3.17) that $C_{1_n} = C_{2_n} = C_{3_n} = C_{4_n} = 0$ for all n except C_{11} and C_{31}. It follows that the modon solutions can be written as follows:

$$\psi^{(0)}(r,\theta) = [\,\frac{\delta^2 a}{\kappa^2 J_1(\kappa a)}\,J_1(\kappa r) - \frac{\kappa^2 c + \delta^2}{\kappa^2} r]\,\sin\theta \qquad r< a, \tag{3.18a}$$

$$\psi^{(0)}(r,\theta) = -\,caK_1(\,\frac{\delta r}{\sqrt{c}})\sin\theta/\,K_1(\frac{\delta a}{\sqrt{c}}) \qquad r > a, \tag{3.18b}$$

where a, c and κ are the modon parameters which are assumed to be functions of X and T.

The relative vorticity $\Delta\psi^{(0)}$ can be calculated easily using the polar Laplacian ,i.e.,

$$\Delta\psi^{(0)} = \frac{1}{r}(r\psi^{(0)}{}_r)_r + \frac{1}{r^2}\,\psi^{(0)}{}_{\theta\theta},$$

with the following recursion formulae:

$$\frac{d}{d\kappa r}J_1(\kappa r) = -\,J_2\,(\kappa r) + \frac{J_1(\kappa r)}{\kappa r}, \tag{3.19a}$$

$$\frac{d}{dmr}K_1(mr) = -\,K_2\,(mr) + \frac{K_1(mr)}{mr}. \tag{3.19b}$$

The relative vorticity can be written in the form

$$\nabla^2\psi^{(0)}(r,\theta) = -\,\delta^2 a\,\frac{J_1(\kappa r)}{J_1(\kappa a)}\,\sin\theta \qquad r < a, \tag{3.20a}$$

$$\nabla^2\psi^{(0)}(r,\theta) = -\,\delta^2 a\,\frac{K_1(mr)}{K_1(ma)}\,\sin\theta \qquad r > a, \tag{3.20b}$$

where $\Delta = \nabla^2$.

A necessary condition for the vorticity to be continuous across $r=a$ is that the radial gradient of $\psi^{(0)}$ (i.e., the azimuthal velocity) must be continuous across $r=a$. This constraint

gives

$$-\frac{J_2(\nu)}{J_1(\nu)} = \frac{\nu}{\gamma}\frac{K_2(\gamma)}{K_1(\gamma)}, \tag{3.21}$$

where $\gamma^2 = \frac{\delta^2 a^2}{c}$ and $\nu = a\kappa$. The expression (3.21) is the modon dispersion relationship. As an example, if $a=c=\delta=1$, it follows that $\kappa = 3.9226$.

Fig.4(a)(b)(c) are contour plots of the streamfunction, vorticity and streaklines for the above example. Fig.4d is a three dimensional plot of the streamfunction depicting the dipole vortices with an anticyclone to the south and a cyclone to the north for the eastward-travelling modon. It turns out (Flierl et al.,1980) that the westward-travelling modon has a reverse cyclone-anticyclone configuration.

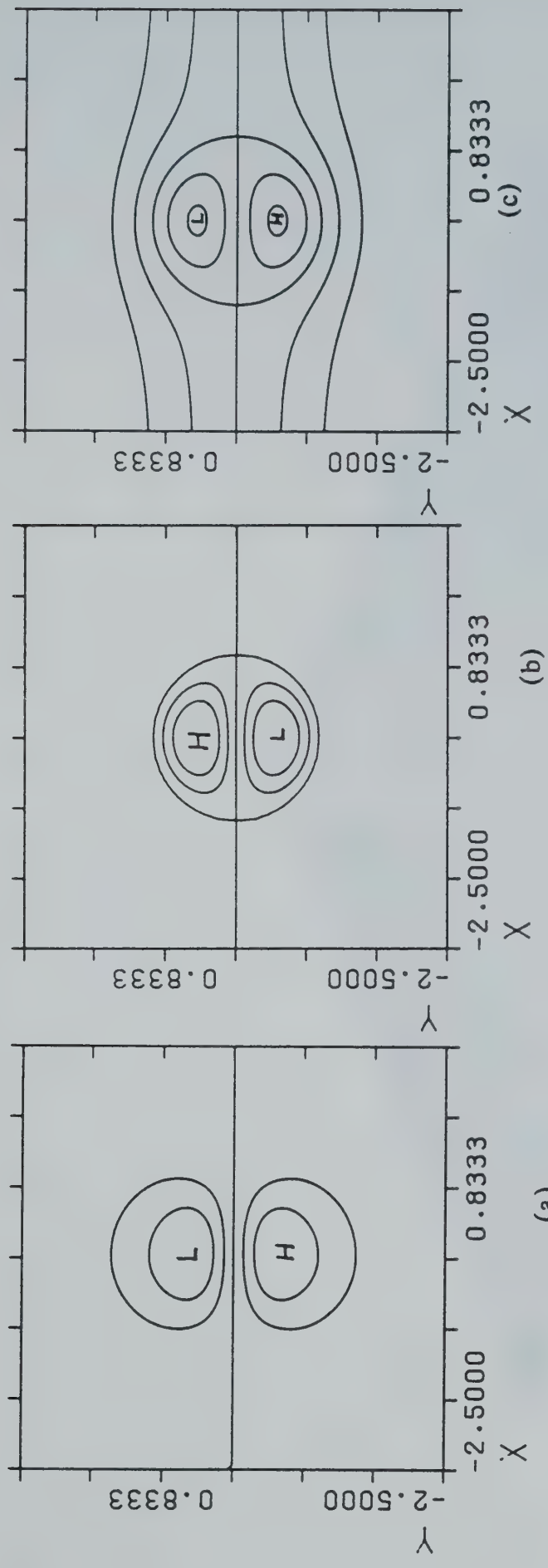

Fig.4. Contour plot of (a) the streamfunction ($\psi'^{(0)}$) (b) the vorticity ($\Delta\psi'^{(0)}$) (c) the streaklines ($\psi'^{(0)} + cy$) for a barotropic modon with $a=c=1.0$ and $\kappa=3.9226$. The contour intervals are ± 0.5 for (a) and (c) but ± 5.0 for (b). The L and H symbols denote the minimum and maximum values of the streamfunction, the vorticity and the streaklines in the modon interior, respectively, which in (a), (b) and (c) are ± 1.61, ± 16.1 and ± 1.08, respectively.

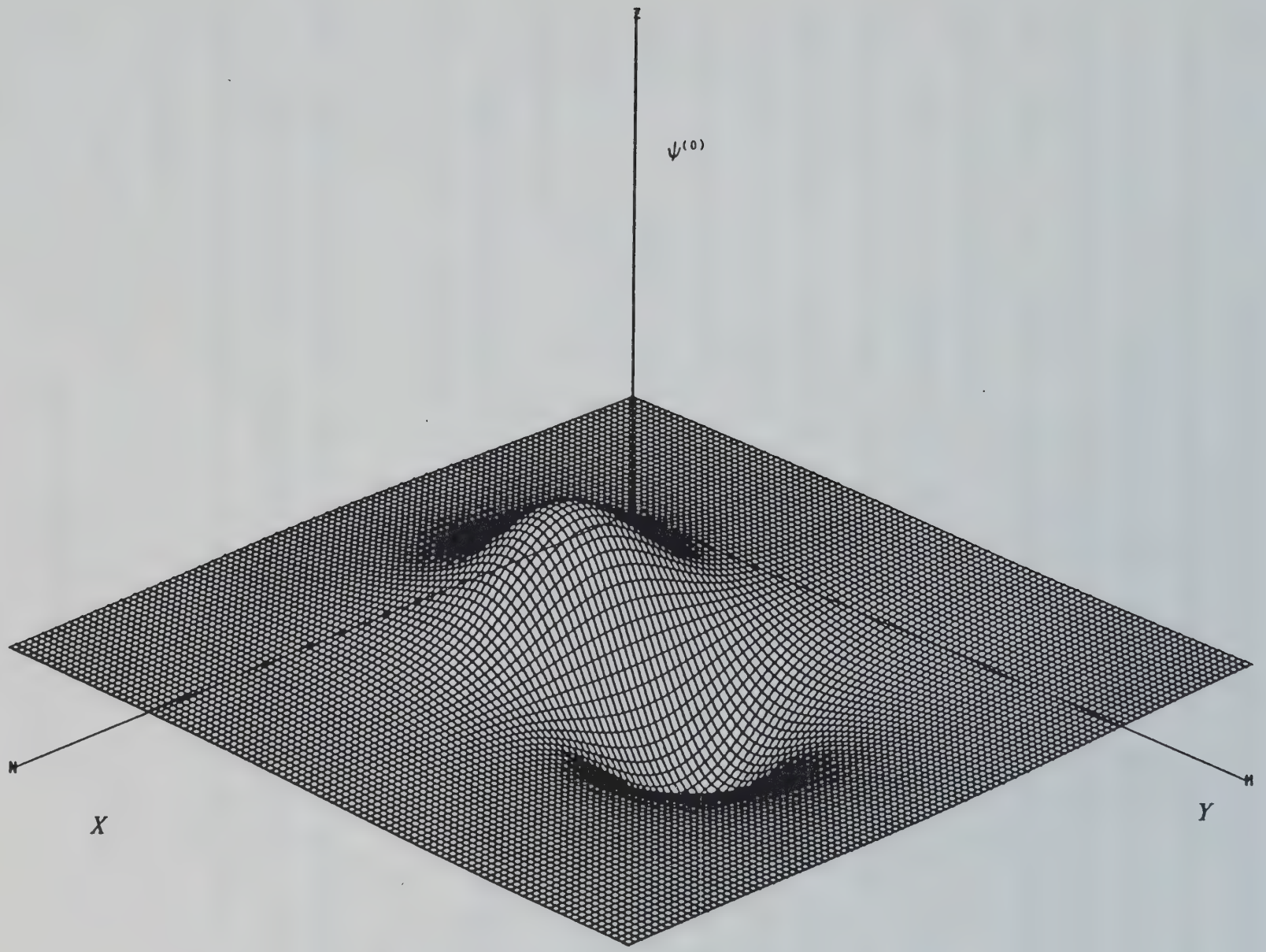

Fig.4d. Three dimensional plot of streamfunction with $a=c=1.0$ and $\kappa=3.9226$.

4. Derivation of the Transport Equations

The solution of the O(1) problem presented in Chapter 3 contained five parameters: $l(X,T)$, $a(X,T)$, $c(X,T)$, $\kappa(X,T)$ and $A(X,T)$. It is the evolution of these parameters which will describe the modulation of the modon (Swaters,1986b). However, while five parameters have been introduced, only two relations have so far been derived to describe the evolution of these parameters, namely the conservation of crests equation (3.5) and the dispersion relation (3.21). Therefore, three additional relations must be obtained to close the mathematical problem for the above five parameters.

There are two approaches one can take to derive the necessary transport equations(Swaters and Flierl,1988). The first of these is to derive the required transport equations as solvability conditions on the $O(\epsilon)$ problem for the asymptotic expansion (3.2). The second approach is to derive the transport relations as the result of area-averaged conservation laws associated with the original governing equation (2.15). Both these approaches are equivalent (Swaters and Flierl, 1988). Swaters(1986b) adopted the conservation law approach because it seemed to be more "physical", and this is the procedure we shall describe here.

Conservation (or more correctly "balance") laws for (2.15) are expressions which can be written in the form (Pedlosky,1987,Sec.3.27):

$$E_t + \nabla\cdot\mathbf{F} = -\epsilon\tau G, \tag{4.1}$$

where E, G and $\mathbf{F}$ are the appropriate scalar densities and vector flux function, respectively, $\nabla = (\partial_x, \partial_y)$ and the subscript t denotes differentiation with respect to time. The three conservation equations that we will use are the vorticity equation, the energy equation and the enstrophy equation.

To begin with, it is noted that the Jacobian can be rewritten in the form

$$J(a,b) = \nabla\cdot[(\hat{e}_3 \times \nabla a)b], \tag{4.2}$$

where $\hat{e}_3 = (0, 0, 1)$. The potential vorticity equation (2.15) can be re-cast into the form (4.1) if

$$E = \nabla\cdot(\frac{\nabla\psi}{H}), \tag{4.3a}$$

$$\mathbf{F} = (\hat{e}_3 \times \nabla\psi)(\nabla\cdot(\frac{\nabla\psi}{H}) + f)/H, \tag{4.3b}$$

$$G = E. \tag{4.3c}$$

The energy equation is obtained by multiplying (2.15) by ψ and re-arranging terms. The first term can be arranged into the form

$$\psi\nabla\cdot(\nabla\psi_t/H) = \nabla\cdot(\psi\nabla\psi_t/H) - (\nabla\psi\cdot\nabla\psi/2H)_t. \tag{4.4a}$$

The term associated with the Jacobian term can be re-arranged as

$$\psi\nabla\cdot[(\hat{e}_3 \times \nabla\psi)(\nabla\cdot(\nabla\psi/H) + f)/H] = \nabla\cdot[\psi(\hat{e}_3 \times \nabla\psi)(\nabla\cdot(\nabla\psi/H) + f)/H]. \tag{4.4b}$$

Combining (4.4a) and (4.4b) implies that the energy conservation equation can be put into the form (4.1) if

$$E = (\nabla\psi\cdot\nabla\psi)/2H, \tag{4.4c}$$

$$\mathbf{F} = -\psi\nabla\psi_t/H - \psi(\hat{e}_3 \times \nabla\psi)(\nabla\cdot(\nabla\psi/H) + f)/H - \epsilon\tau\psi\nabla\psi/H, \tag{4.4d}$$

$$G = 2E. \tag{4.4e}$$

The enstrophy is defined as the square of the potential vorticity. Thus the enstrophy equation is derived by simply multiplying (2.15) by $[\nabla\cdot(\nabla\psi/H) + f]/H$. The enstrophy equation can therefore be put into the form of (4.1) if

$$E = (\nabla\cdot(\nabla\psi/H) + f)^2/H, \tag{4.5a}$$

$$\mathbf{F} = (\hat{e}_3 \times \nabla\psi)(\nabla\cdot(\nabla\psi/H) + f)^2/H^2, \tag{4.5b}$$

$$G = 2[E - (\nabla\cdot(\nabla\psi/H) + f)f/H]. \tag{4.5c}$$

Following the arguments of Swaters(1986b), the three conservation equations (4.3), (4.4) and (4.5) will be sufficient to close the problem for the evolution of the modon

parameters. However, first we have to examine the structure of the conservation laws when the asymptotic expansion (3.2) is substituted into (4.1). Let us first note that when (3.2) is substituted into the general conservation density term E, G and flux term $\mathbf{F}$, expressions of the form

$$E = E^{(0)} + \epsilon E^{(1)} + \dots , \tag{4.6a}$$

$$\mathbf{F} = \mathbf{F}^{(0)} + \epsilon \mathbf{F}^{(1)} + \dots , \tag{4.6b}$$

$$G = G^{(0)} + \epsilon G^{(1)} + \dots , \tag{4.6c}$$

will be obtained. Note that under the multiple-scale assumption the density term will be re-written

$$E_t = - clE_\xi + \epsilon E_T. \tag{4.7a}$$

The gradient will be re-written as

$$\nabla = (\partial_x, \partial_y) = (l\partial_\xi, \partial_y) + \epsilon \hat{e}_1 \partial_X = \nabla + \epsilon \hat{e}_1 \partial_X. \tag{4.7b}$$

For convenience, we let $\nabla = (l\partial_\xi, \partial_y)$ and $\nabla_X = \hat{e}_1 \partial_X$. As a result, the flux term in the conservation law becomes

$$\nabla\cdot\mathbf{F} = \nabla\cdot\mathbf{F}^{(0)} + \epsilon \nabla_X\cdot\mathbf{F}^{(0)} + \epsilon\nabla\cdot\mathbf{F}^{(1)} + O(\epsilon^2), \tag{4.7c}$$

where $O(\epsilon^2)$ means that all the other terms are order ϵ^2 or higher order. Therefore, the perturbation form of the conservation law (4.1) can be written in the form

$$- clE^{(0)}_\xi + \nabla\cdot\mathbf{F}^{(0)} + \epsilon E^{(0)}_T - \epsilon cl E^{(1)}_\xi + \epsilon \nabla_X\cdot\mathbf{F}^{(0)} + \epsilon\nabla\cdot\mathbf{F}^{(1)} + \dots = - \epsilon\tau G^{(0)} + O(\epsilon^2). \tag{4.8}$$

Following Swaters(1986b), we can obtain the transport equation for $A(X,T)$ as follows. Consider (4.8) evaluated for the potential vorticity density (4.3a) and flux (4.3b), respectively. It is possible to show that since $\psi^{(0)} \to 0$ as $r \to \infty$ and if we demand that $\psi^{(1)} \to 0$ as $r \to \infty$, it follows that the leading term in (4.8) as $r \to \infty$ is

$$[f(AH)_X]_y = 0, \tag{4.9a}$$

from the $\nabla\cdot\mathbf{F}^{(1)}$ term in (4.8), i.e., all the O(1) and the other O(ϵ) terms are zero. Since $f=1/R_0+\delta^2 y$, it follows from (4.9a) that

$$(AH)_X = 0. \tag{4.9b}$$

Equation (4.9b) can be interpreted as the long wave approximation to (2.15) (Swaters,1986b). Swaters(1986b) has shown that the "long waves" $A(X,T)$ eventually decouple from the other transport equations. Thus with no loss of generality we, following Swaters(1986b), can choose $A \equiv 0$.

The other two transport equations that are required are obtained by averaging the energy and enstrophy conservation equations over the fast variable domain (i.e. $-\infty < (\xi,y) < \infty$) (Swaters,1986b). These transport equations can be put into the form

$$-cl\langle E^{(0)}{}_{\xi}\rangle + \langle\nabla\cdot\mathbf{F}^{(0)}\rangle + \epsilon\langle E^{(0)}\rangle_T - \epsilon cl\langle E^{(1)}{}_{\xi}\rangle + \epsilon\nabla_X\cdot\langle\mathbf{F}^{(0)}\rangle + \epsilon\langle\nabla\cdot\mathbf{F}^{(1)}\rangle + O(\epsilon^2) = -\epsilon\tau\langle G^{(0)}\rangle + O(\epsilon^2), \tag{4.10}$$

where $\langle(*)\rangle$ is defined as

$$\langle(*)\rangle = \int_{-\infty}^{\infty}\int_{-\infty}^{\infty}(*)d\xi dy.$$

The calculation of the energy and enstrophy transport equations is complicated. First, note that $E^{(1)}$ and $\mathbf{F}^{(1)}$ in (4.10) will be continuous at $r = a$ and both will vanish as $r \to \infty$ because $\nabla\psi^{(1)} \to 0$ as $r \to \infty$ and $\psi^{(0)}$ as well as $\psi^{(1)}$ are assumed differentiable (Swaters (1988) has shown how to explicitly construct $\psi^{(1)}$ so that all these regularity conditions can be met.). Therefore, the term $\langle E^{(1)}{}_{\xi}\rangle$ in (4.8b) can be evaluated as follows:

$$\langle E^{(1)}{}_{\xi}\rangle = \int_{-\infty}^{\infty}\int_{-\infty}^{\infty} E^{(1)}{}_{\xi}d\xi dy$$

$$= \int_{-\infty}^{\infty} E^{(1)}\Big|_{-\infty}^{\infty} dy$$

$$= \int_{-\infty}^{\infty} [E^{(1)}(\infty) - E^{(1)}(-\infty)]\, dy$$
$$= 0,$$

since $E^{(1)}(\infty)=0=E^{(1)}(-\infty)$. A similar result also follows for $<E^{(0)}{}_{\xi}>$, $<\nabla\cdot\mathbf{F}^{(0)}>$ and $<\nabla\cdot\mathbf{F}^{(1)}>$. As a result, the only surviving terms left after averaging are

$$<E^{(0)}>_T + \nabla_X\cdot<\mathbf{F}^{(0)}> = -\tau<G^{(0)}>. \tag{4.11}$$

The leading order density and flux terms for the energy and enstrophy can be written respectively,

$$E^{(0)} = H(\nabla\psi^{(0)})^2/2, \tag{4.12a}$$

$$\mathbf{F}^{(0)} = [\,(A+\psi^{(0)})Hcl^2\,\psi^{(0)}{}_{\xi\xi} + H(A+\psi^{(0)})(\,\nabla^2\psi^{(0)} + f)\,\psi^{(0)}{}_{y},$$
$$(A+\psi^{(0)})Hcl\,\psi^{(0)}{}_{y\xi} - H(A+\psi^{(0)})(\,\nabla^2\psi^{(0)} + f)\,l\psi^{(0)}{}_{\xi}\,] \tag{4.12b}$$

$$G^{(0)} = 2E^{(0)}. \tag{4.12c}$$

$$E^{(0)} = (\Delta\psi^{(0)} + f)^2/H \tag{4.13a}$$

$$\mathbf{F}^{(0)} = \frac{1}{H}[\,-\psi^{(0)}{}_{y}\,(\Delta\psi^{(0)} + f)^2/H,\; l\psi^{(0)}{}_{\xi}\,(\Delta\psi^{(0)} + f)^2/H] \tag{4.13b}$$

$$G^{(0)} = 2[E^{(0)} - (\Delta\psi^{(0)} + f)f/H]. \tag{4.13c}$$

The calculations for the averaged energy and enstrophy transport equations are not difficult but are rather lengthy. The following are the key steps in performing the computations:

1. Do as much integration by parts as possible.
2. Use polar coordinates rather than Cartesian coordinates, i.e.,

$$<(*)> = \int_0^{2\pi}\int_0^{\infty} (*)lrdrd\theta.$$

3. Do the angular part of the integration first because most of the results turn out to be

zero due to the trigonometric integrations (this is the reason why the y-component of both the energy and enstrophy fluxes integrate to zero).

4. Use the following derivative definitions

$$\psi_{\xi\xi} = -\frac{c_1\kappa}{l^2}\,[\kappa J_1(\kappa r)\cos^2\theta\sin\theta + \frac{J_2(\kappa r)}{r}\,\sin\theta(4\sin^2\theta - 3)], \qquad r < a$$

$$\psi_{\xi\xi} = \frac{c_3 m}{l^2}\,[mK_1(mr)\cos^2\theta\sin\theta - \frac{K_2(mr)}{r}\,\sin\theta(4\sin^2\theta - 3)], \qquad r > a$$

where $c_1 = \delta^2 a/J_1(\kappa a)\,\kappa^2$, $c_3 = -ca/K_1(ma)$ and m is given by (3.11b).

5. Use

$$\int_0^a r^2 J_1(\kappa r)dr = \frac{a^2}{\kappa}J_2(\kappa a),$$

with a similar expression for $K_1(mr)$ except the integration limits range from a to ∞.

6. Use

$$\int_0^a rJ^2{}_n(\kappa r)\,dr = \frac{r^2}{2}[J^2{}_n(\kappa r) - J_{n+1}(\kappa r)\,J_{n-1}(\kappa r)]\,|_0^a,$$

where n is a positive integer. A similar expression is used for $K_1(mr)$ except the integration limits range from a to ∞.

After substantial algebra and the application of the dispersion relation, the averaged energy transport equation can be put into the form

$$\partial_T(Hla^2c^2E_1) + \partial_X(Hla^2c^3E_1) = -2\tau Hla^2c^2E_1, \tag{4.14a}$$

where

$$E_1 = \frac{\gamma^2}{4\nu^2}\,(\gamma^2 + \nu^2)(1 + \frac{4R}{\gamma}), \tag{4.14b}$$

with $R = K_2(\gamma)/K_1(\gamma)$. The averaged enstrophy transport equation can be put into the form

$$\partial_T(lc^2E_2/H) + \partial_X(lc^3E_2/H) = -2\tau lc^2E_2/H, \tag{4.15a}$$

where

$$E_2 = \frac{\gamma^2}{2}(\gamma^2 + \nu^2)R^2. \tag{4.15b}$$

Physically, the quantities $Hla^2c^2E_1$, lc^2E_2/H correspond to the averaged kinetic energy and relative enstrophy, respectively. With the transport equations (4.14) and (4.15), the number of equations and unknowns is the same and so, in principle, the modulation problem for the modon parameters forms a closed system of equations.

5. The Steady-State Solution

The frictionally and topographically forced evolution of the modon parameters is determined by the solutions to equations (3.5), (3.21), (4.14a) and (4.15a). In this chapter, we obtain nonlinear ordinary differential equations which will describe the exact nonlinear *steady-state* response of the modon to orographic forcing and frictional damping. Physically, the steady-state solutions will correspond to the situation in which the modon is instantaneously adjusting to the external forcing. This assumption is reasonable provided the forcing is being "gradually" or "weakly" applied.

The steady-state interaction equations are obtained by assuming $\partial_T \equiv 0$ in (3.5), (3.21), (4.14a) and (4.15a), i.e.,

$$(cl)_X = 0, \tag{5.1a}$$

$$(la^2c^3E_1H)_X = -2\tau la^2c^2E_1H, \tag{5.1b}$$

$$(lc^3E_2/H)_X = -2\tau lc^2E_2/H, \tag{5.1c}$$

$$\gamma K_1(\gamma)J_2(\nu) + \nu K_2(\gamma)J_1(\nu) = 0. \tag{5.1d}$$

The boundary condition on the solution to (5.1) is

$$c = l = a = 1 \text{ and } \kappa = \kappa_0 = 3.9226, \tag{5.1e}$$

as $X \to -\infty$ where $H(X)$ satisfies the condition that $H(X) \to 1$ as $X \to -\infty$.

From (5.1a) and (5.1e), we obtain

$$l = \frac{1}{c}. \tag{5.2}$$

Substituting (5.2) into (5.1b) and (5.1c) yields

$$(a^2c^2E_1H)_X = -2\tau a^2cE_1H, \tag{5.3a}$$

$$(c^2E_2/H)_X = -2\tau cE_2/H. \tag{5.3b}$$

Equations (5.3) cannot be integrated directly and a numerical solution of (5.3) and (5.1d) is required. The procedure adopted in this thesis is to eliminate the κ_X derivatives in (5.3) in favour of a_X and c_X by exploiting the dispersion relationship (5.1d). It follows from (5.1d) that

$$\left(\frac{\kappa_X}{\kappa} + \frac{a_X}{a}\right) = (1 + M)\left(\frac{a_X}{a} - \frac{c_X}{2c}\right), \tag{5.4a}$$

where

$$M \equiv -R(\gamma^2 + \nu^2)/(4\gamma + \gamma^2/R + R\nu^2), \tag{5.4b}$$

and

$$R \equiv \frac{K_2(\gamma)}{K_1(\gamma)}. \tag{5.4c}$$

Substitution of (5.4) into (5.3) yields the following dynamical system

$$a_X = \frac{E_2E_{23}(2\tau - cH_X/H) - E_1E_{33}a^2(2\tau + cH_X/H)}{\mathrm{DET}}, \tag{5.5a}$$

$$c_X = \frac{E_2E_{22}(-2\tau + cH_X/H) + E_1E_{32}a^2(2\tau + cH_X/H)}{\mathrm{DET}}, \tag{5.5b}$$

with

$$E_{22} = ac[2E_1 + E_{1_\gamma}\gamma + E_{1_\nu}\nu\,(M+1)], \tag{5.5c}$$

$$E_{23} = a^2[2E_1 - (E_{1_\gamma}\gamma + E_{1_\nu}\nu\,(M+1))/2], \tag{5.5d}$$

$$E_{32} = c[E_{2_\gamma}\gamma + E_{2_\nu}\nu\,(M+1)]/a, \tag{5.5e}$$

$$E_{33} = [2E_2 - (E_{2_\gamma}\gamma + E_{2_\nu}\nu\,(M+1))/2], \tag{5.5f}$$

and

$$\mathrm{DET} = E_{22}E_{33} - E_{23}E_{32}, \tag{5.5g}$$

where subscripts with respect to γ and ν correspond to their respective partial derivatives, and where the modon wavenumber $\kappa(X)$ is understood to be an implicit function of the modon radius $a(X)$ and the translation speed $c(X)$ via the dispersion relationship (5.1d). Equations (5.5a), (5.5b) and (5.1d) can be solved to determine $c(X)$, $a(X)$ and $\kappa(X)$. (IMSL routine, DIVPRK, is used to numerically solve the two ordinary differential equations.)

To verify the validity of the equations (5.5), we compared our solutions of (5.5) with no topography (i.e., $H \equiv 1$) but assuming that damping is present (e.g., $\tau = 0.2$) with the analytical and numerical results obtained by Swaters and Flierl(1988). It turns out that our solutions for the modon radius, the translation speed and the modon wavenumber are exactly the results obtained by Swaters and Flierl(1988).

It is possible to re-write (5.3) in the following form. First, we introduce the arrival time T_A of the modon at position X as calculated by integrating the modon translation speed, i.e.,

$$T_A = \int_{X_0}^{X} \frac{1}{c(s)} ds, \tag{5.6a}$$

where $X_0 = -4$ corresponds to our assumed initial position. Therefore, using the following change of variable

$$\frac{d}{dX} = \frac{dT_A}{dX}\frac{d}{dT_A} = \frac{1}{c(X)}\frac{d}{dT_A}, \tag{5.6b}$$

we can formally integrate equations (5.3) into the following forms

$$a^2c^2E_1H(X) = E_{10}\exp(-2\tau T_A), \tag{5.7a}$$

$$c^2E_2/H(X) = E_{20}\exp(-2\tau T_A), \tag{5.7b}$$

where

$$E_{10} = E_1(c=a=1,\kappa=\kappa_0) = 3.14, \tag{5.8a}$$

$$E_{20} = E_2(c=a=1,\kappa=\kappa_0) = 59.7. \tag{5.8b}$$

It is important to note that (5.7) is a highly implicit way of writing (5.3) because of the appearance of T_A in the argument of the exponential. However, note that if $\tau = 0$ (i.e., the inviscid problem), then (5.7) represents two exact nonlinear *algebraic* relationships for the modon parameters. The relationships (5.7) and the modon dispersion relation (5.1d) can, in this situation, be therefore solved directly without resorting to a numerical solution of (5.3). We will examine these undamped topographic solutions in the next chapter.

As well, note that in the limit of no topographic variability (i.e., $H(X)\equiv 1$), (5.7) reduces again to a set of nonlinear *algebraic* relationships of the form

$$a^2c^2E_1 = E_{10}\exp(-2\tau T_A), \tag{5.9a}$$

$$c^2E_2 = E_{20}\exp(-2\tau T_A). \tag{5.9b}$$

Equations (5.9) and (5.1d) can be solved to determine a, c and κ as a function of T_A. In this

situation the zonal position of the dissipation modon is given by

$$X_c = X_0 + \int_0^{T_A} c(s)ds. \tag{5.9c}$$

Swaters and Flierl(1988) compared the theoretical predictions of (5.9a,b,c) and (5.1d) with a high-resolution numerical solution of (2.15) assuming a modon initial condition and $H(X)\equiv 1$. The comparison between the two was very good, implying that higher order terms in the perturbation expansion are not important. Not only were the decay properties of the averaged energy and enstrophy reproduced very accurately, but local properties such as the location and magnitude of the extrema in the streamfunction and vorticity fields, the zonal position coordinate and the dilation of the modon dipole were accurately reproduced. The numerical simulation also confirmed that very little energy was radiated away from the decaying modon in the form of linear Rossby waves. This latter assumption is implicit in the adiabatic ansatz on which our theory is based.

6. The Inviscid and Viscous Topographic Solution

In the last chapter, we obtained nonlinear ordinary differential equations which described the exact nonlinear steady-state response of the modon to orographic forcing and frictional damping. In this chapter, we examine both the inviscid and the viscous solutions with different topographies. For the inviscid case, the solution is then compared with the approximate linear solutions found by Swaters(1986b). For small amplitude topography, the solutions found by Swaters are a good approximation to the nonlinear solutions we present here. However, the conclusion made by Swaters(1986b) that the magnitude of the vorticity extrema of the modon increases during the interaction is shown to be incorrect. In fact, we will show that the magnitudes of the vorticity extrema *decrease* during the interaction. Also, the viscous solutions are studied for the different topographic configurations.

6.1 The ridge topography

The first example is a Gaussian ridge topography given by

$$H(X) = 1 - \mu h(X), \tag{6.1a}$$

where

$$h(X) \equiv \exp(-X^2), \tag{6.1b}$$

and where the topographic height parameter $\mu=0.2$ (i.e., the maximum ridge height corresponds to 20% of the mean fluid depth). The topography is illustrated in Fig.5.

For the inviscid case (i.e., $\tau = 0$), equations (5.7) are reduced to the nonlinear algebraic equations

$$a^2c^2E_1H(X) = E_{10}, \tag{6.2a}$$

$$c^2E_2/H(X) = E_{20}, \tag{6.2b}$$

where

$$E_{10} = E_1(c=a=1,\kappa=\kappa_0) = 3.14, \tag{5.8a}$$

$$E_{20} = E_2(c=a=1,\kappa=\kappa_0) = 59.7. \tag{5.8b}$$

The results of solving (6.2) and (5.1d) for $H(X)$ given by (6.1) are shown in Fig.6(a), (b) and (c). We can compare the exact nonlinear solutions for a, c, l and κ with the linear

solutions obtained by Swaters(1986b). Swaters showed that assuming $0<\mu<<1$ the approximate linear solutions could be written in the form

$$l = 1 + 0.69\mu h(x), \tag{6.3a}$$

$$a = 1 + 0.84\mu h(x), \tag{6.3b}$$

$$c = 1 - 0.69\mu h(x), \tag{6.3c}$$

$$\kappa = \kappa_0[\,1 - 0.79\mu h(x)], \tag{6.3d}$$

where a general topographic $h(X)$ is assumed. It is noted that (6.3d) is slightly different from Swaters' equation (5.7) in his 1986b paper because the equation (3.11b) in his paper has a small computational error.

The exact nonlinear and the approximate linear solutions convey the same physics, i.e., when the modon travels into a shallower (deeper) region, its radius increases (decreases), speed decreases (increases) and modon wavenumber decreases (increases). However, the linear solutions suggest a strengthening of the maximum vorticity as the modon approaches the ridge (see Fig.7), whereas the nonlinear suggests the opposite, i.e., a weakening. This discrepancy does not depend on μ. For example, if μ is decreased to 0.1, the discrepancy persists. Fig.8 shows that the modon radius increases and its absolute vorticity extrema decreases as the modon enters the shallow region of the ridge topography.

Fig.6d shows that the normalized averaged energy and enstrophy, which are written in the following forms,

$$\hat{\mathrm{E}}\mathrm{n} = \frac{la^2c^2E_1}{E_{10}}, \tag{6.4a}$$

$$\hat{\mathrm{E}}\mathrm{s} = \frac{lc^2E_2}{E_{20}}, \tag{6.4b}$$

increase (decrease) as the modon enters a shallow (deep) region. The increase in the normalized averaged energy can be interpreted in the following way. The steady-state averaged energy equation (5.1b) states that following the modon the depth-averaged horizontal kinetic energy is constant. Consequently, it follows that if the total depth of the atmosphere decreases (increases) due to the presence of a topographic feature, then the horizontal kinetic energy must correspondingly increase (decrease).

The arrival time T_A of the modon at position X is calculated by integrating the nonlinear modon speed, i.e.,

$$T_A = \int_{X_0}^{X} \frac{1}{c(s)} ds, \tag{6.5}$$

where $X_0 = -4$ corresponds to our assumed initial position. The result of the integration is shown in Fig.9. (The integration is performed using Simpson's Rule.) The interaction of the modon with the ridge-topography leads to a change in the slope of $T(X)$, which is confined to a relatively small region about $X \simeq 0.0$ (which corresponds to the location of the maximum of the topographic amplitude).

For the viscous case, the range of τ in which the solutions of the equation (5.5) are valid is $0 < \tau < 0.06$. Beyond this range, the damping effect of the friction is so strong that the equation (5.5) and the dispersion relation (5.1d) cannot be simultaneously satisfied. Fig.10 shows that as τ increases, the damping effect increases. For an example, $\tau = 0.05$ is arbitarily selected so as to study the modon response.

Fig.11 is a comparison of the modon response between the effect of the friction alone and the combined effects of the friction and topography. Fig.11(b) shows that as the modon starts to propagate, the dissipation rate due to the friction and the friction plus topography are the same. As soon as the modon interacts with the topography, the two curves begin to separate. Without the topography, the modon speed decreases slowly. With topography, the modon speed decreases sharply in the shallow region of the ridge, but the modon regains some of the lost speed when the modon enters the deeper region of the ridge. However, long after the modon has passed through the ridge, the overall effect is that the modon speed decreases. In fact, the speed decreases much faster in the combined effect of the friction plus topography than just friction alone.

This higher dissipation rate due to the combined action of friction plus topography can be explained as follows. As the modon moves into the shallow region associated with the ridge topography, the modon speed decreases. But the presence of friction acts to further

decelerate the modon. Hence there is a *nonlinear* coupling between the two effects which will imply that the modon will slow down more rapidly than simply the *sum* of these two effects individually. As the modon enters the deeper region, the modon speed starts to increase, but the friction continues to decelerate the modon.

Fig.11(a) shows that the time required to reach the same location is longer in the presence of friction plus topography than the friction alone. Fig.11(c)(d) illustrate that the modon radius increases and the modon wavenumber decreases as a result of the frictional dissipation and the topographic forcing. Fig.11(e)(f) show that the energy and enstrophy (both being normalized) slowly decrease, as do the maximum vorticity and the streamfunction extrema (normalized also) (see Fig.11(g)(h)).

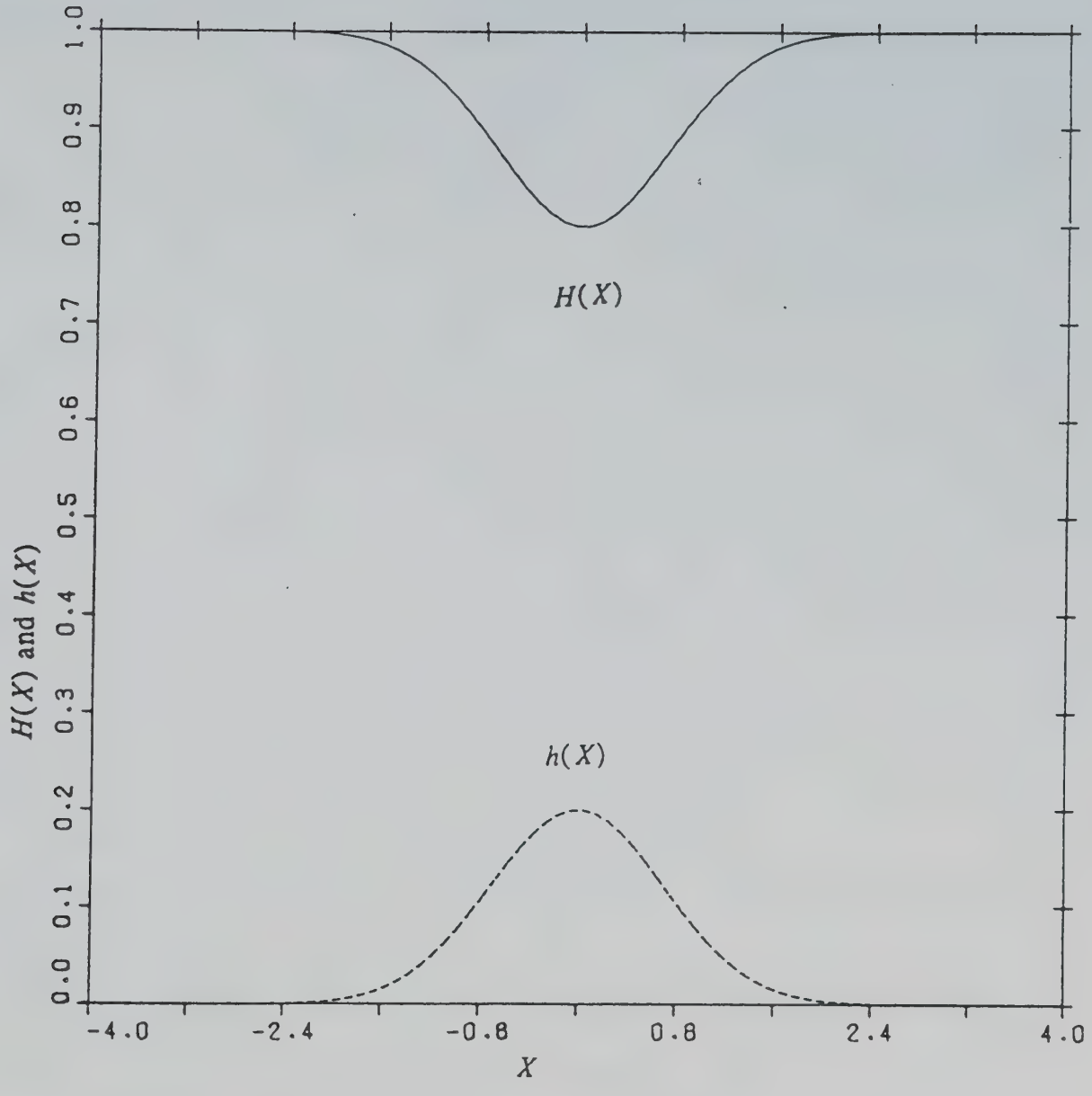

Fig.5. Depth of fluid $H(X)$ and ridge topography $h(X)$ given by the equations (6.1a) and (6.1b) respectively with $\mu=0.2$.

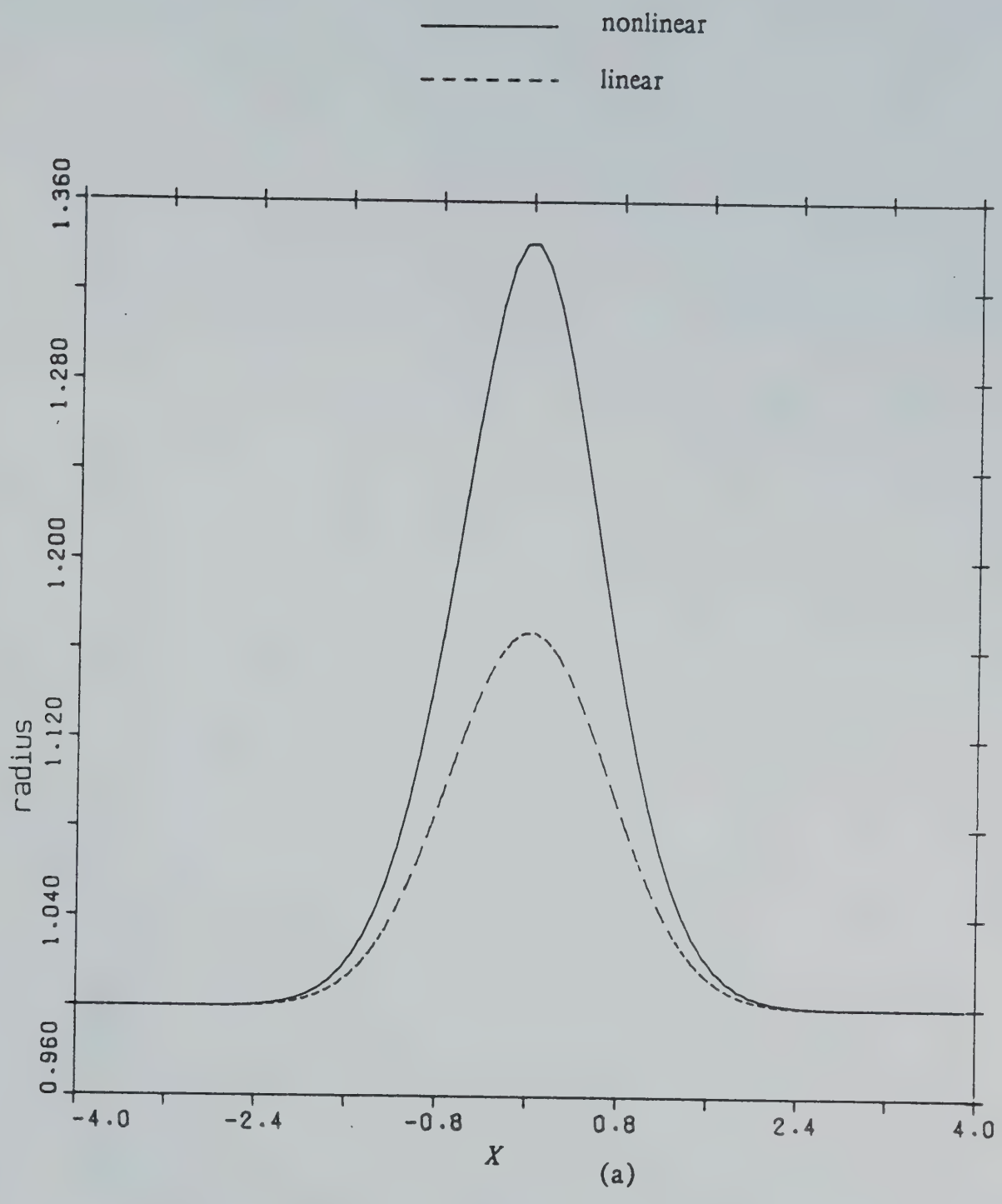

Fig.6 Comparison between the exact nonlinear and linearized "steady-state" topographically-modulated (a) modon radius (b) modon speed (c) modon wavenumber, (d) plots of the normalized average energy and enstrophy when the eastward-travelling modon propagates towards a ridge given by the equation (6.1b) with $\mu=0.2$ and $\tau=0$.

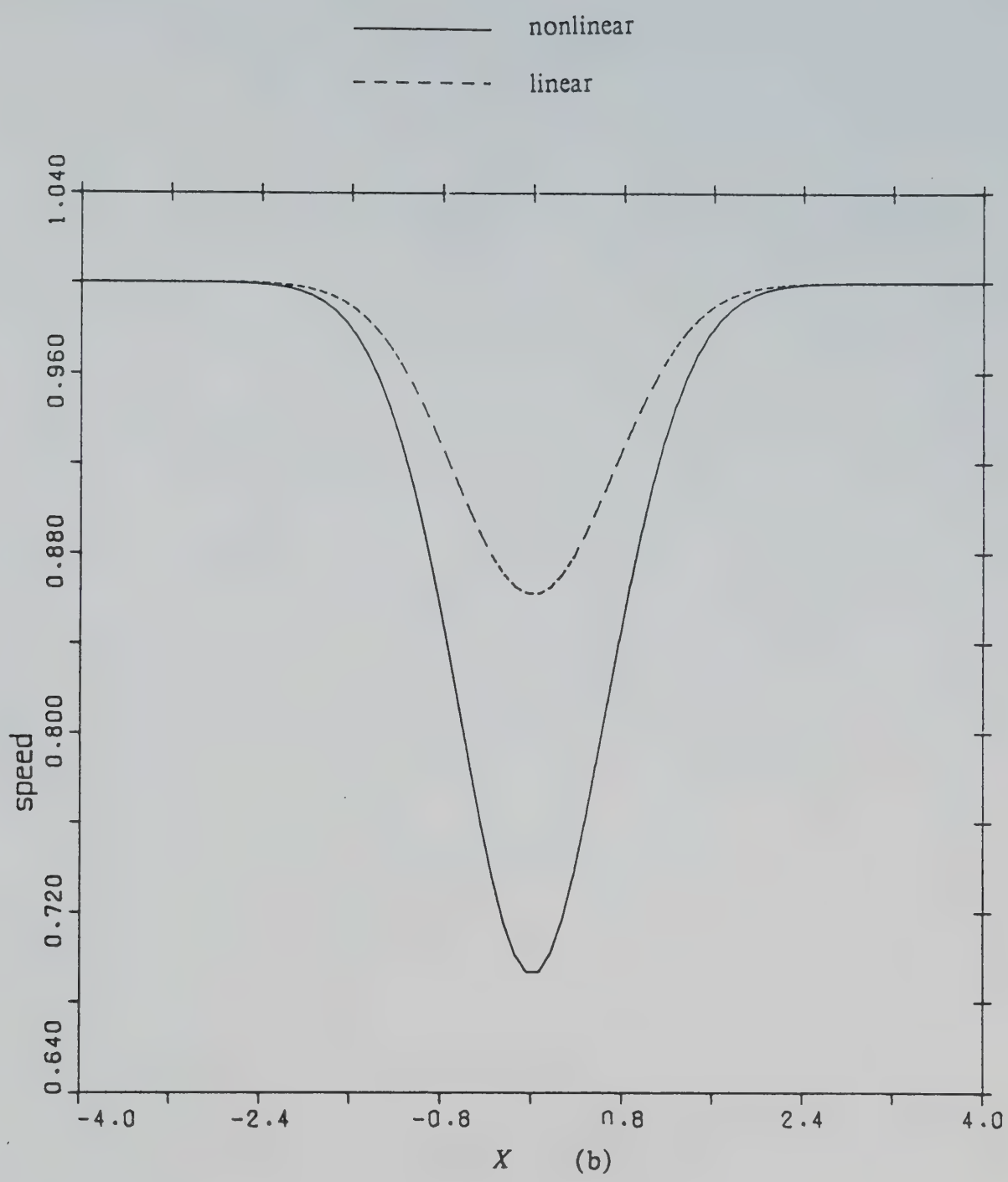
nonlinear
linear
1.040
0.960
0.880
0.800
0.720
0.640
speed
-4.0
-2.4
-0.8
0.8
2.4
4.0
X

(b)

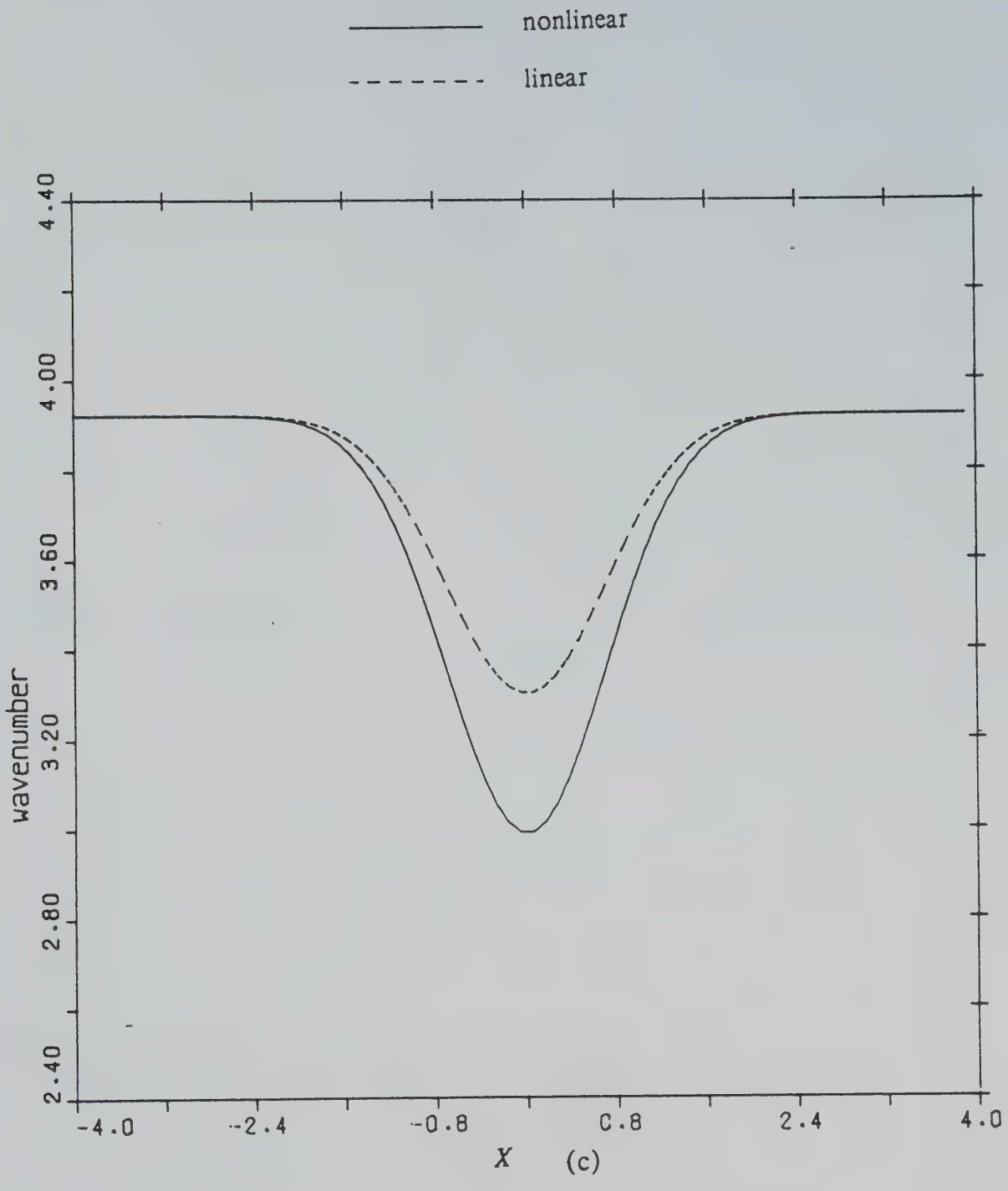
nonlinear
linear
4.40
4.00
3.60
3.20
2.80
2.40
wavenumber
-4.0
-2.4
-0.8
0.8
2.4
4.0
X
(c)

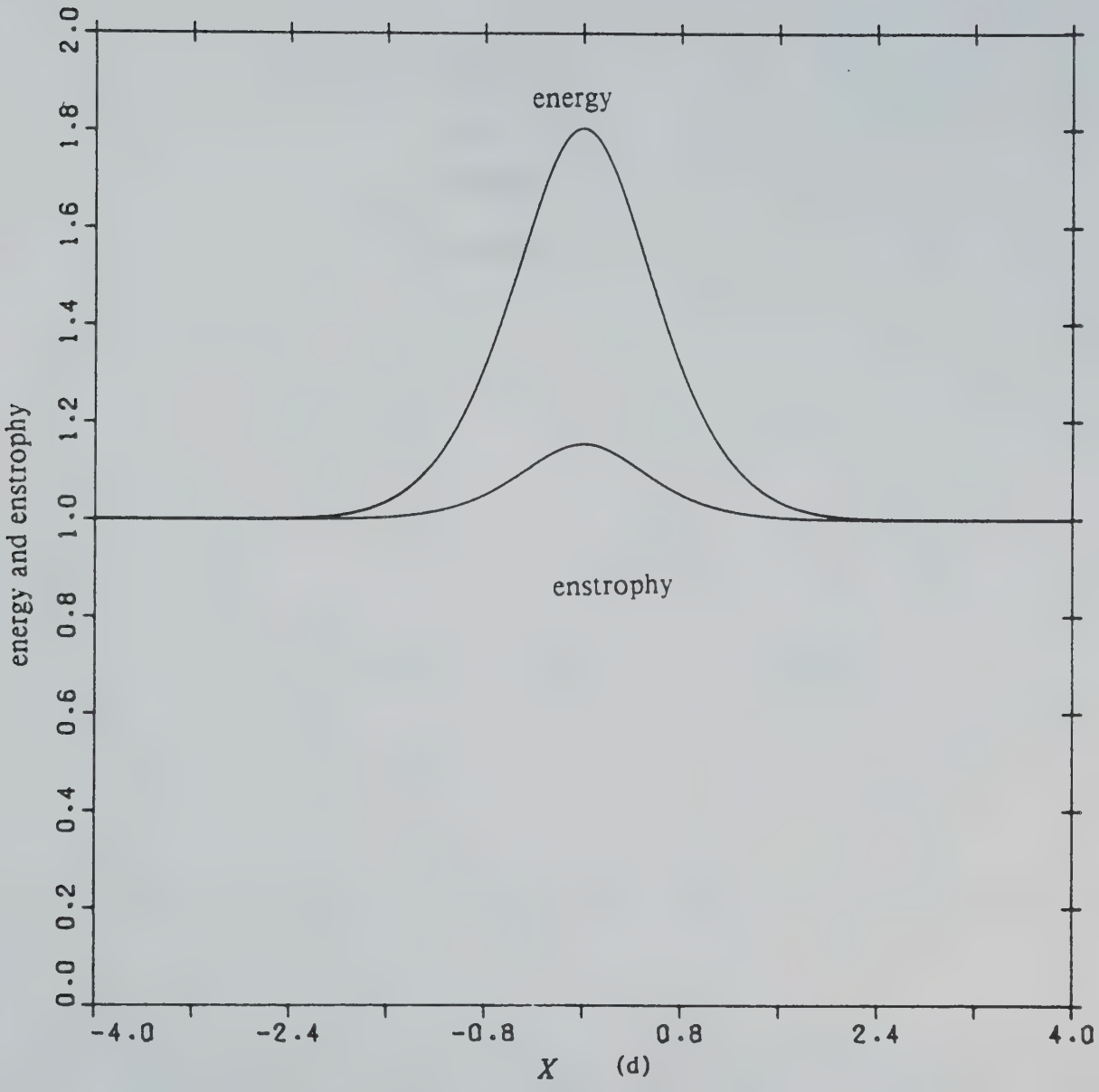
energy
enstrophy
energy and enstrophy
0.0
0.2
0.4
0.6
0.8
1.0
1.2
1.4
1.6
1.8
2.0
-4.0
-2.4
-0.8
0.8
2.4
4.0
X
(d)

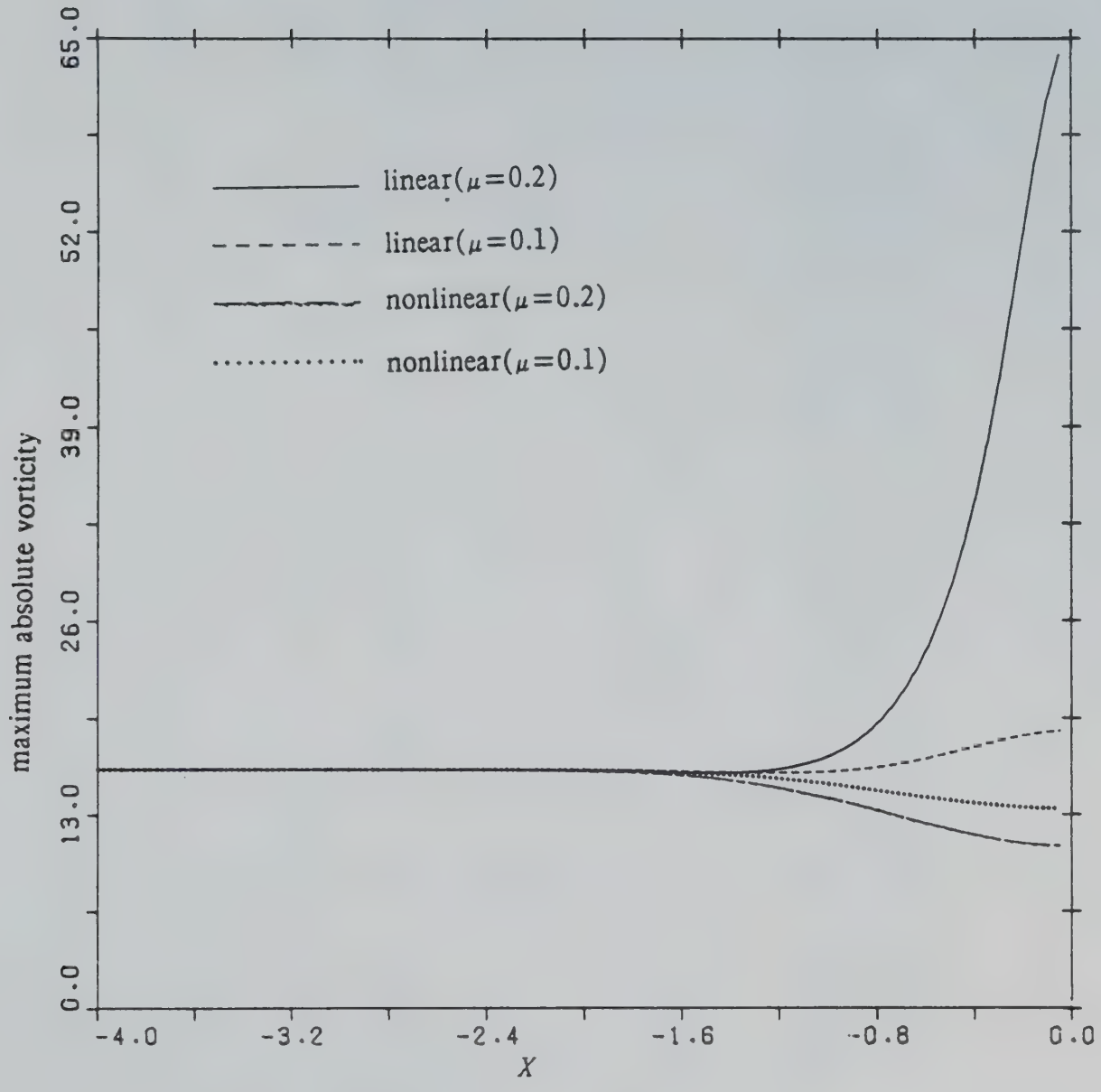

Fig.7. Comparison between the computed topographically-modulated maximum absolute vorticity based on the Swaters (1986b) linear solutions for the modon parameters and the exact nonlinear solutions determined in this thesis. The assumed topography is the ridge-like feature given by the equation (6.1b) with $\mu=0.2$ and $\mu=0.1$ and $\tau=0$.

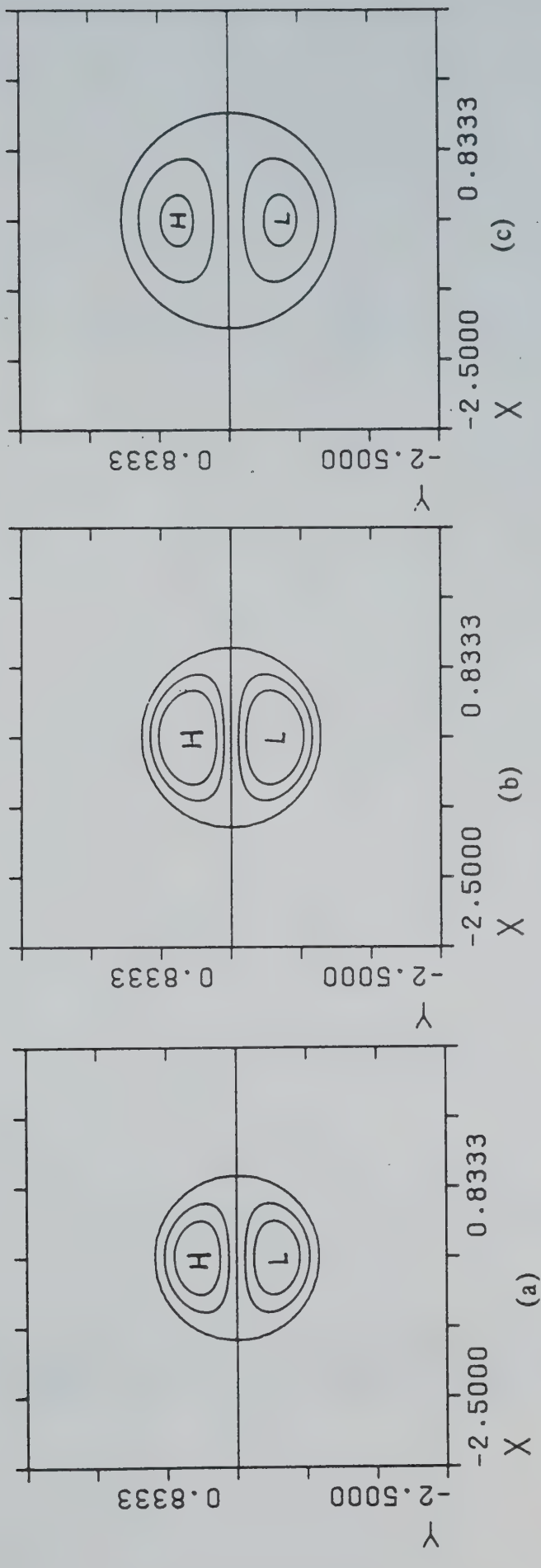

Fig.8. Sequences of plots of the vorticity as the modon propagates towards the ridge given by the equation (6.1b) with $\mu=0.2$. The contour interval in (a),(b) and (c) is ± 5.0. The L and H symbols denote the minimum and maximum values of the vorticity in the modon interior, respectively, which in (a) $T=0$, maximum vorticity of 16.1 (b) $T=2.90$, maximum vorticity of 16.0 (c) $T=3.50$, maximum vorticity of 10.7.

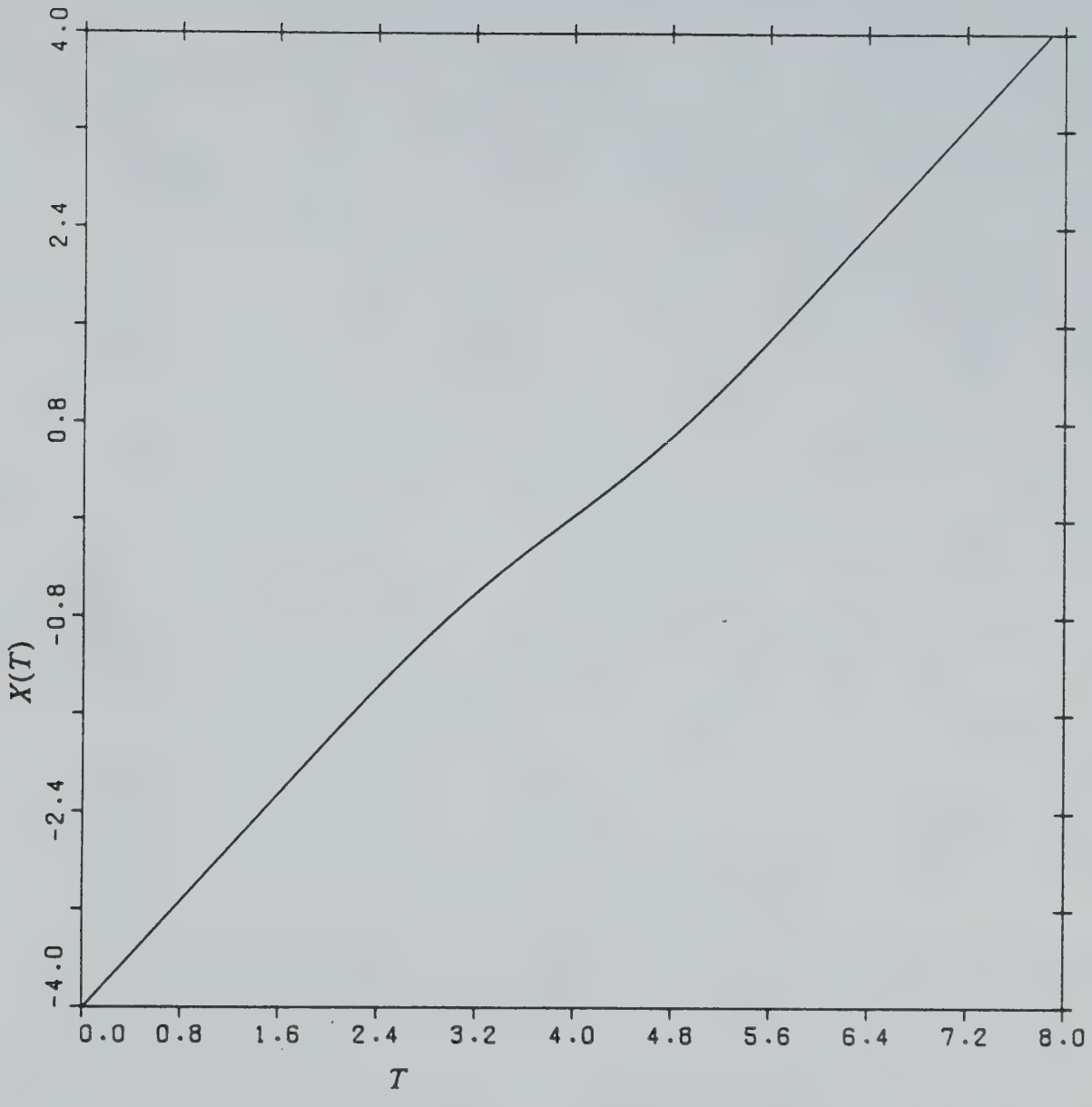

Fig.9. Plot of slow space $X(T)$ vs. T. $T(X)$ is computed by the equation (6.5), using ridge topography given by equation (6.1b) with $\mu=0.2$ and $\tau=0$.

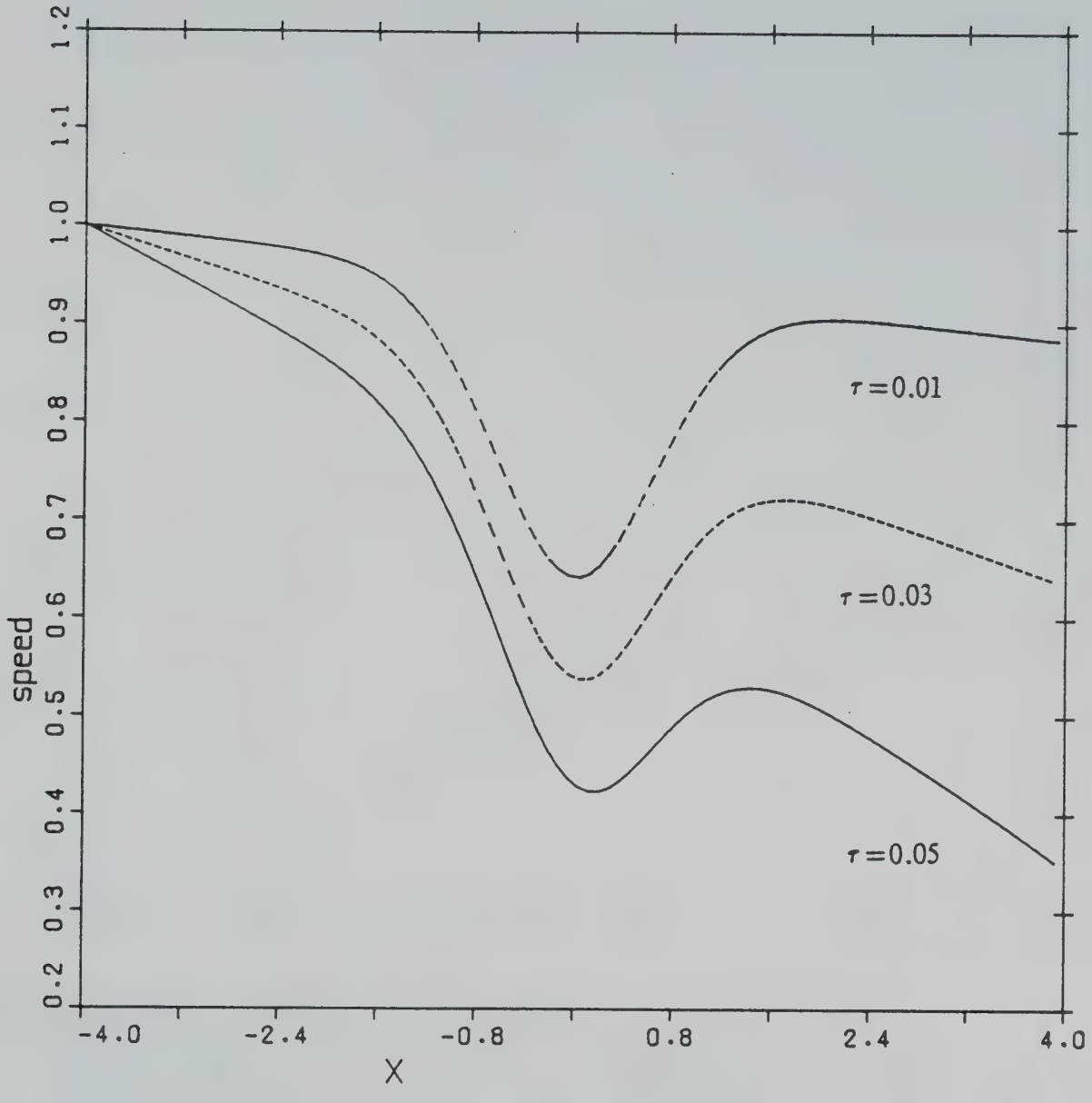

Fig.10. Plot of the modon speed $c(X)$ vs. X with τ changing from 0.01 to 0.03 to 0.05 in the ridge topography given by the equation (6.1b) with $\mu=0.2$.

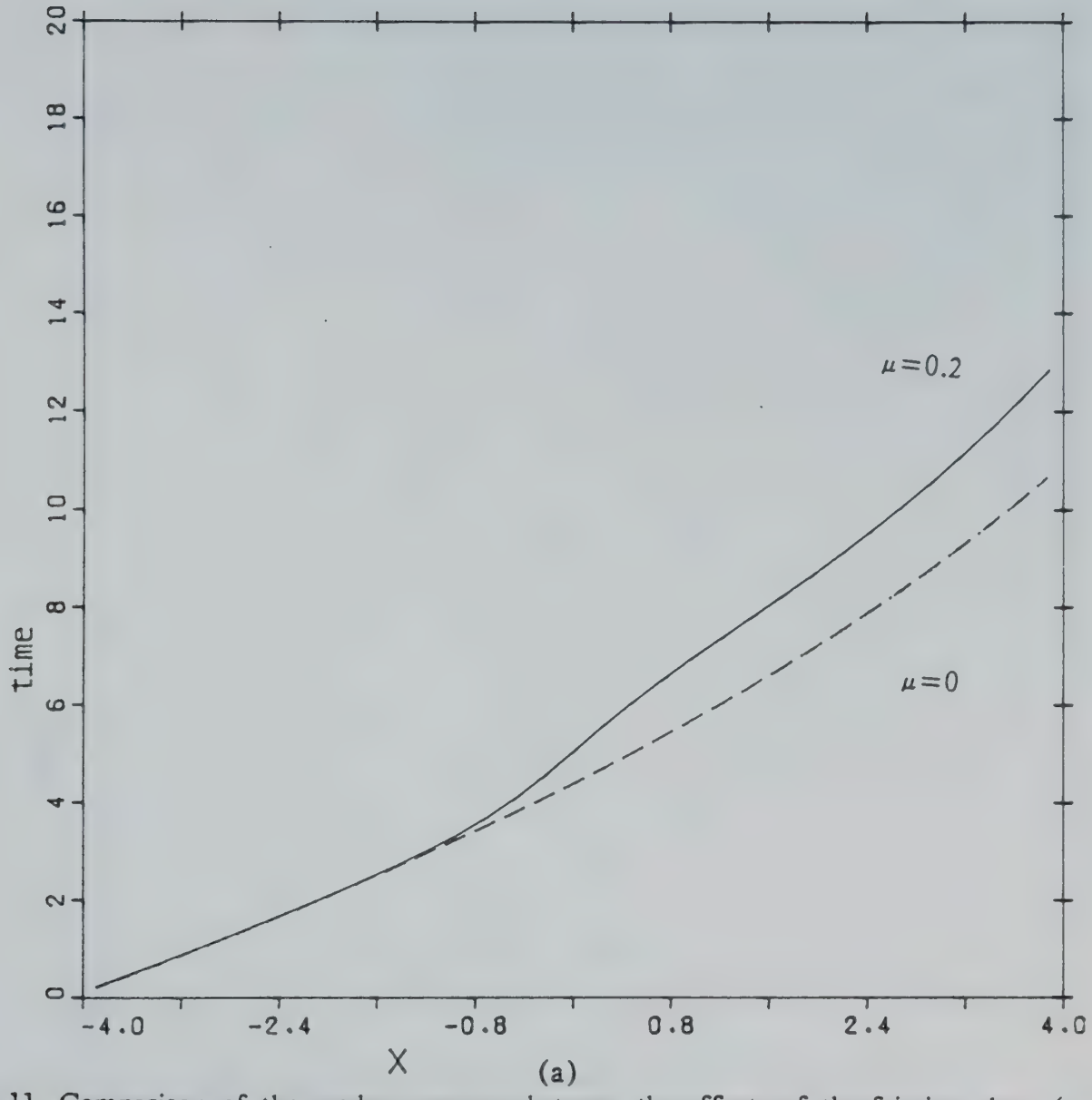

Fig.11. Comparison of the modon response between the effects of the friction alone ($\mu=0$) and the combined effects of friction and topography ($\mu=0.2$). Plots of the exact nonlinear "steady-state" frictionally- and topographically-modulated (a) the arrival time (b) the modon speed (c) the modon radius (d) the modon wavenumber (e) the normalized average energy (f) the enstrophy (g) the maximum vorticity (h) streamfunction when the eastward-travelling modon propagates towards a ridge given by the equation (6.1b) with $\mu=0.2$ and $\tau=0.05$.

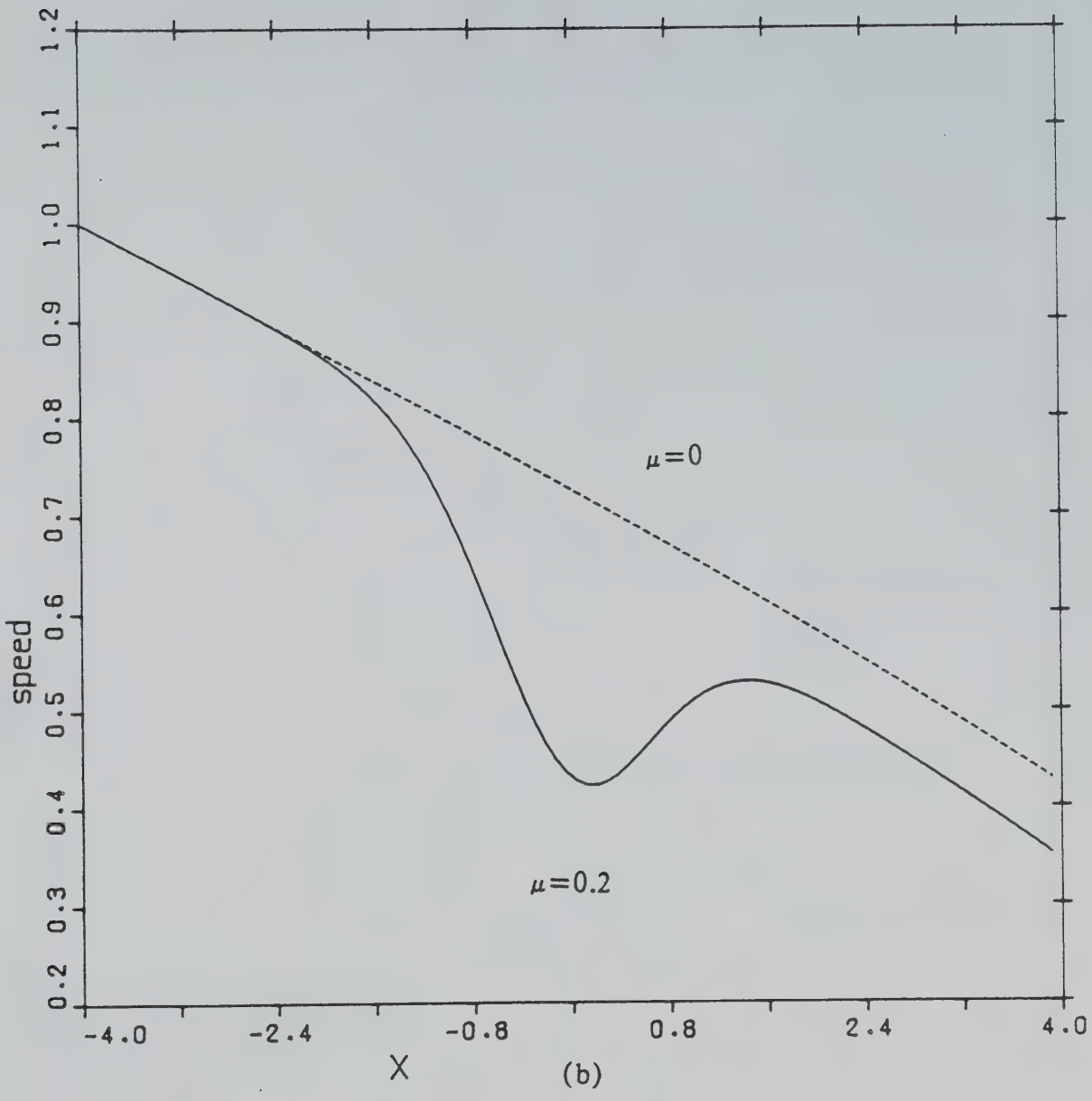

speed vs. X ridge

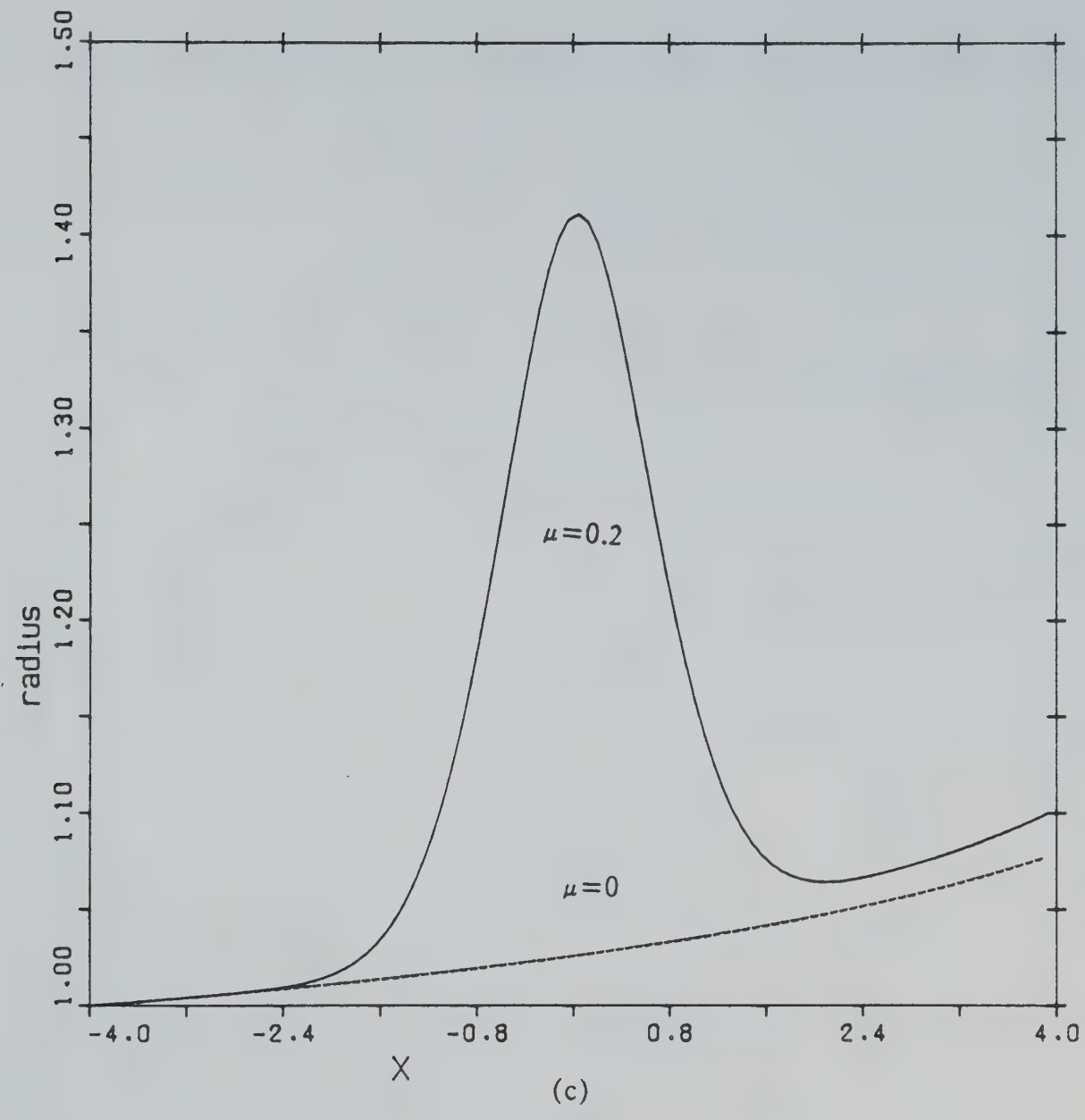

radius vs. X ridge

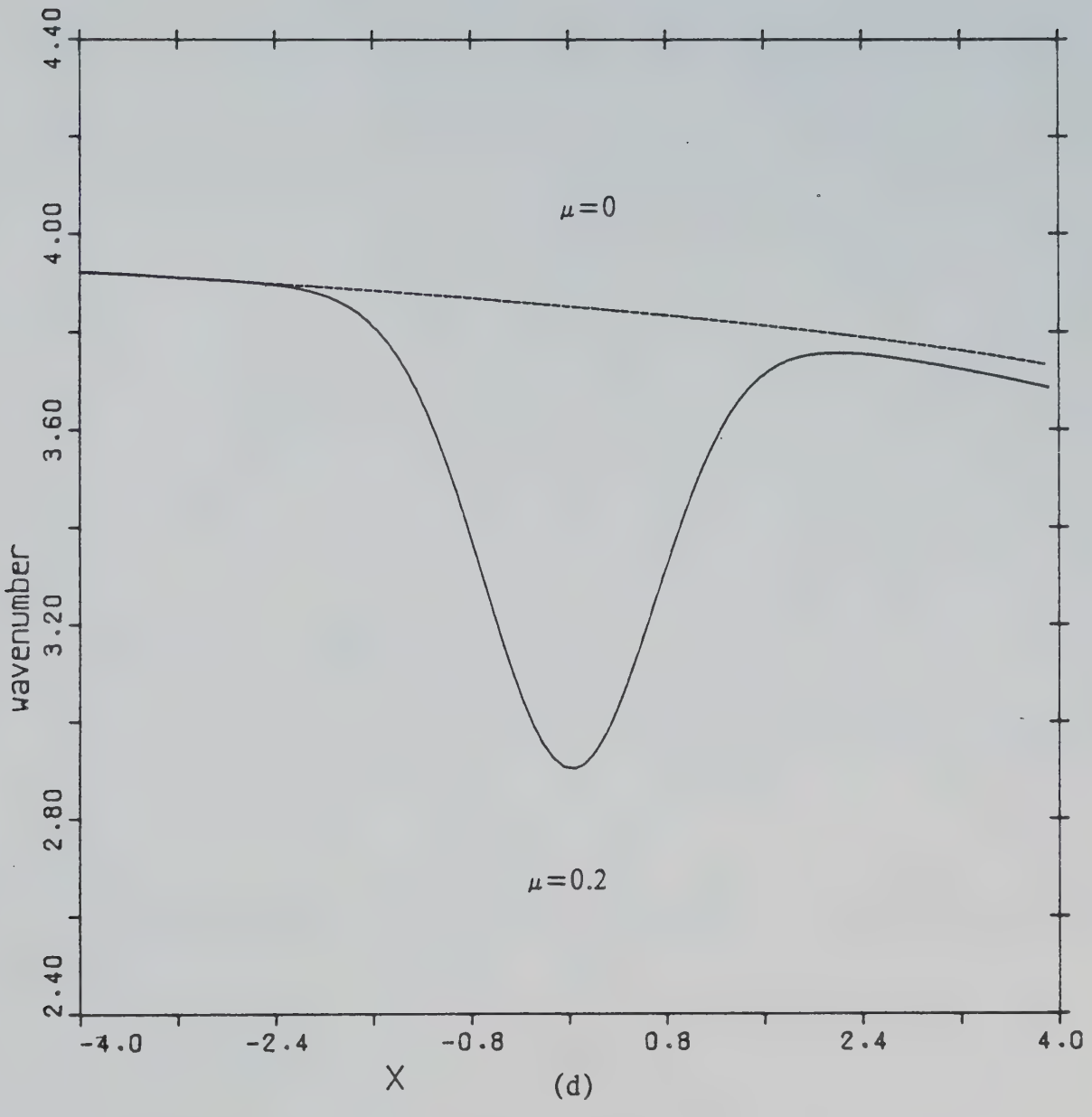

wavenumber vs. X ridge

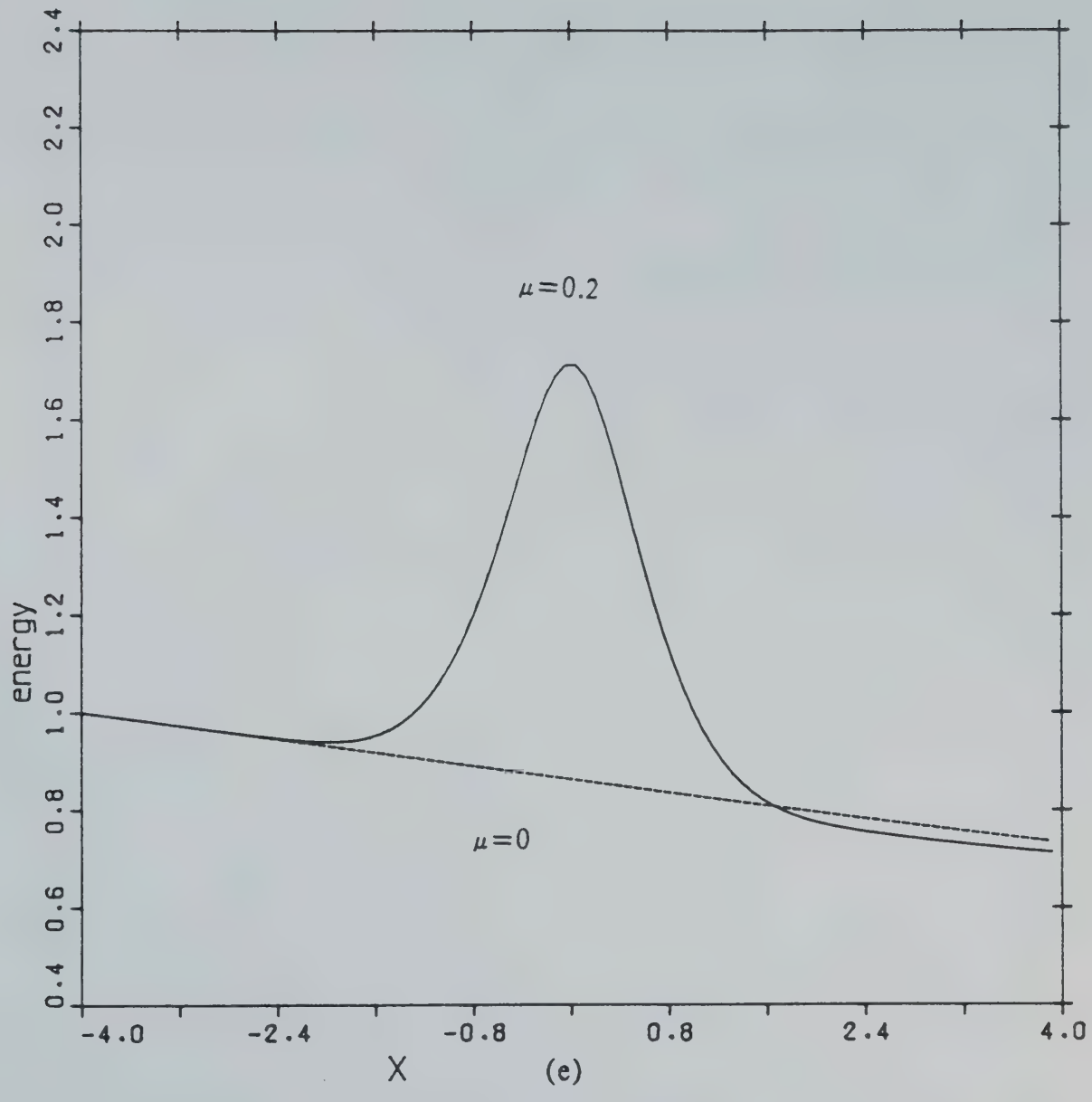

energy vs. X ridge

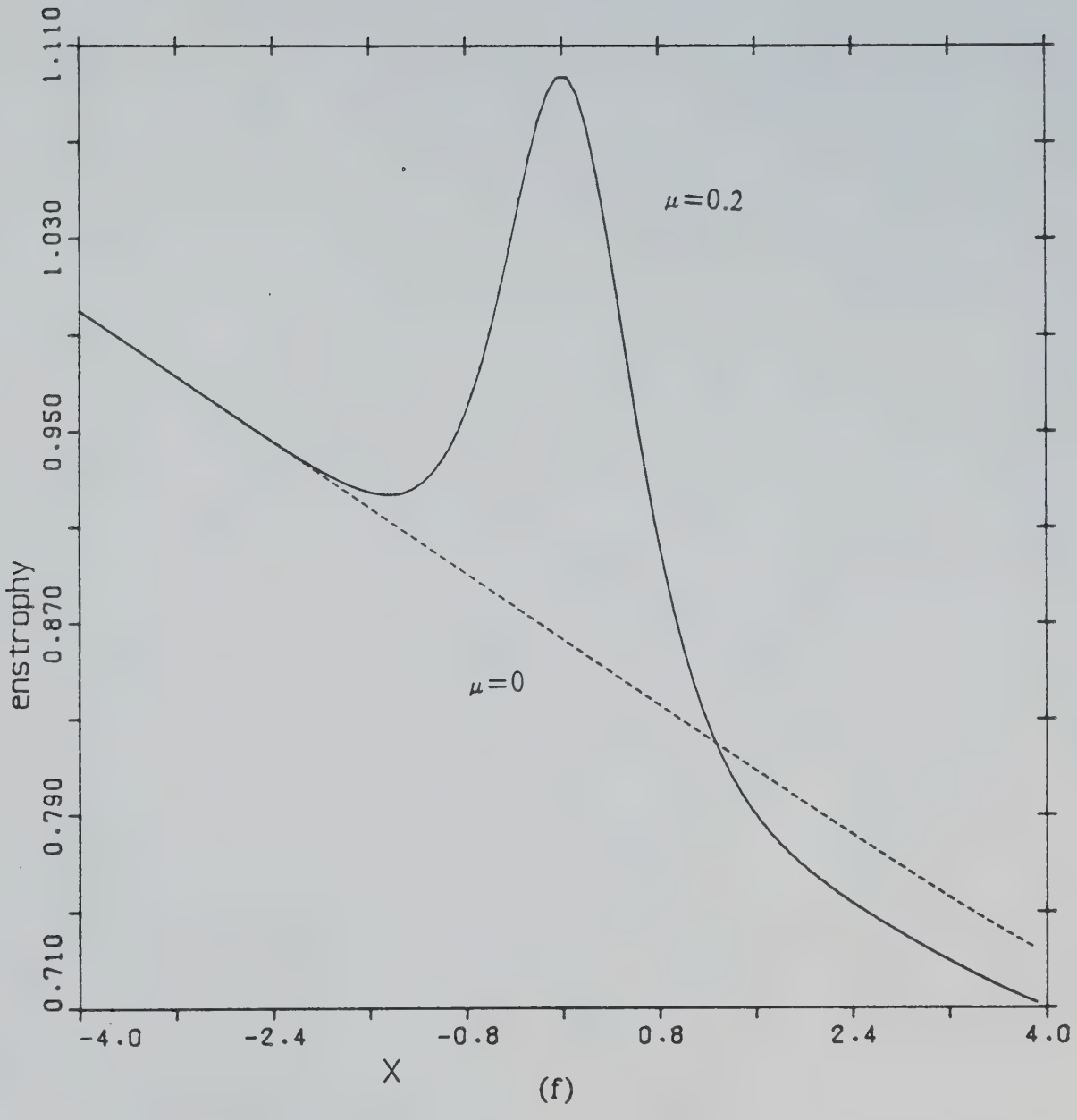

enstrophy vs. X ridge

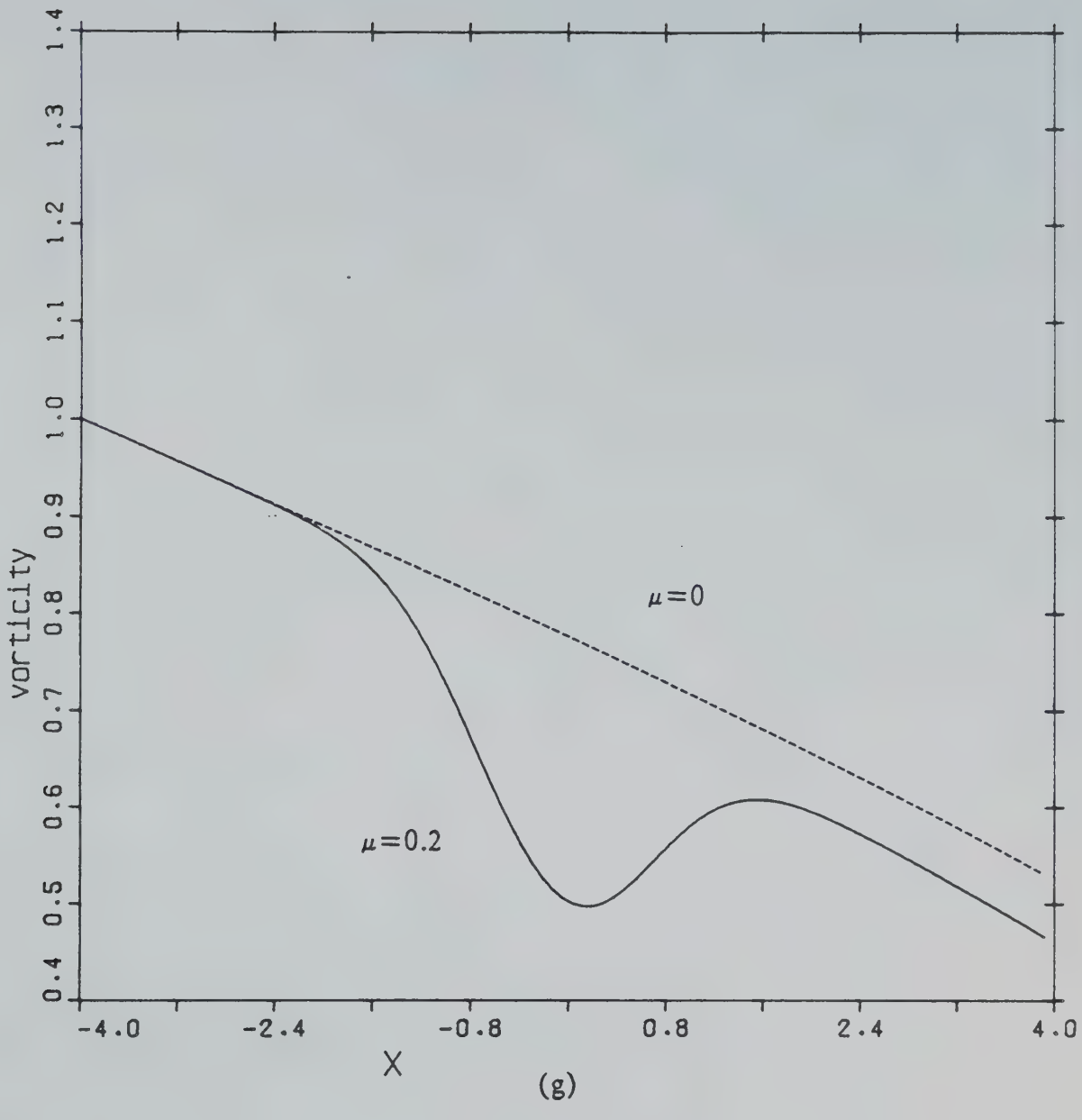

vorticity vs. X ridge

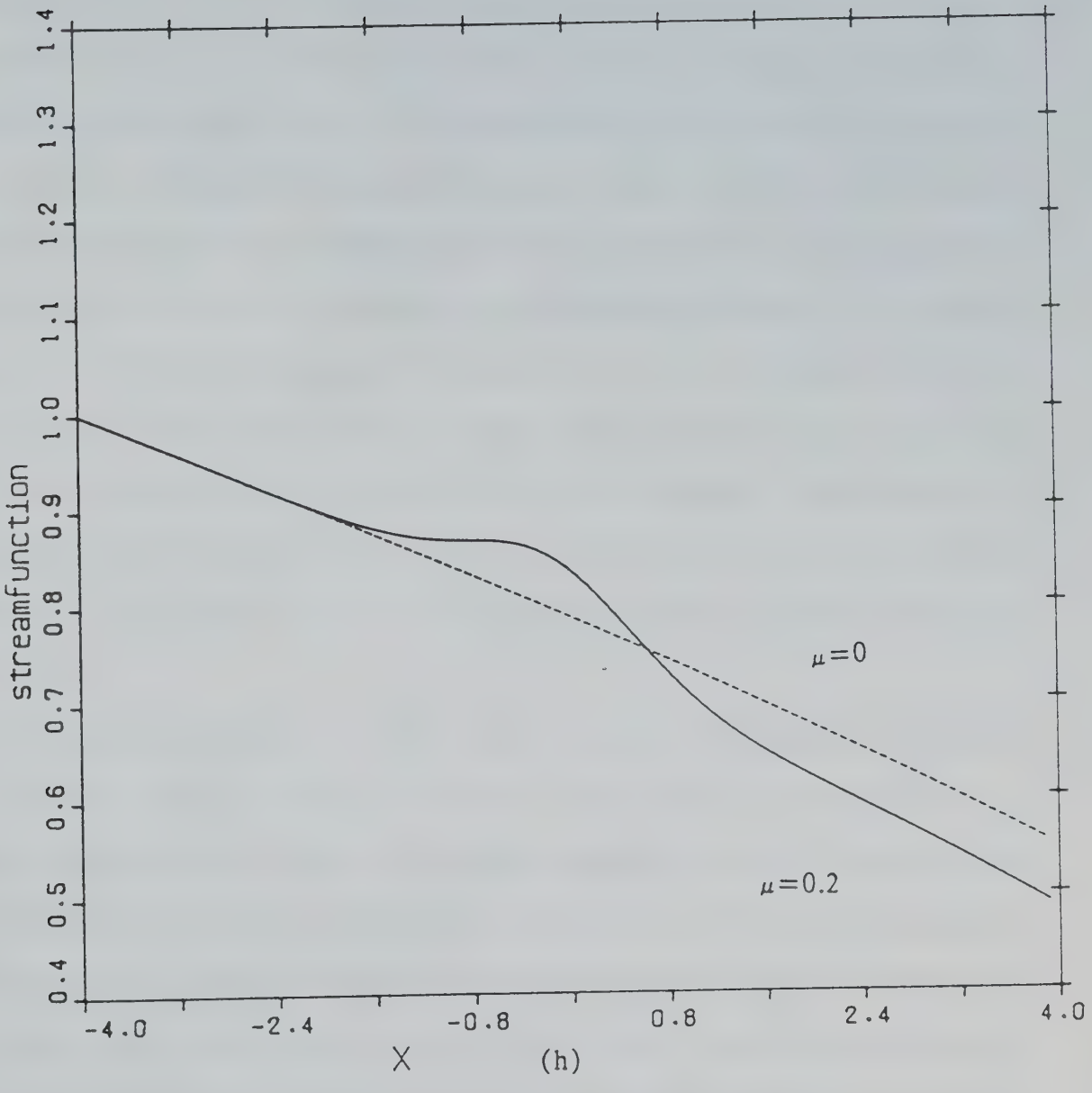

streamfunction vs. X ridge

6.2 The Valley Topography

If the topographic height parameter, μ, becomes negative such as $\mu = -0.2$, a valley topography results (Fig.12). For an inviscid interaction (i.e., $\tau = 0$), Fig.13 shows that as the modon enters the deep (shallow) region of the valley, the radius decreases (increases), the speed increases (decreases) and the modon wavenumber increases (decreases).

In addition, Fig.13 is a comparison between the exact nonlinear "steady-state" topographically-modulated modon radius, the translation speed and the modon wavenumber when the eastward-travelling modon propagates towards a ridge and a valley. These figures show that the extremum values of the modon parameters are higher for the ridge topography than for the valley topography. For example, the extremum speed achieved by the modon situated at the top of the ridge topography is higher than that at the bottom of the valley topography. In other words, the responses of the modon parameters due to the ridge topography is not anti-symmetric to that due to the valley topography. This difference in magnitudes of the modon parameters is because the term H_X/H in the equations (5.5) is *not* anti-symmetric in μ . The absolute value of this term for the ridge is larger than that of the valley.

For the viscous interaction, $\tau = 0.05$ is used for the sake of comparison. The effect due to the valley plus friction is essentially the same as that of the ridge topography, i.e., only the radius slowly increases while all the other parameters decrease. However, one noticeable difference is that the rate of the dissipation due to friction in the valley topography is much slower than that of the ridge topography. Fig.14(a) shows that the arrival time due to the valley plus friction is faster than that due to friction alone because the modon speed due to the valley plus the friction decelerates more slowly than that of friction alone (see Fig.14(b)). This slower deceleration is also shown in the radius, wavenumber, energy, enstrophy, maximum vorticity and streamfunction (Fig.14(c)(d)(e)(f)(g)(h)). The slower rate of dissipation due to the valley plus friction is because the rate of dissipation is reduced when the modon enters the deeper region of the valley.

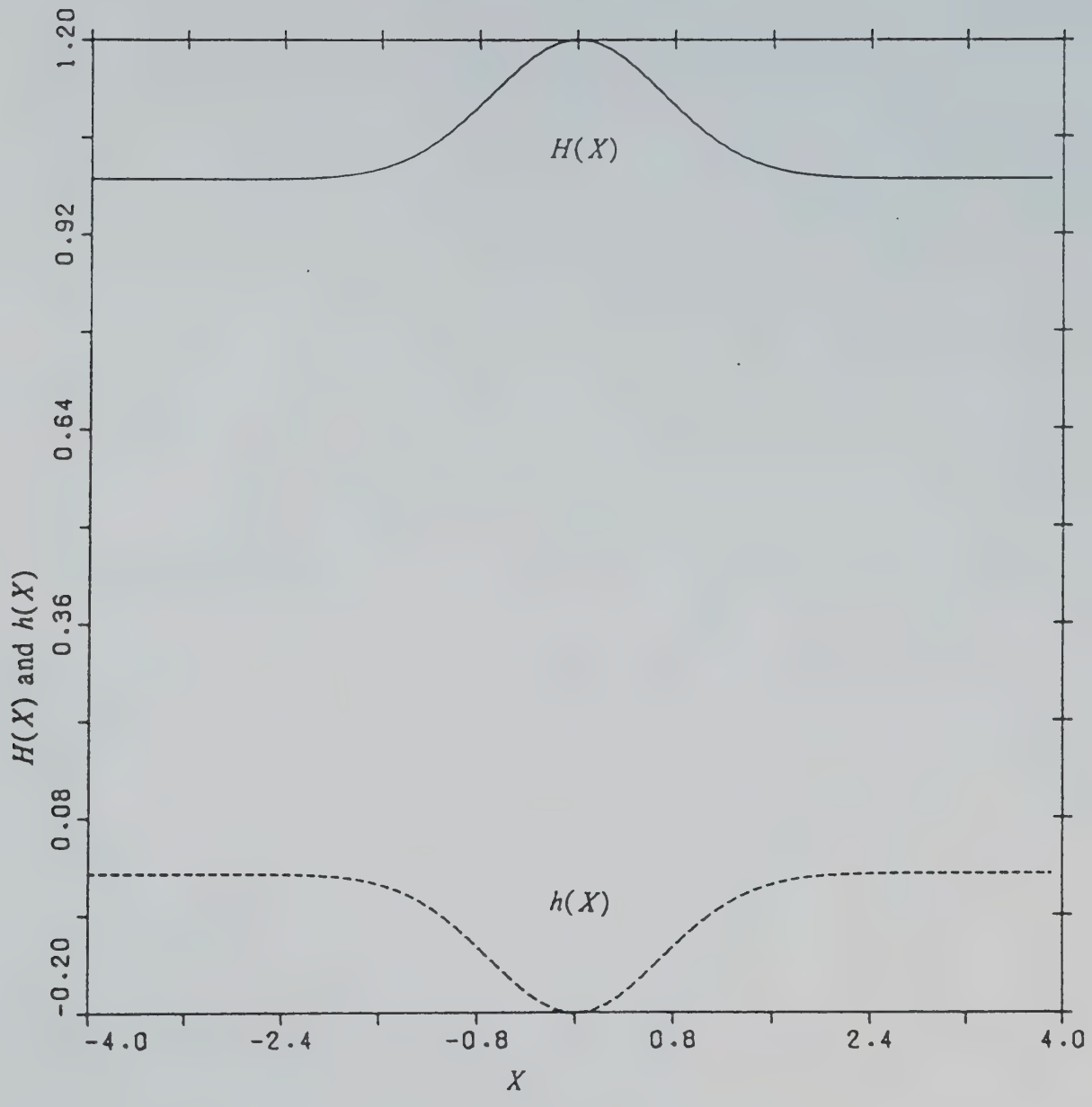

Fig.12. Depth of fluid $H(X)$ and valley topography $h(X)$ given by the equations (6.1a) and (6.1b) respectively with $\mu = -0.2$.

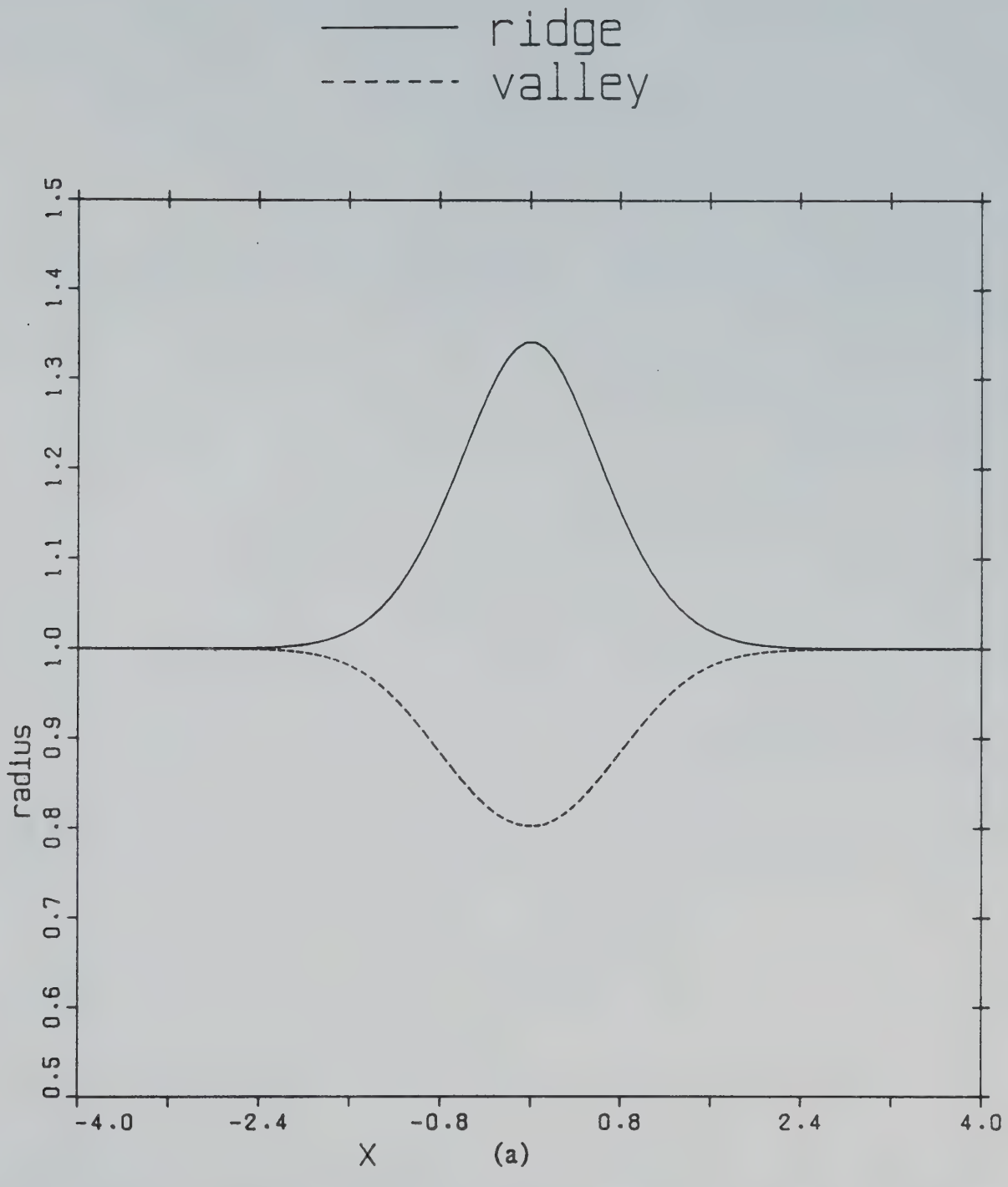

Fig.13. Comparison between the exact nonlinear "steady-state" topographically-modulated (a) modon radius (b) modon speed (c) modon wavenumber when the eastward-travelling modon propagates towards a ridge and a valley given by the equation (6.1b) with $\mu=0.2$ and -0.2, respectively and $\tau=0$.

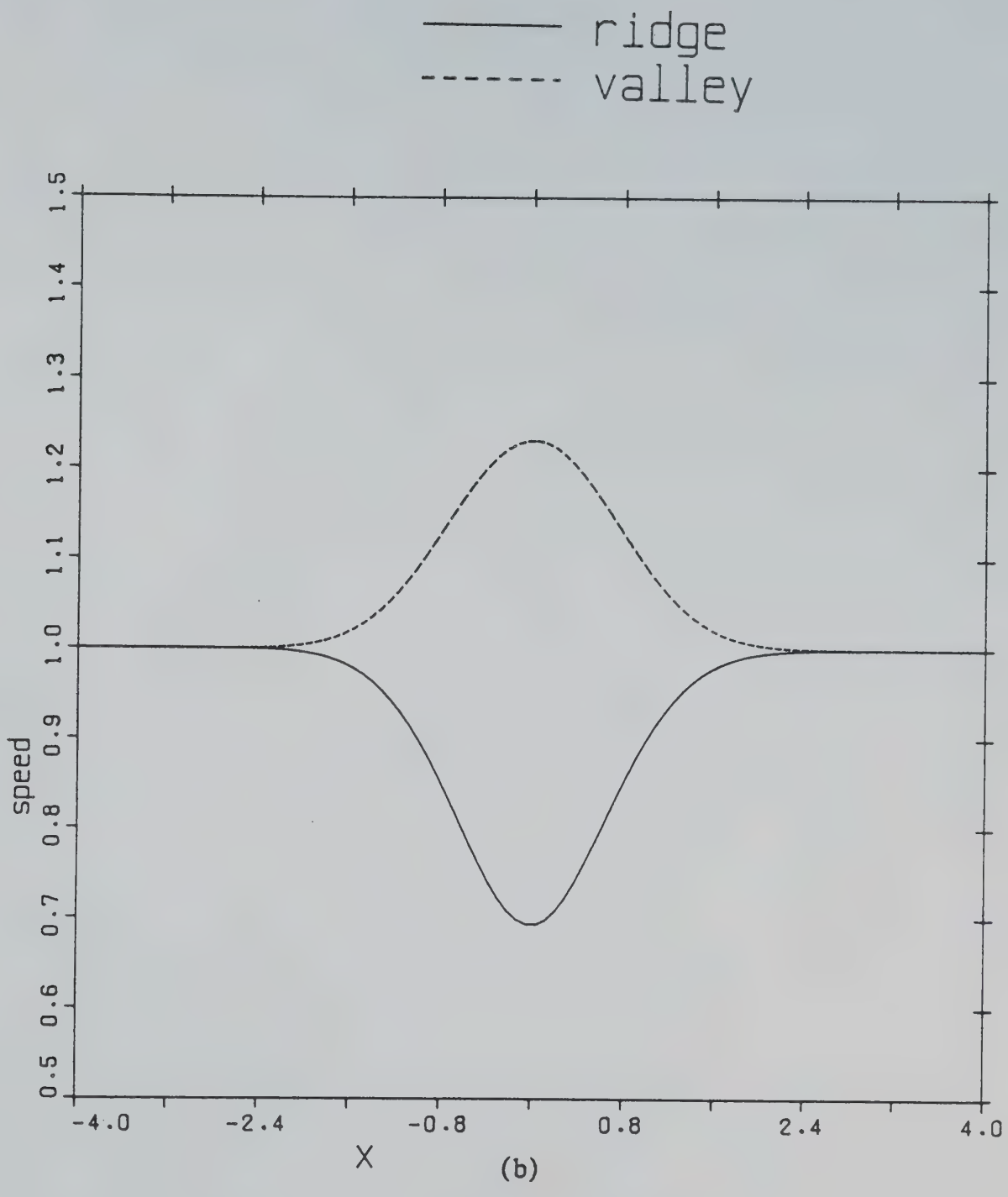
ridge
valley
speed
1.5
1.4
1.3
1.2
1.1
1.0
0.9
0.8
0.7
0.6
0.5
-4.0
-2.4
-0.8
0.8
2.4
4.0
X

(b)

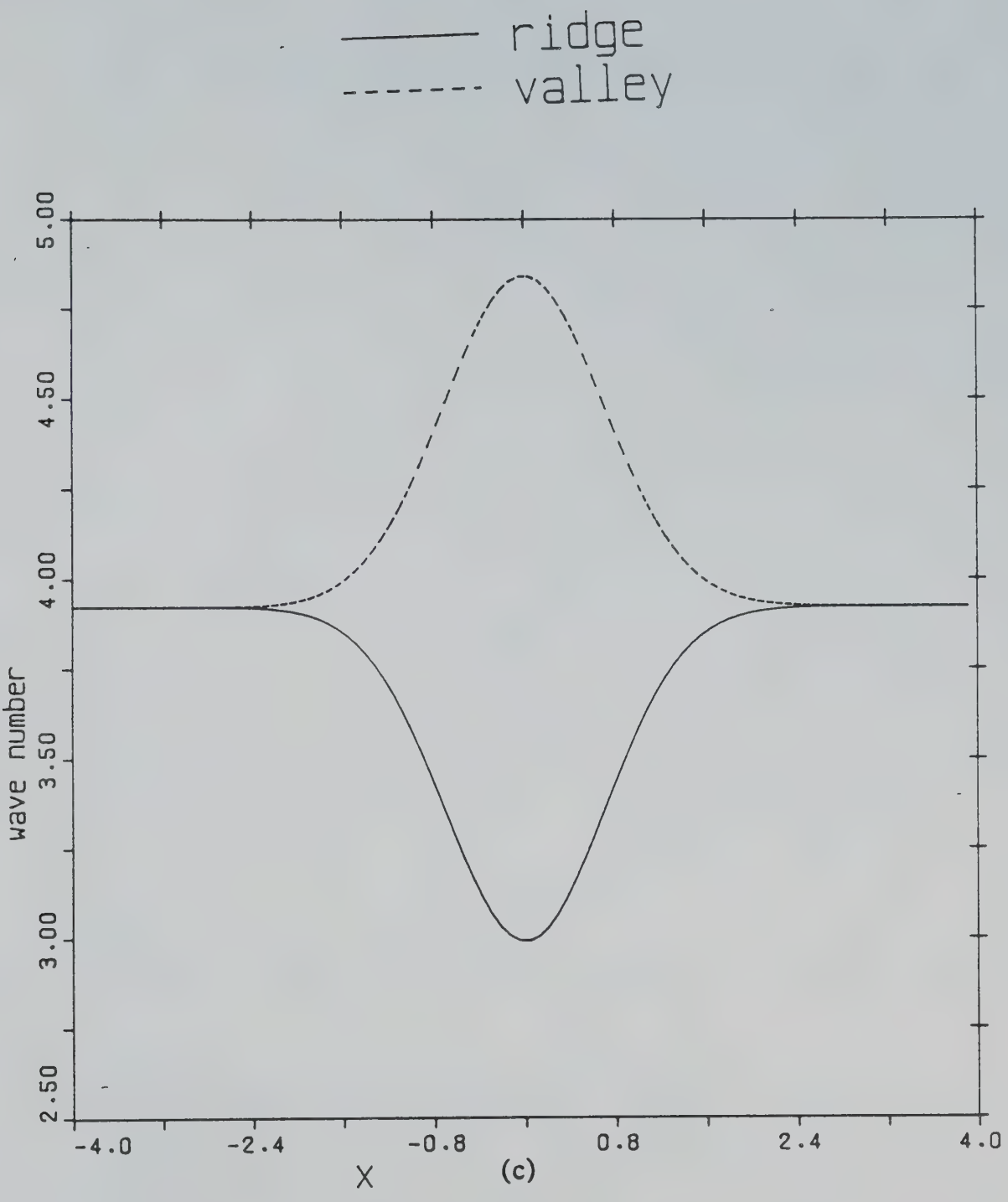
ridge
valley
wave number
5.00
4.50
4.00
3.50
3.00
2.50
-4.0
-2.4
-0.8
0.8
2.4
4.0
X
(c)

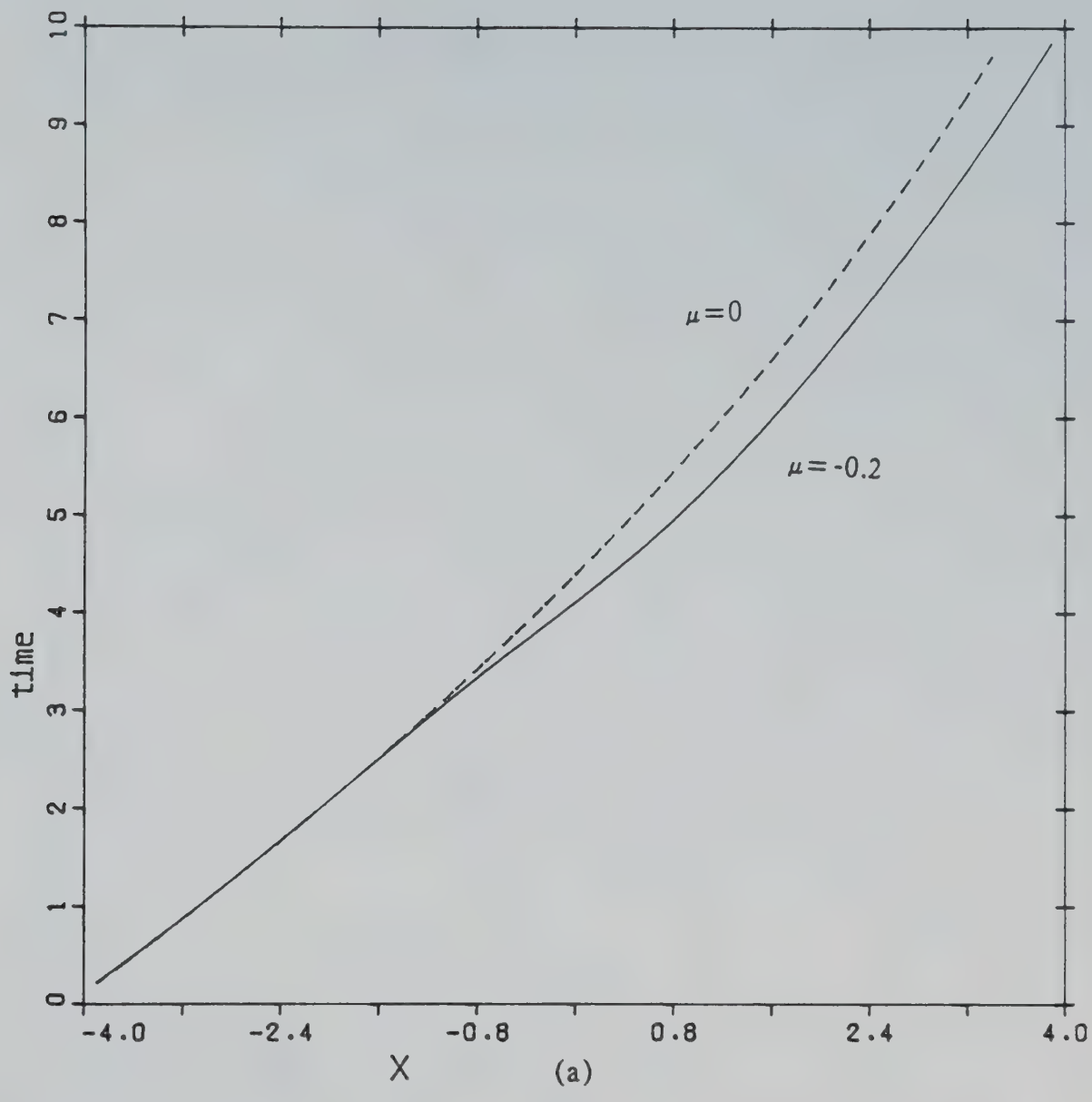

Fig.14.Comparison of the modon response between the effects of the friction alone ($\mu=0$) and the combined effects of friction and topography ($\mu=-0.2$). Plots of the exact nonlinear "steady-state" frictionally- and topographically-modulated (a) the arrival time (b) the modon speed (c) the modon radius (d) the modon wavenumber (e) the normalized average energy (f) the enstrophy (g) the maximum vorticity (h) streamfunction when the eastward-travelling modon propagates towards a valley given by the equation (6.1b) with $\mu=-0.2$ and $\tau=0.05$.

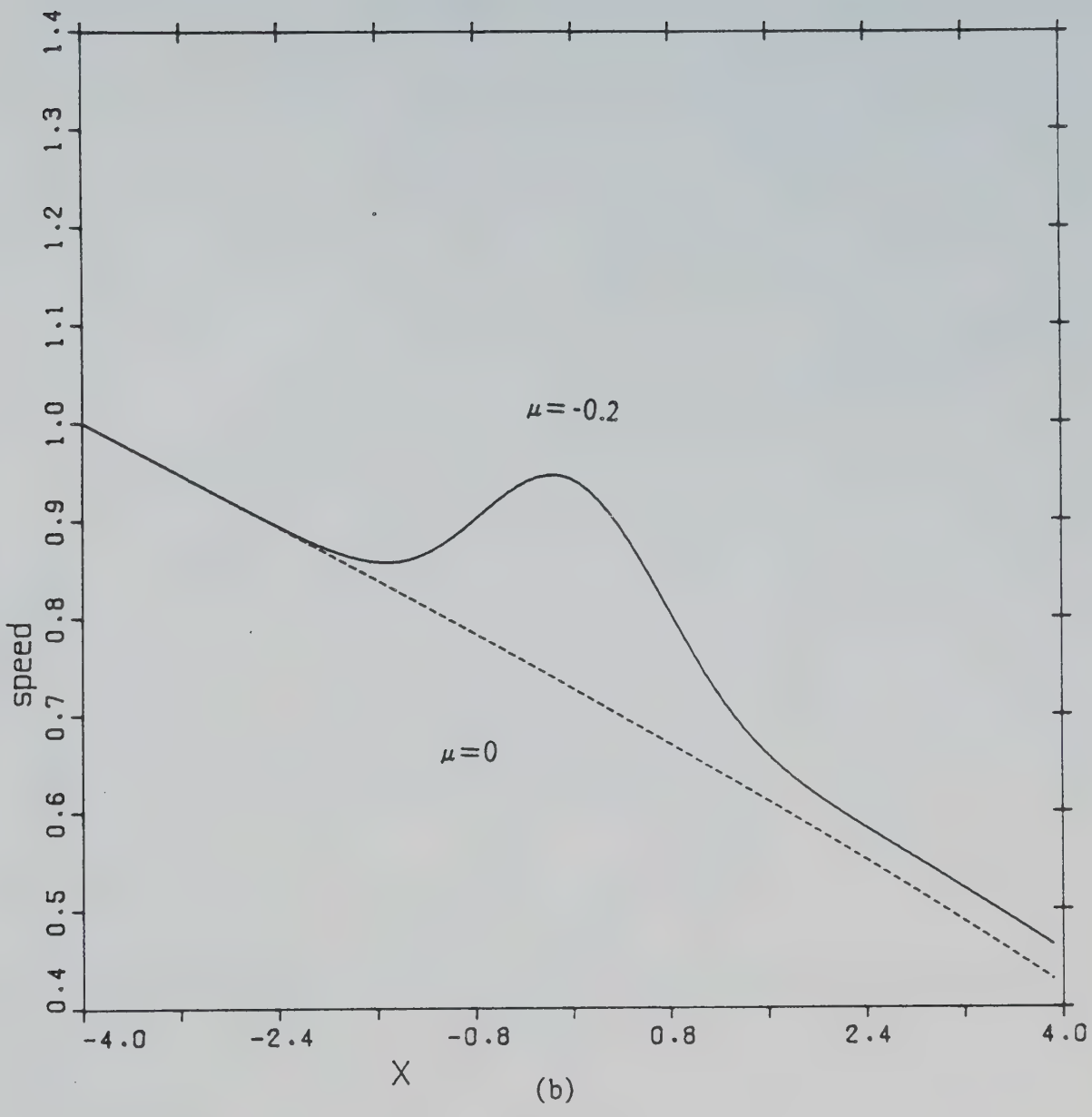

speed vs. X valley

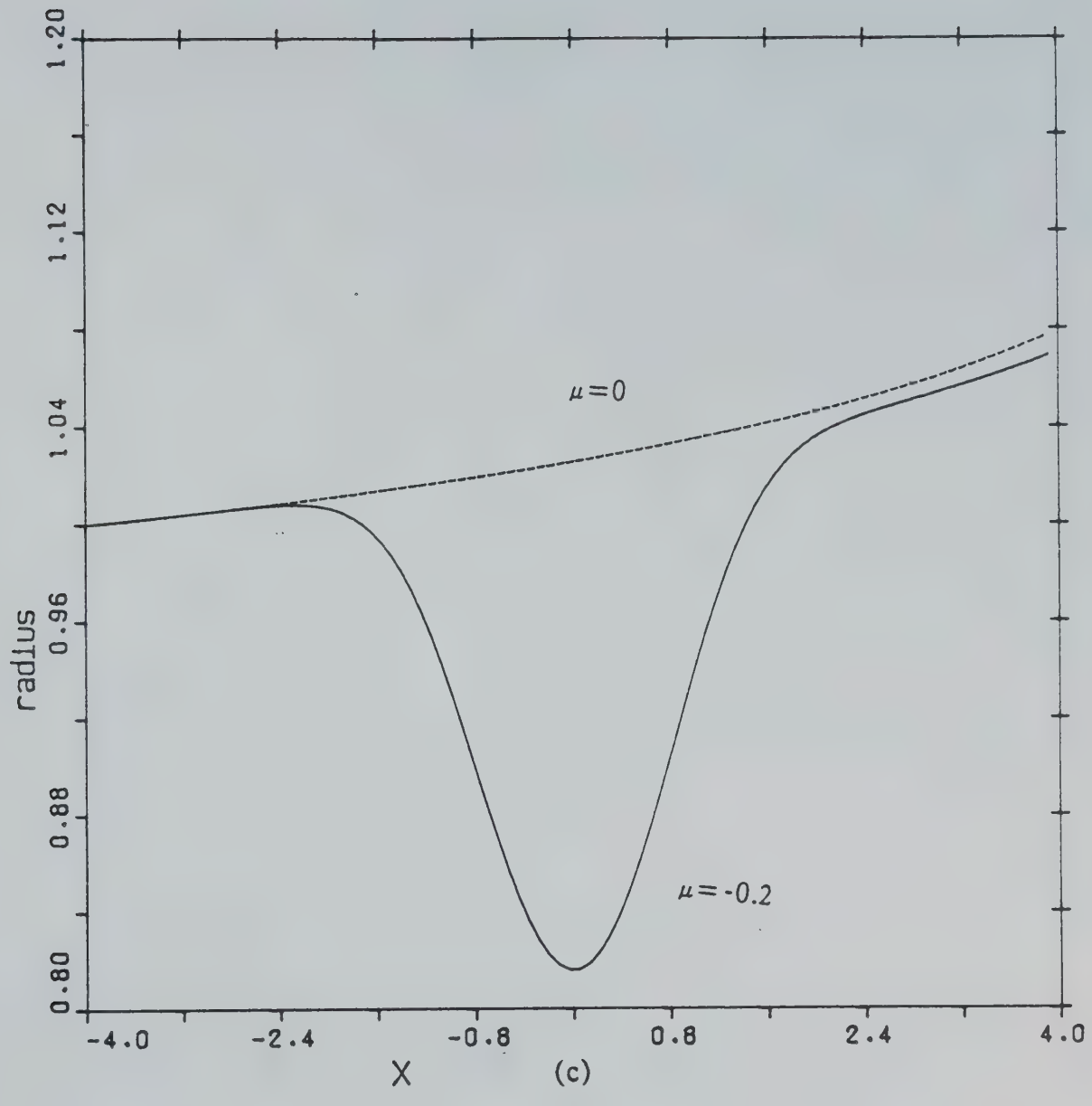

radius vs. X valley

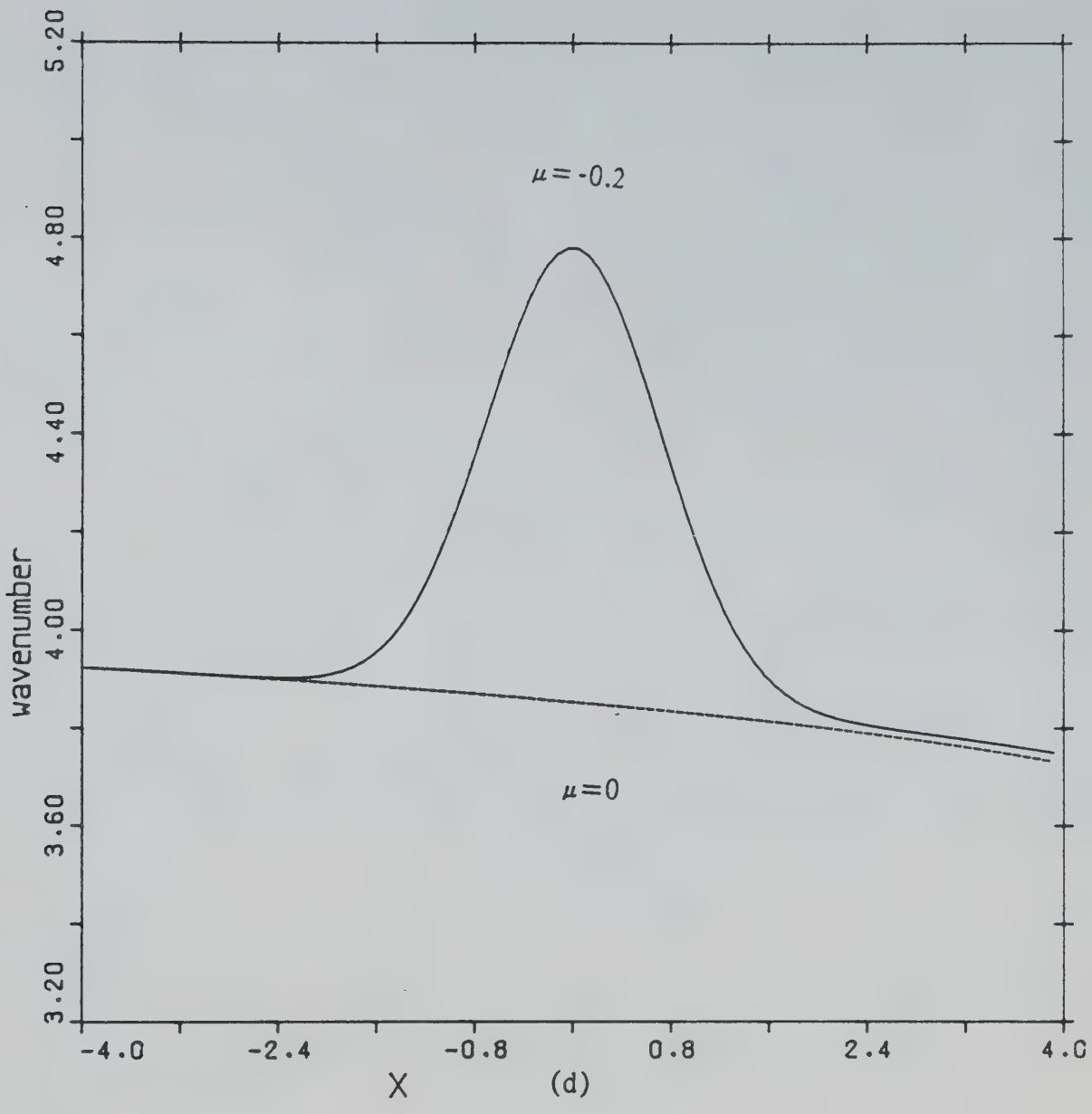

wavenumber vs. X valley

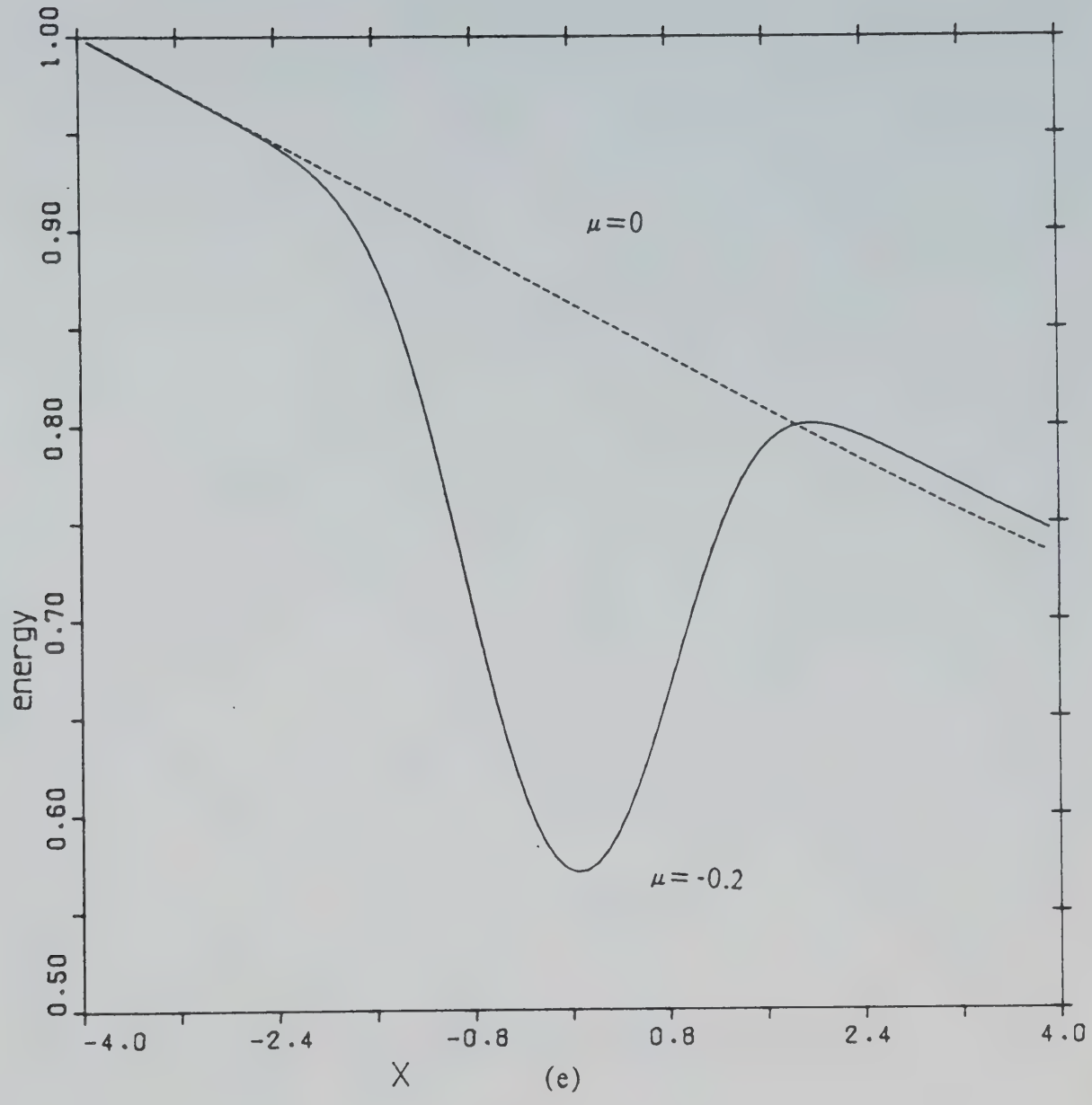

energy vs. X valley

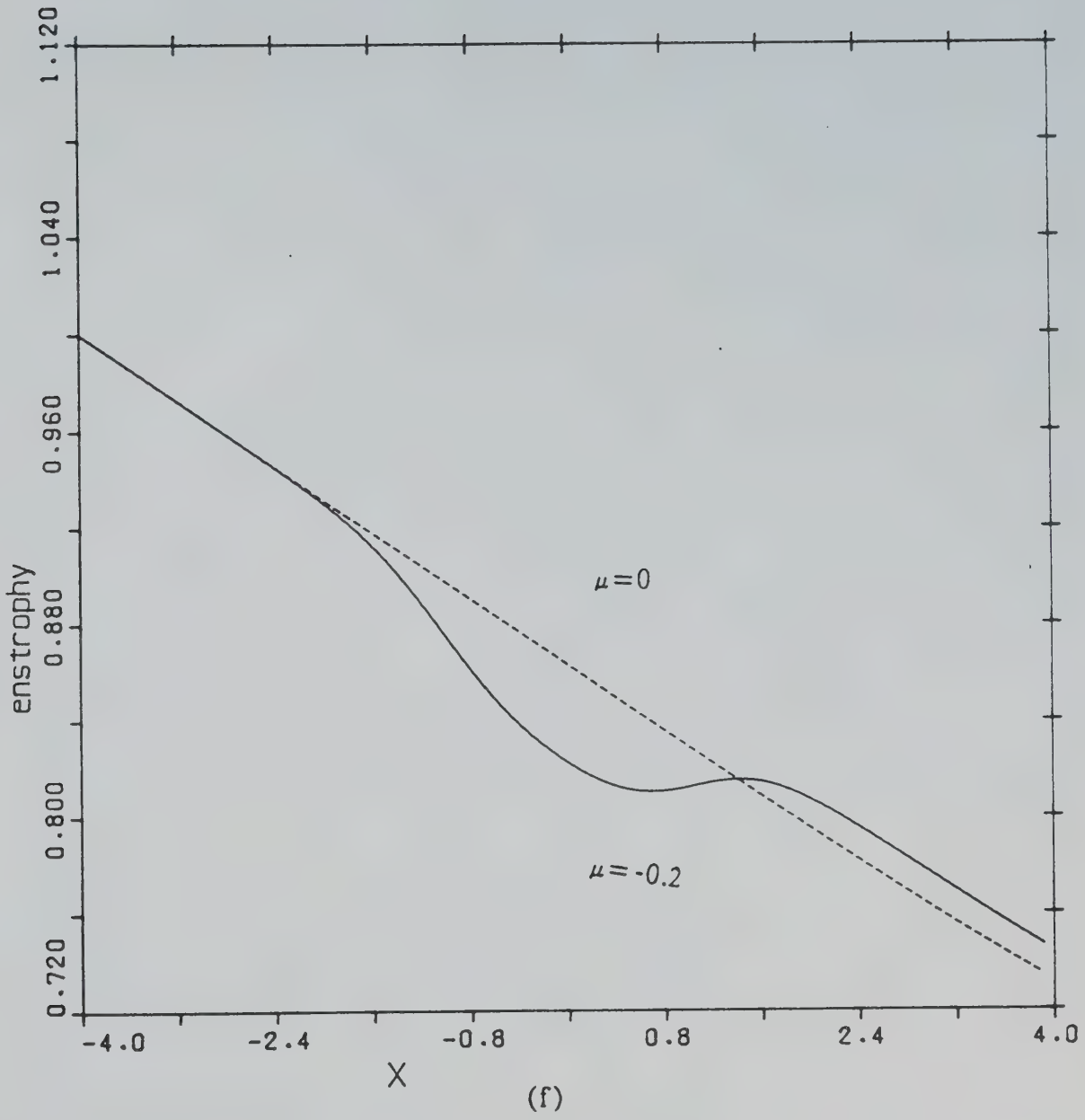

enstrophy vs. X valley

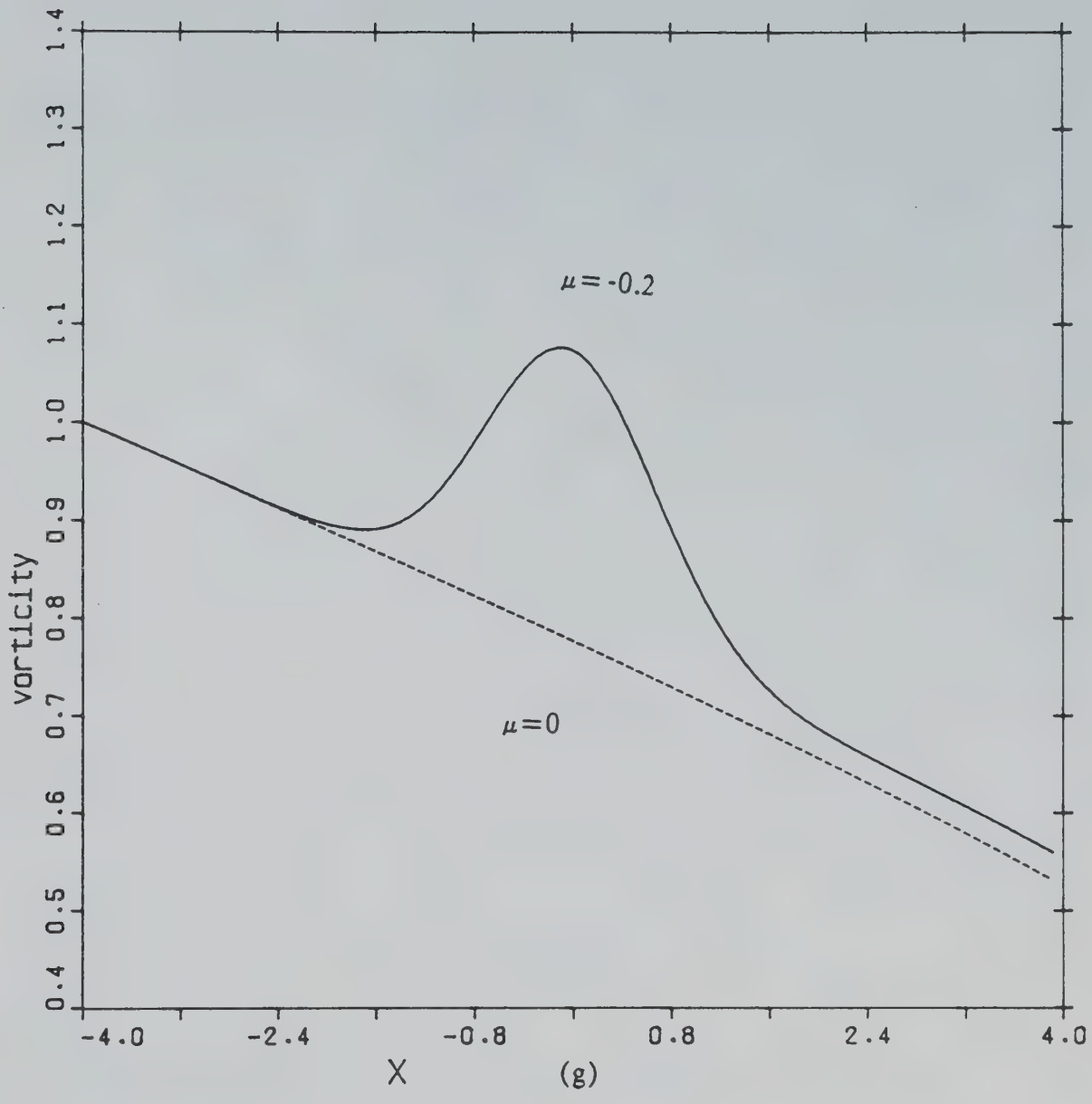

vorticity vs. X valley

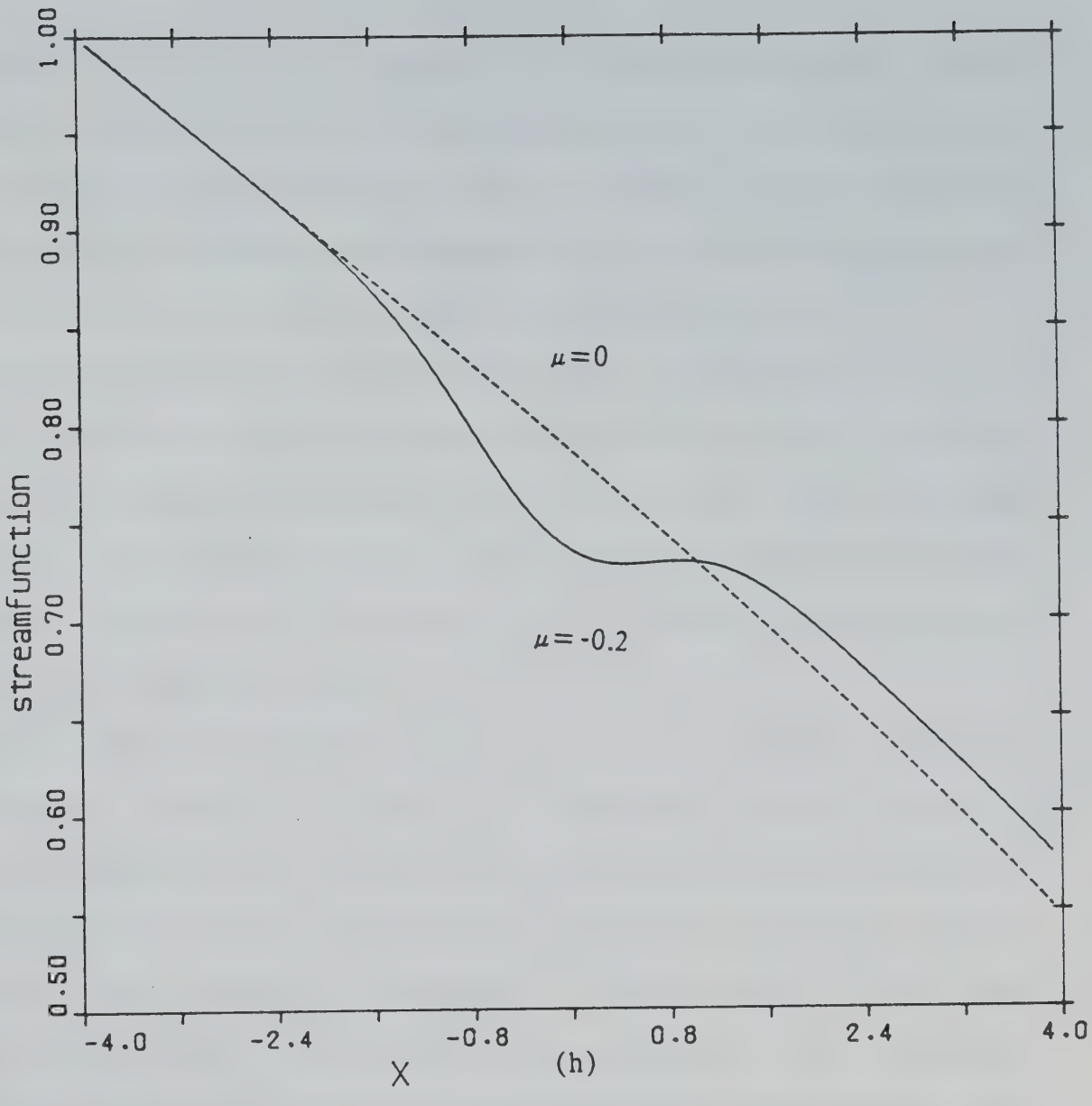

streamfunction vs. X valley

6.3 The Shelf topography

The final example of topography is a shelf (Fig.15) which takes the form of

$$h(X) = \frac{1}{2}(1 + \tanh(X)), \tag{6.6}$$

where $\mu = 0.2$ in (6.1a) is chosen for comparison with the previous topographies. The results of the inviscid modon-shelf interaction are essentially the same as those for the ridge. In brief, the steady-state modon parameters are: the radius increases, the speed decreases and the modon wavenumber decreases, and the normalized average energy and enstrophy increase as the eastward travelling modon enters the shallow region of the shelf (Fig.16).

For the viscous shelf-modon interaction, the range of τ in which equations (5.3) and (5.1d) can be simultaneously satisfied is between 0 and 0.02 with the μ=0.1, a range much lower than the ridge and valley topographies. μ=0.2 is not considered because the equation (5.3) and (5.1d) cannot be satisfied. This lower value of τ is chosen because the modon speed decreases faster to zero in the shelf-topography than with the previous topographies. For an illustration, τ =0.01 is arbitrarily chosen.

Fig.17(e) shows that the energy decreases on the level ground of the bottom of the shelf and starts to increase as the depth of the atmosphere decreases. However, the acceleration is reduced by friction. Once on the level ground associated with the top of the shelf, the increased modon speed starts to slow down due to the action of frictional dissipation. The other figures can be explained in a similar manner, i.e., the speed, wavenumber, energy, enstrophy, vorticity extrema and streamfunction extrema decrease while only the radius increases (see Fig.17(b)(c)(d)(e)(f)(g)(h)). Fig.17(a) shows that the arrival time with the shelf plus friction is slower than with friction alone because the modon speed with the shelf plus friction decreases faster than that of friction alone.

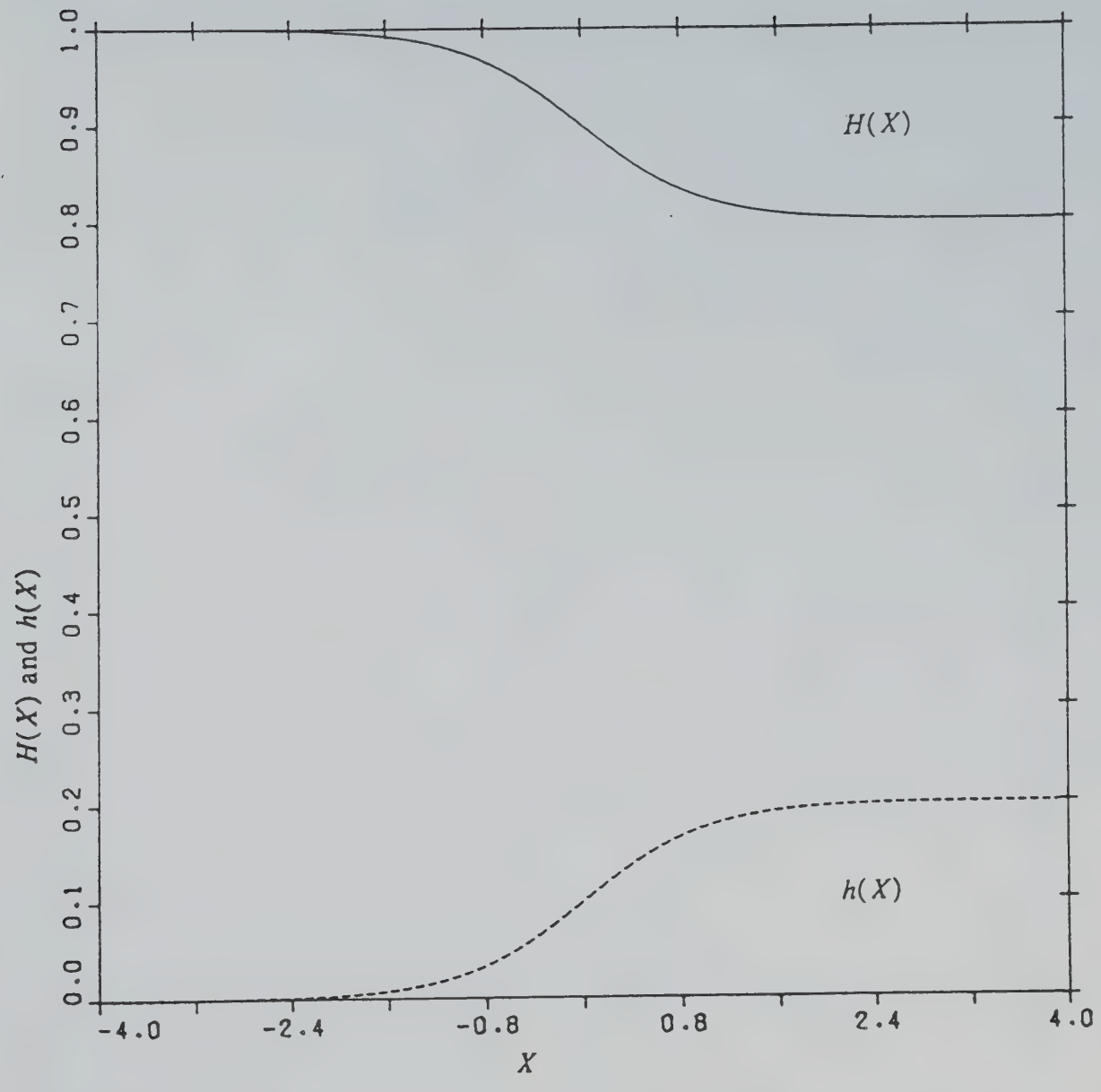

Fig.15. Depth of fluid $H(X)$ and shelf topography $h(X)$ given by the equations (6.1a) and (6.6) respectively with $\mu=0.2$.

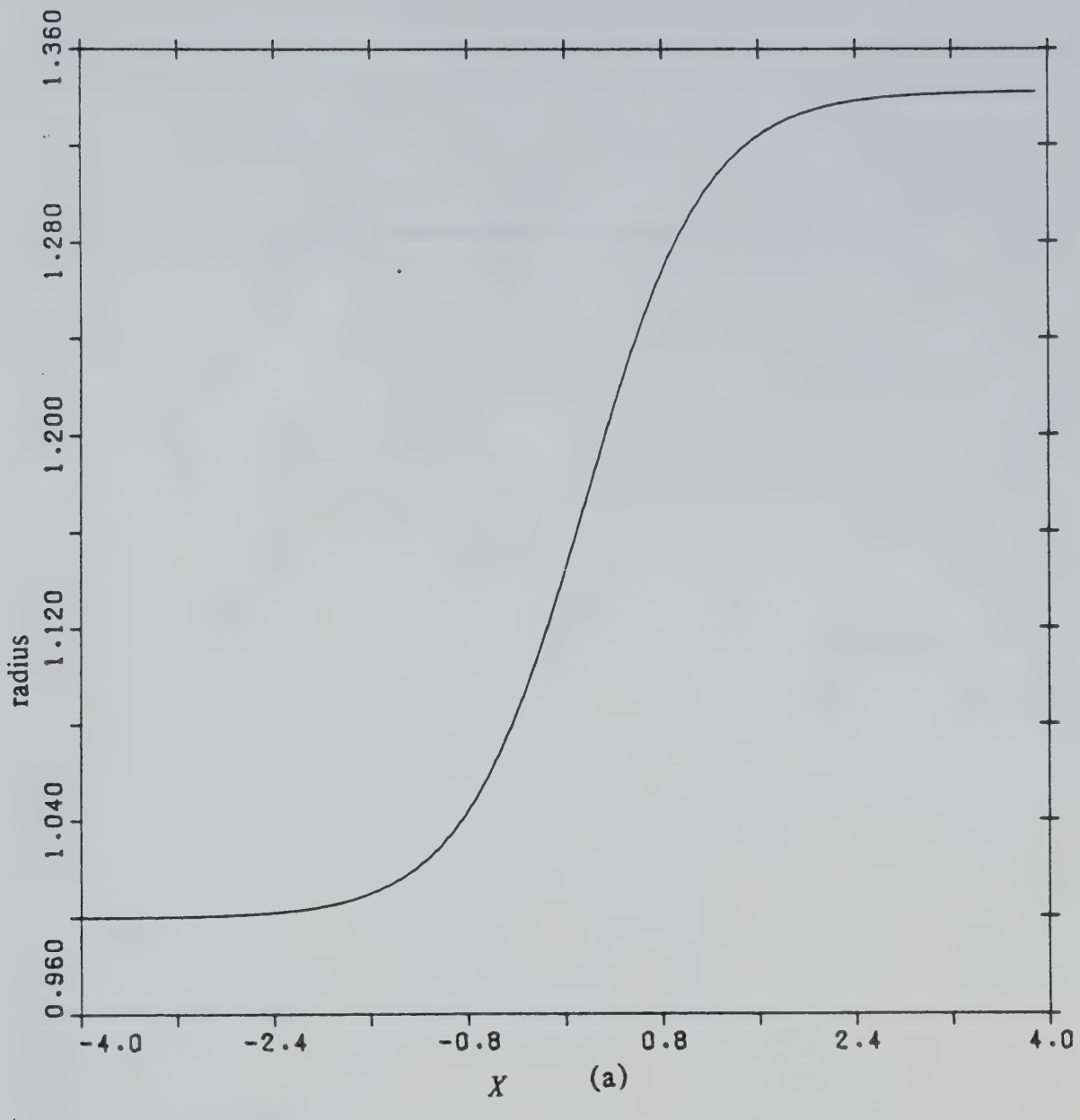

Fig.16. Plots of the exact nonlinear "steady-state" topographically-modulated (a) modon radius (b) modon speed (c) modon wavenumber (d) normalized average energy and enstrophy when the eastward-travelling modon propagates towards a shelf given by the equation (6.6) with $\mu=0.2$ and $\tau=0$.

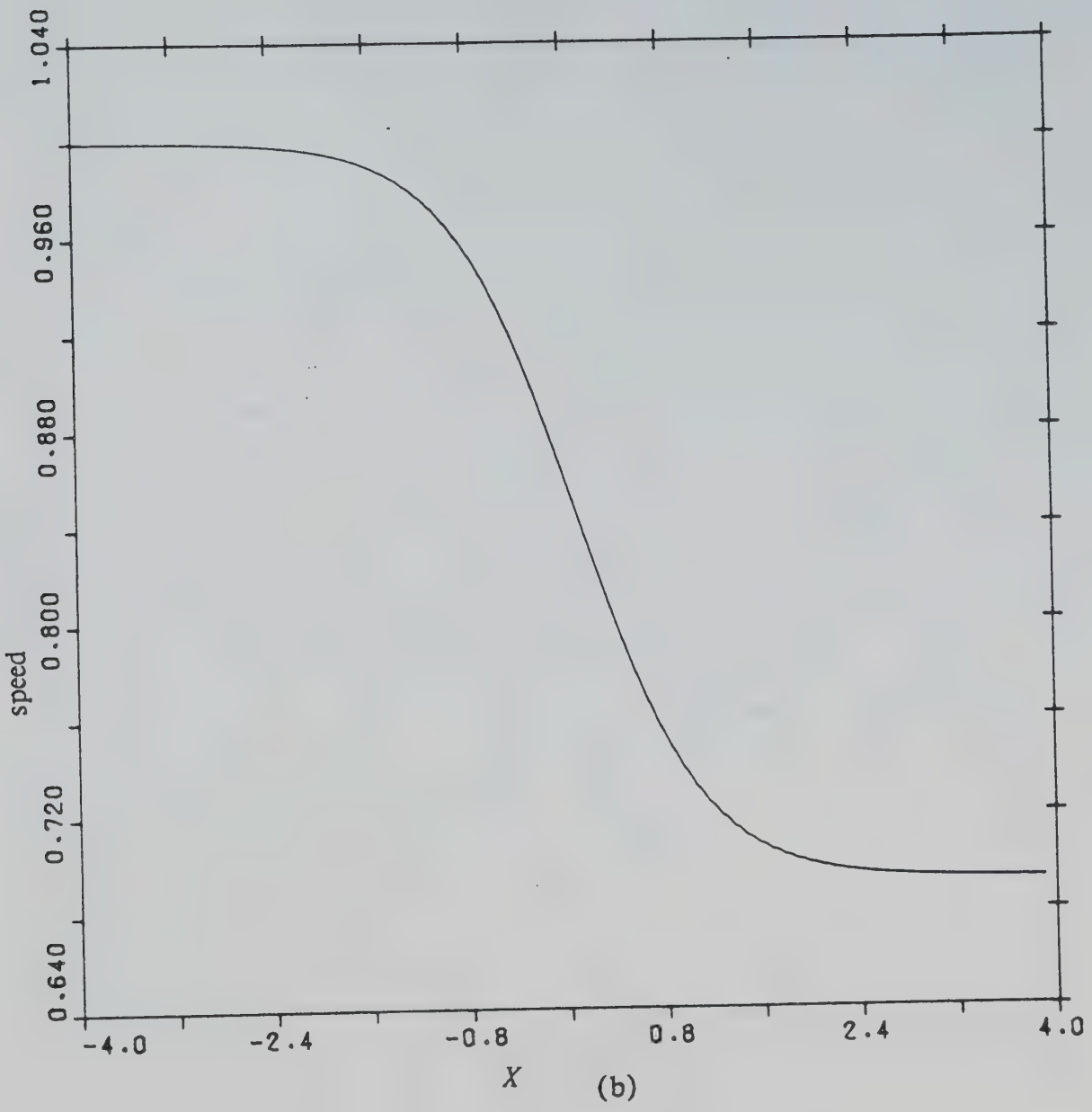

(b)

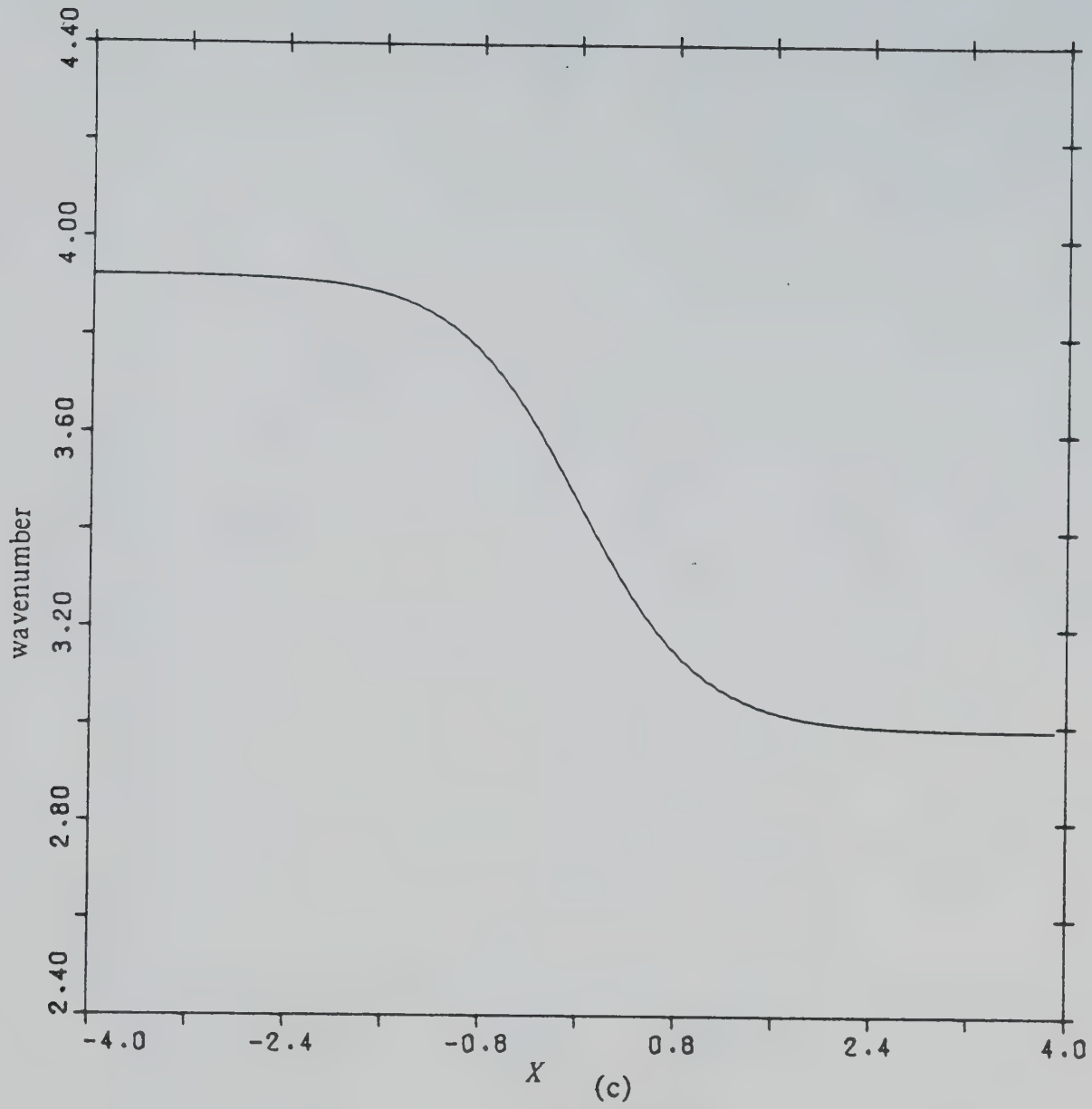

(c)

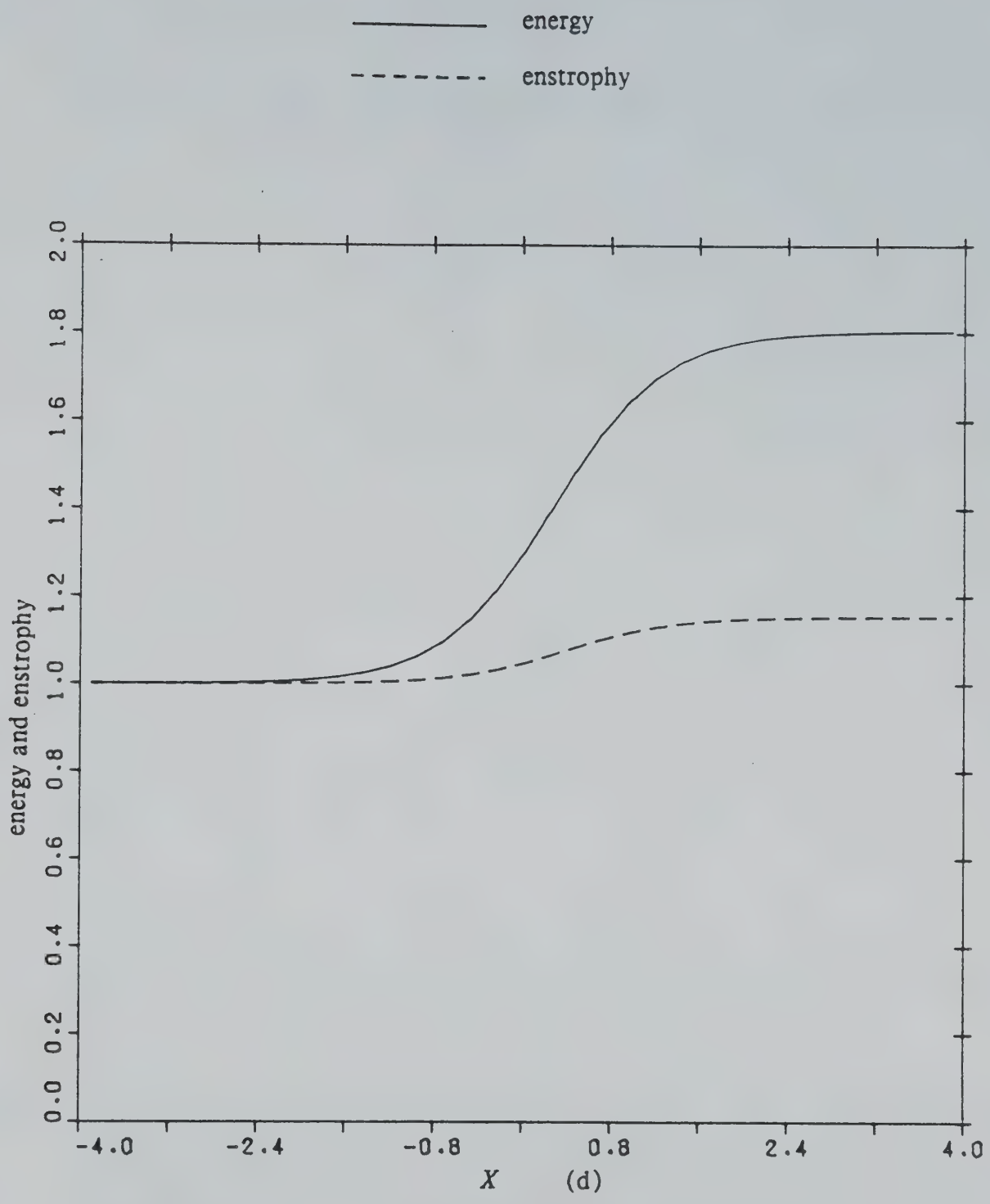
energy
enstrophy
energy and enstrophy
0.0
0.2
0.4
0.6
0.8
1.0
1.2
1.4
1.6
1.8
2.0
-4.0
-2.4
-0.8
0.8
2.4
4.0
X (d)

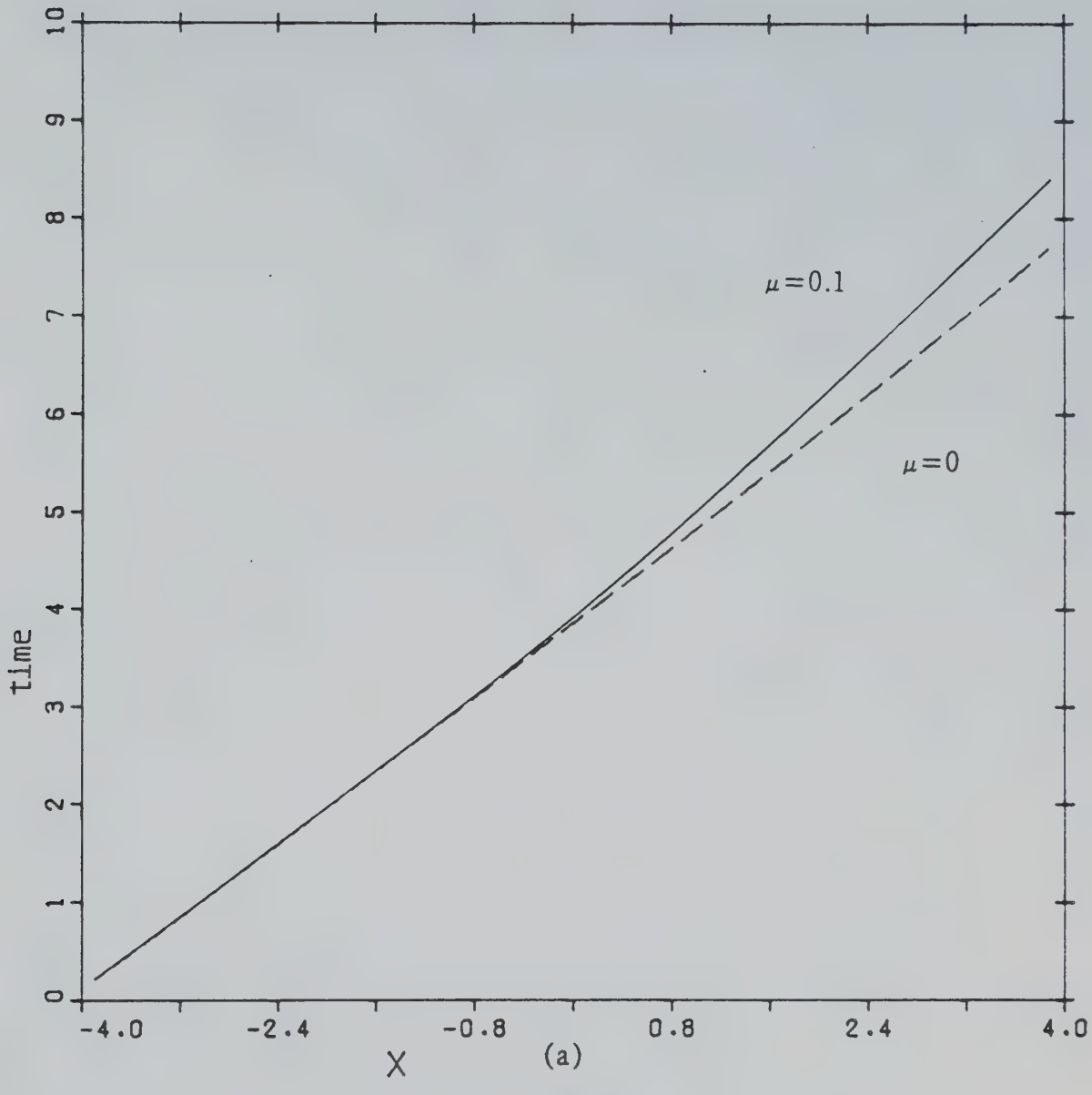

Fig.17. Comparison of the modon response between the effects of the friction alone ($\mu=0$) and the combined effects of friction and topography ($\mu=0.1$). Plots of the exact nonlinear "steady-state" frictionally- and topographically-modulated (a) the arrival time (b) the modon speed (c) the modon radius (d) the modon wavenumber (e) the normalized average energy (f) the enstrophy (g) the maximum vorticity (h) streamfunction when the eastward-travelling modon propagates towards a shelf given by the equation (6.6) with $\mu=0.1$ and $\tau=0.01$.

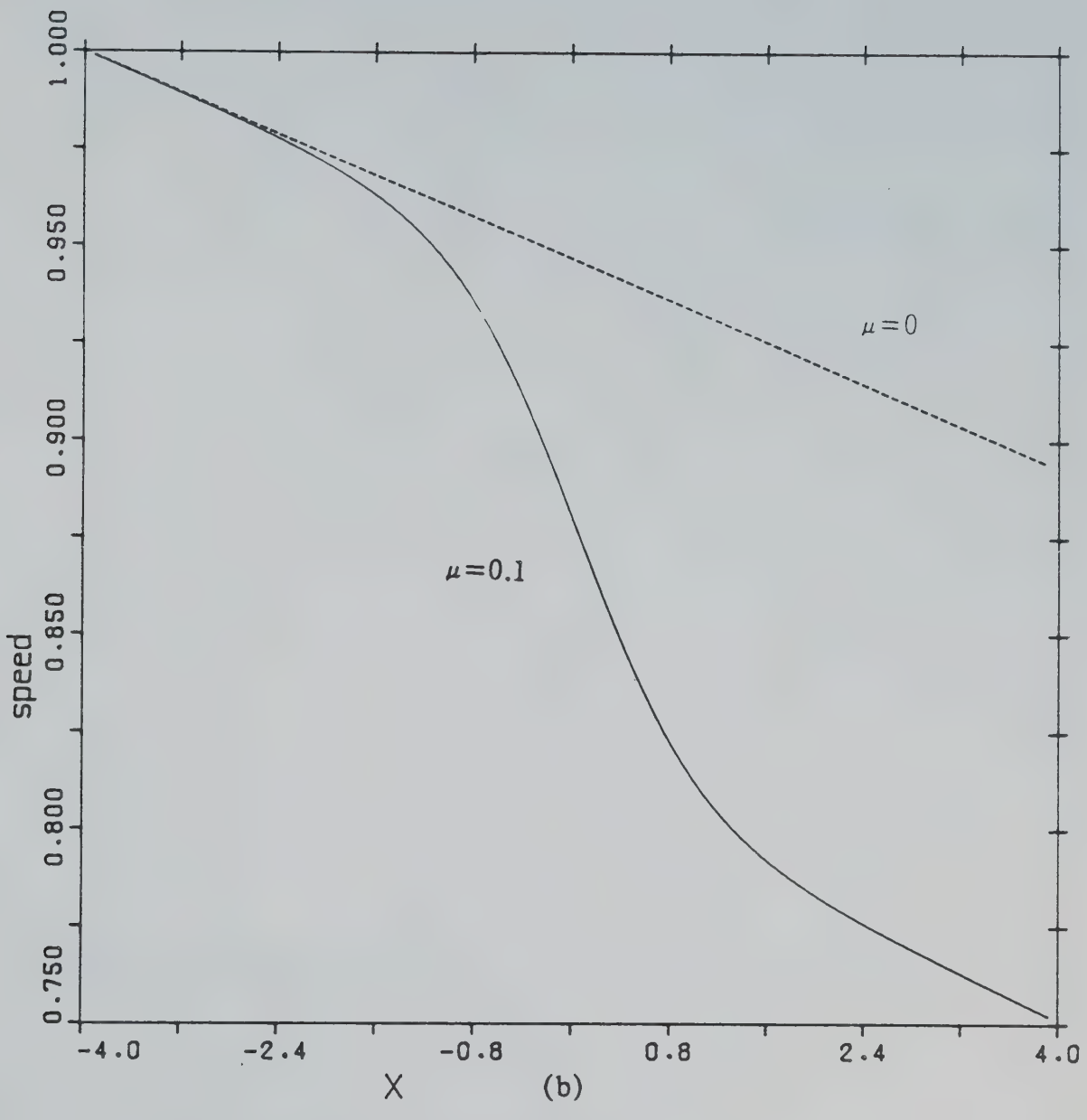

speed vs. X shelf

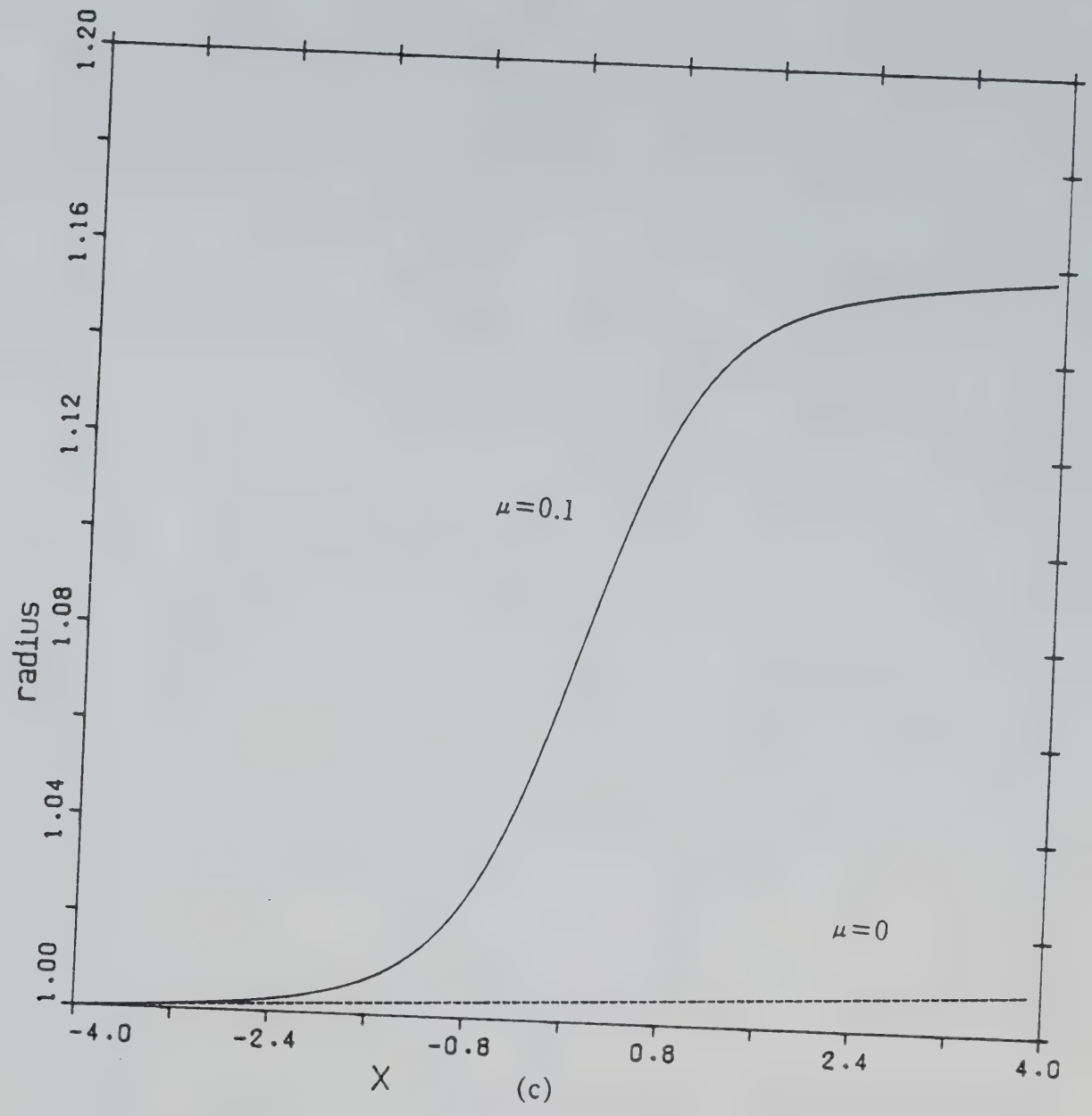

radius vs. X shelf

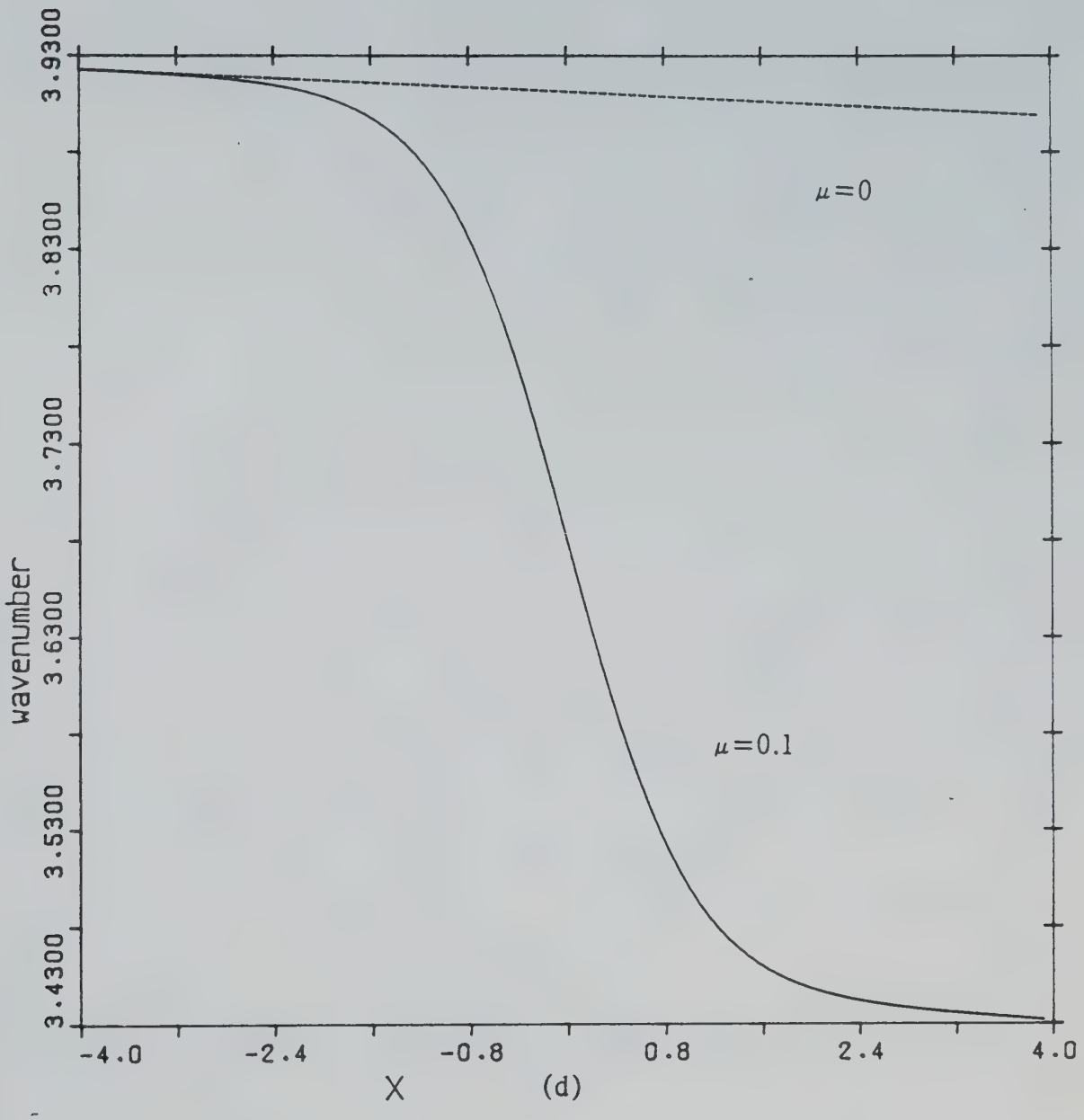

wavenumber vs. X shelf

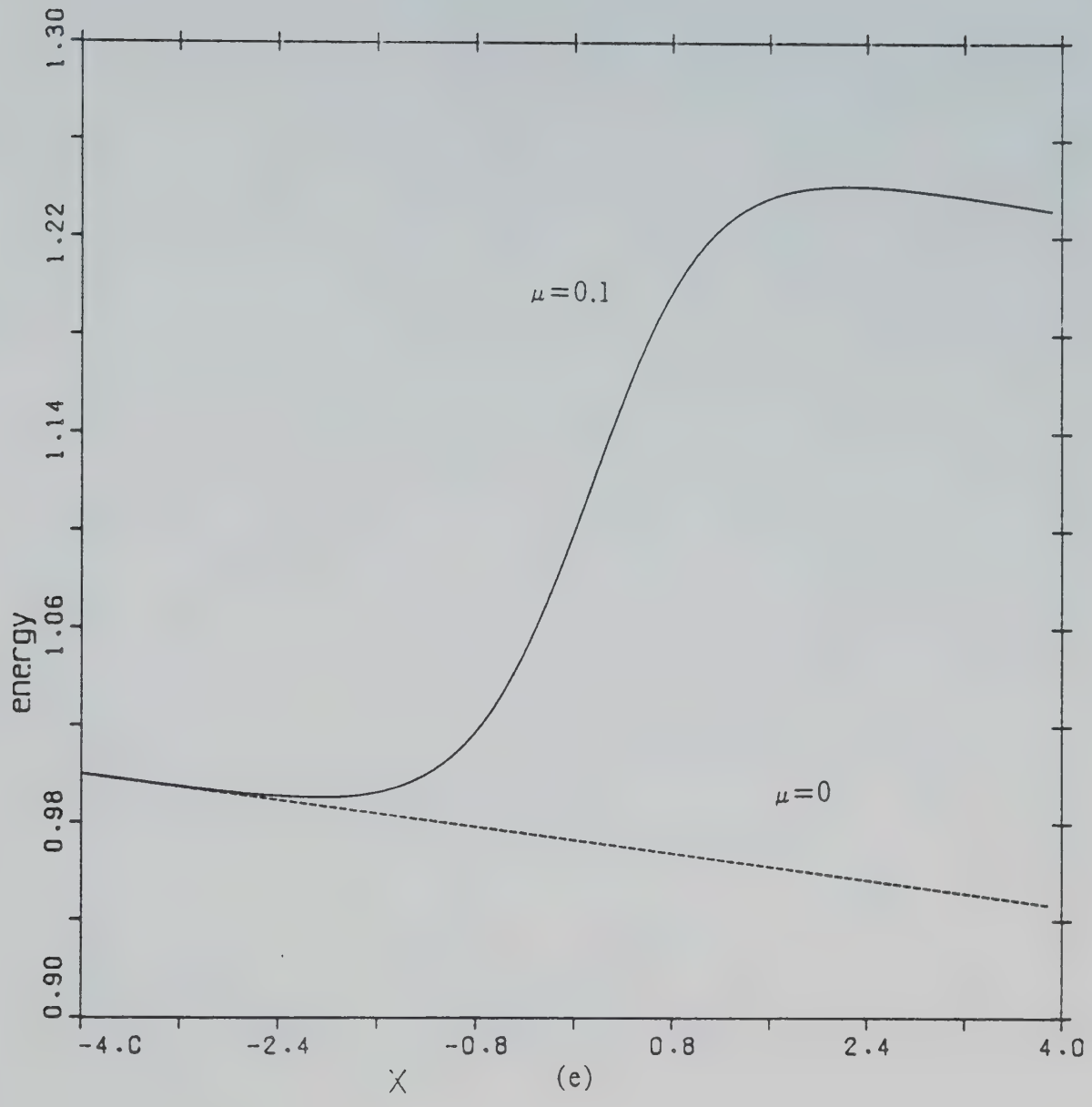

energy vs. X shelf

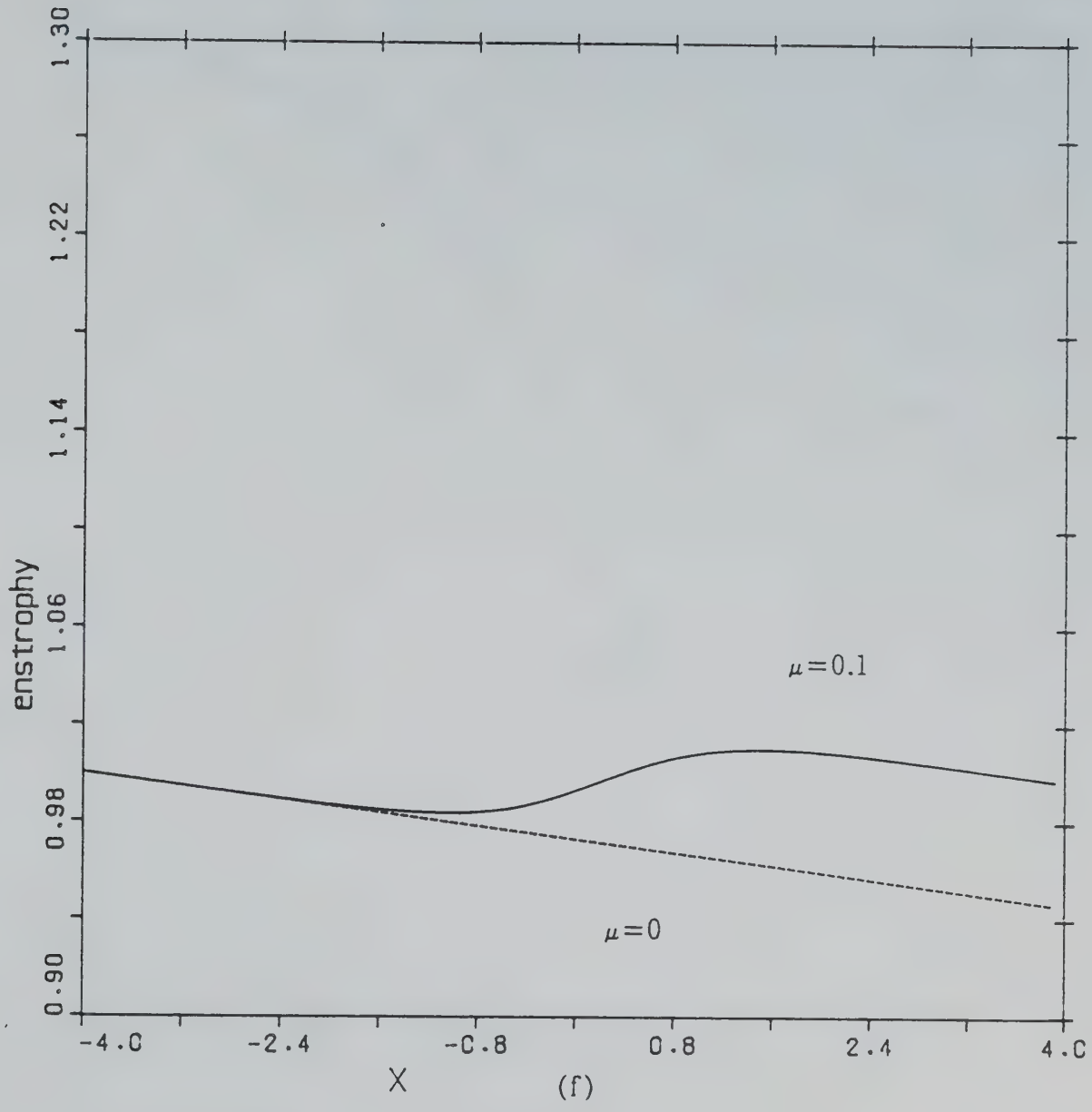

enstrophy vs. X shelf

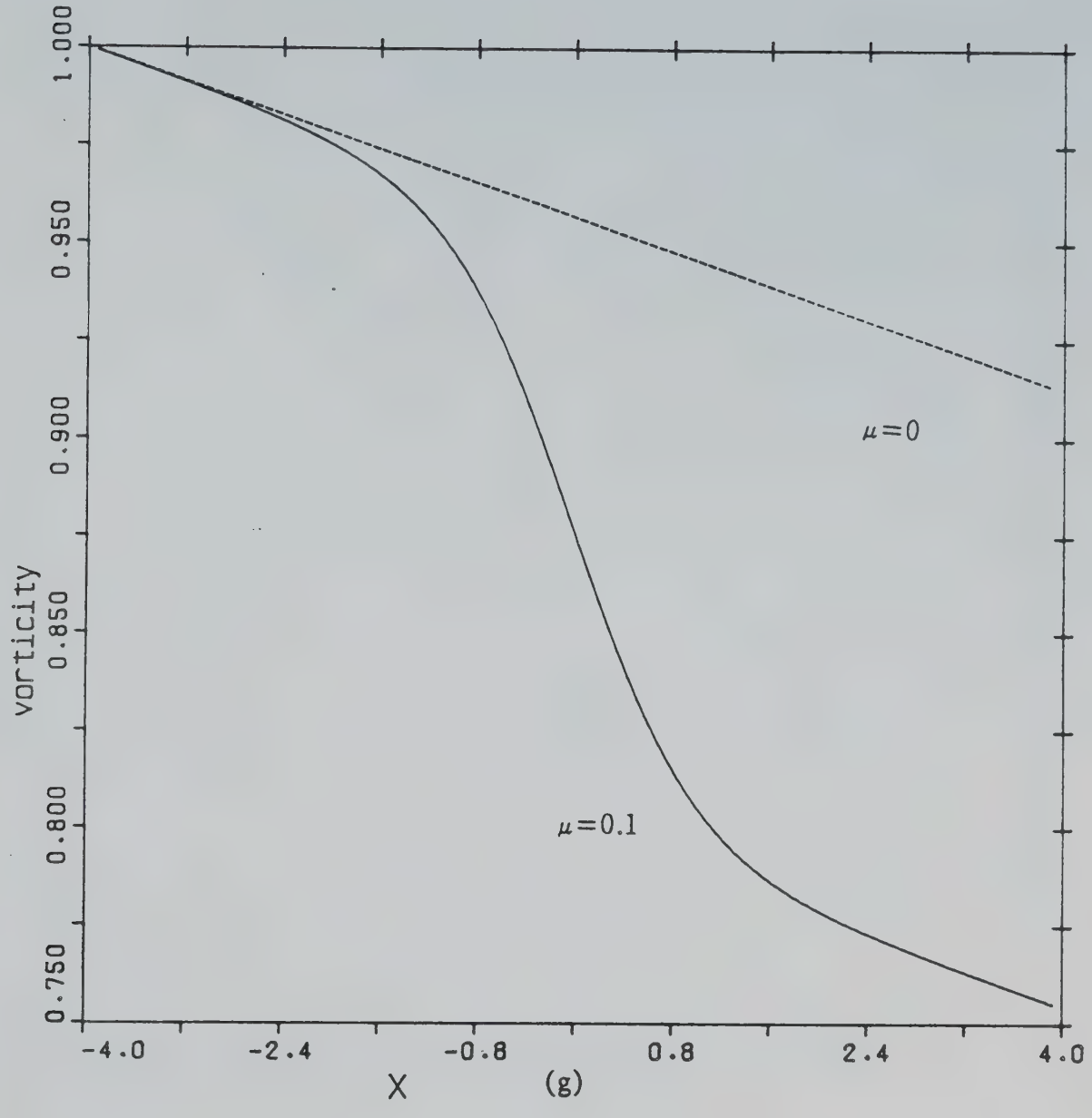

vorticity vs. X shelf

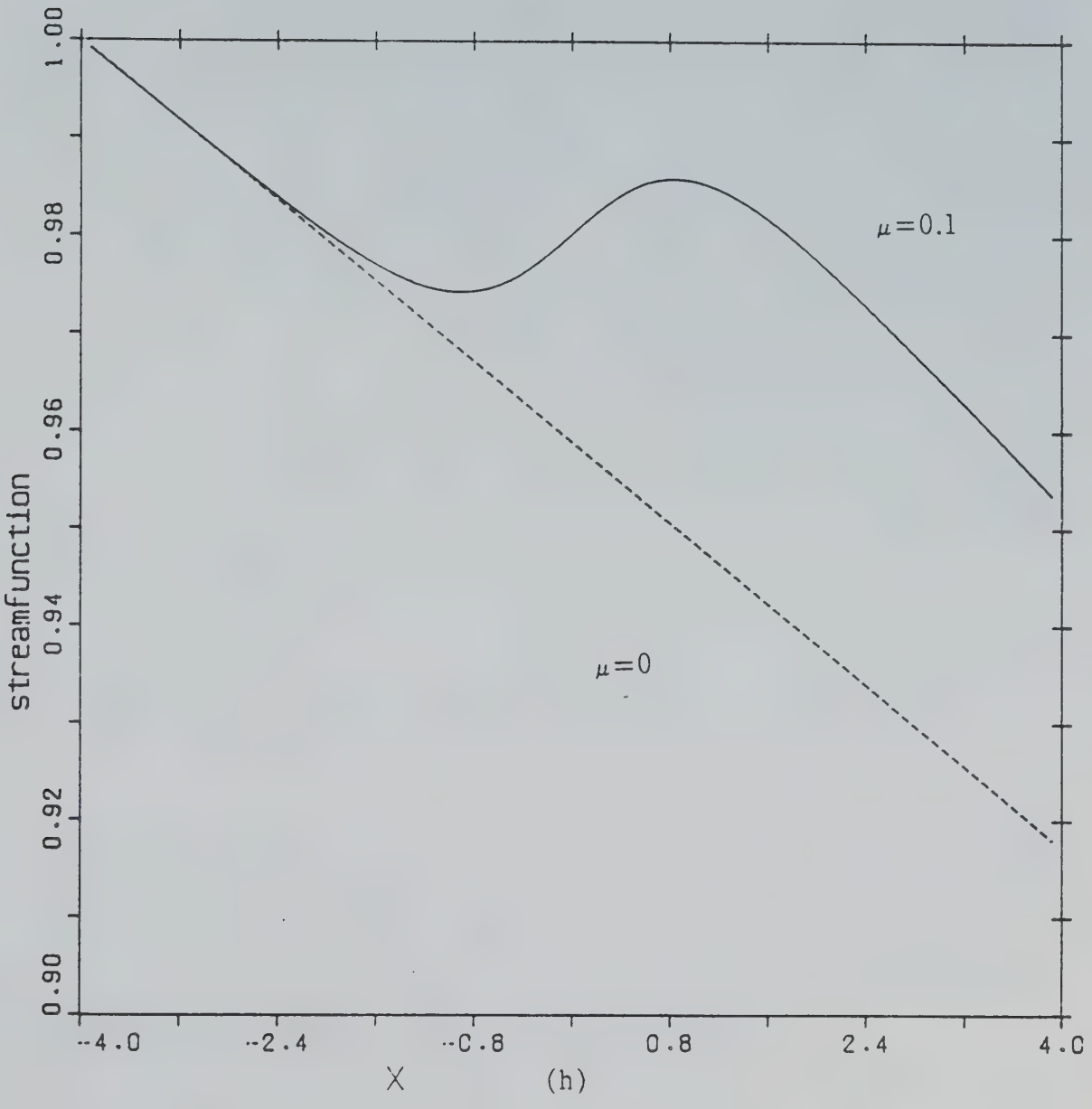

streamfunction vs. X shelf

7. Conclusions

We have derived an analytical asymptotic theory which describes the propagation of the modon under the influence of the combined effects of weak frictional dissipation and finite-amplitude but slowly-varying topography.

We began by formulating the problem in terms of the shallow-water potential vorticity equation which included orographic terms and a Rayleigh dissipation term. In order to highlight the essential features of the interaction, we restricted the modon to propagate zonally in a viscid, homogeneous, hydrostatic and incompressible atmosphere. Assuming that the horizontal length scale associated with the topography was much larger than the undeformed modon radius and the nondimensional dissipation parameter was small, a multiple-scale perturbation theory was developed to describe the modulated modon. To determine the evolution of the modon parameters (i.e., the modon radius, the translation speed and the modon wavenumber), we followed Swaters(1986b) and derived transport equations based on globally-averaged energy and enstrophy equations.

For the "steady-state" modon-topographic interaction including friction, we numerically solved the transport equations. Our principal conclusions are as follows:

1. For the inviscid topographic interaction, as the modon propagates towards a shallow (deep) region, the modon radius increases (decreases), the translation speed and the modon wavenumber decrease (increase), maximum vorticity weakens (strengthens) and the normalized average energy and enstrophy increase (decrease).
2. The absolute extremum values of the modon parameters achieved are higher in the ridge topography than in the valley topography because the absolute value of the term H_X/H in equations (5.5) is higher in the ridge than that in the valley, or equivalently because H_X/H is not anti-symmetric in the topographic amplitude parameter μ.
3. For the viscous topographic interaction, the modon radius increases while the modon speed, modon wavenumber, energy, enstrophy, maximum vorticity and streamfunction decrease. When a ridge or a shelf is present, the topography acts to accelerate the

dissipation process. If a valley is present, the effects of frictional dissipation are reduced. With the same topographic height parameter (i.e., μ), the modon speed decelerates faster in the shelf than in the ridge. Therefore, the rate of dissipation in the shelf is faster than that in the ridge.

There are several areas in which the theory developed in this thesis can be improved. First, it turns out that equations (3.5), (4.14) and (4.15) can be combined and rewritten as nonlinear hyperbolic system of equations (A.6) (see the Appendix for the derivation). A complete solution of this matrix system (A.6) will provide a complete description of the modon-topographic interaction including frictional effects. These equations will probably need to be solved numerically because an analytical approach is likely very difficult. In fact, we have used the method of *acceleration front analysis* (see, for example, Varley and Dunwoody,1965; Varley and Cumberbatch,1965; Seymour and Mortell,1974; Whitham,1974) to analyze the formation of singularities in the solutions of the nonlinear hyperbolic equation (A.6). We found (not shown in this thesis) that the singularities do not form on the "lead characteristic". Swaters and his colleagues are trying to show that the singularities may form behind the lead characteristic. They believe that the formation of singularities implies that the theory has "broken" down and is an indication of a topographically-induced instability in the modon. This instability may be one of the factors that leads to the destruction of the modon near a ridge topography as shown by Carnevale et al.(1988).

Second, a more realistic assumption would be to allow the modon to have meridional motion as well. However, the analytic solution would be very complicated. Numerical simulations of the quasi-geostrophic potential vorticity equation including topography (Carnevale et al.,1988) for a modon demonstrate the importance of the two-dimensional motion. As well, the theory developed in this thesis has also completely neglected baroclinic effects. More realistic modelling of the propagation characteristics of a modon in a stratified atmosphere is another area of possible research. Finally, the Rayleigh parameterization of the frictional processes is very crude and further work in this regard is also another area of

possible research.

Bibliography

Aref, H., and E. D. Siggia, 1980: Vortex dynamics of the two-dimensional turbulent shear layer. *J. Fluid Mech.*, **100**, 705-737.

Austin, J. F., 1980: The blocking of middle latitude westerly winds by planetary waves. *Q. J. R. Meteorol. Soc.*, **106**, 327-350.

Basdevant, C., Y. Couder and R. Sadourny, 1984: Vortices and vortex-couples in two-dimensional turbulence, or long-lives couples are Batchelor's couples. *Lect. Notes Phys.*, 230, 327-346.

Benzi, R., B. Saltzman and A. C. Wiin-Nielsen, 1986: Anomalous atmospheric flows and blockings. *Adv. Geophys.*, **29**, 459pp.

Boyd, J. P., 1985: Equational solitary waves. Part3: Westward-traveling modons. *J. Phys. Oceangr.*, **15**, 46-54.

Carnevale, G. F., G. K. Vallis, R. Purini and M. Briscolini, 1987: Propagation of barotropic modons over topography. *Geophys. Astrophys. Fluid Dynamics*, **41**, 45-101.

Charney, J. G., and J. G. Devore, 1979: Multiple flow equilibria in the atmosphere and blocking. *J. Atmos. Sci.*, 36, 1205-1216.

Courant, R., and D. Hilbert, 1962: Methods of Mathematical Physics. *Interscience, New York*, 407-635pp.

Dole, R. M., and N. D. Gordon, 1983: Persistent anomalies of the extratropical Northern Hemisphere wintertime circulation: Geographical distribution and regional persistence characteristics. *Mon. Weather Rev.*, **111**, 1567-1586.

Egger, J., 1978: Dynamics of blocking highs. *J. Atmos. Sci.*, **35**, 1788-1801.

Flierl, G. R., V. D. Larichev, J. C. McWilliams and G. M. Reznik, 1980 :The dynamics of baroclinic and barotropic solitary eddies. *Dyn. Atmos. & Oceans.*, **5**, 1-41.

----------, M. E. Stern and J. A. Jr. Whitehead, 1983: The physical significance of modons: Laboratory experiments and general integral constraints. *Dyn. Atms. & Oceans.*, 7, 233-263.

----------, 1987: Isolated Eddy Models in Geophysics. *Ann. Rev. Fluid Mech.*, **19**, 493-530.

Frederiksen, J. S., 1984: The onset of blocking and cyclogensis in southern hemisphere synoptic flows: linear theory. *J. Atmos. Sci.*, **41**, 1116-1131.

Ghil, M. and S. Childress, 1987: Topics in Geophysical Fluid Dynamics: Atmospheric Dynamics, Dynamo theory, and Climate Dynamics. *Springer-Verlag*, 485pp.

Gill, A. E., 1982: Atmosphere-Ocean Dynamics. *Academic Press*, 662pp.

Gimshaw, R. H. J., 1970: The solitary wave in water of variable depth: Part I. *J. Fluid Mech.*, **42**, 639-656.

----------, 1971: The solitary wave in water of variable depth: Part II. *J. Fluid Mech.*, **46**, 611-622.

Green, J. S. A., 1977: The weather during July 1976: Some dynamics considerations of the drought. *Weather*, **32**, 120-128.

Haines, K., and J. Marshall, 1987: Eddy-forced coherent structures as a prototype of atmospheric blocking. *Q. J. R. Meteorol. Soc.*, **113**, 681-704.

Illari, L., 1984: A diagnostic study of the potential vorticity in a warm blocking anticyclone. *J. Atmos. Sci.*, **41**, 3518-3526.

Laedke, E. W., and K. H. Spatschek, 1985: Dynamical properties of drift vortices. *Phys. Fluids*, **28**, 1008-1010.

Lamb, H., 1932: Hydrodynamics, *Dover*, 738pp.

Larichev, V., and G. Reznik, 1976: Two-dimensional Rossby Soliton an exact solution. POLYMODE News. No.19 (Simultaneous Russian Publication in Reports of U.S.S.R. Academy of Sciences, 1976, 231, No.5).

LeBlond, P. H., and L. A. Mysak, 1978: Waves in the Ocean. *Elsevier*, 602pp.

Makino, M., T. Kamimura and T. Taniuti, 1981: Dynamics of two-dimensional solitary vortices in a low-beta plasma with convective Motion. *J. Phys. Soc. Japan*, **50**, 980-989.

McWilliams, J.C., 1980: An application of equivalent modons to atmospheric blocking. *Dyn. Atmos. & Ocean.*, **5**, 43-66.

----------, G. R. Flierl, V. D. Larichev and G. M. Reznik, 1981: Numerical studies of barotropic modons. *Dyn. Atmos. & Ocean.*, **5**, 219-238.

----------,and N. J. Zabusky, 1982: Interactions of isolated vortices I. *Geophys. Astrophys. Fluid Dynamics.*, **19**, 207-227.

----------, 1983: Interactions of isolated vortices II. *Geophys. Astrophys. Fluid Dynamics.*, **24**, 1-22.

----------, 1982: Isolated vortices in planetary fluid motion. *Proc. Ninth U. S. Congress on Applied Mechanics*, 283-289.

----------, 1984: The emergence of isolated, coherent vortices in turbulent flow. *J. Fluid Mech.*, **146**, 21-43.

Mied, R. P., and G. J. Lindemann, 1982: The birth and evolution of eastward-propagating modons. *J. Phys. Oceangr.*, **12**, 213-230.

Miyakoda, K., C. T. Gordon, R. Caverly, W. F. Stern, J. Sirutis and W. Bourke, 1983: Simulation of a blocking event in January 1977. *Mon. Wea. Rev.*, **111**, 846-869.

Mo, K. C., J. Pfaendtner and E. Kalnay, 1987: A GCM study on the maintenance of the June 1982 blocking in the southern hemisphere. *J. Atmos. Sci.*, **44**, 1123-1142.

Orszag, S. A., and C. M. Bender, 1978: Advanced Mathematical Methods for scientists and engineers. *McGraw-Hill New York*, 593pp.

Pedlosky, J., 1987: Geophysical Fluid Dynamics, *Springer-Verlay,* 624pp.

Pierrehumbert, R. T., and P. Malguzzi, 1984: Forced coherent structures and local multiple equilibria in a barotropic atmosphere. *J. Atmos. Sci.,* **41**, 246-257.

Rex, D. F., 1950a: Blocking action in the middle troposphere and its effect on regional climate. Part I: An aerological study of blocking action. *Tellus,* **2**, 196-211.

--------, 1950b: Part II: The climatology of blocking action. *Tellus,* **2**, 275-301.

Seymour, B. R. and M. P. Mortell, 1974: Nonlinear Geometrical Acoustics. *Mechanics Today,* Vol 2, 256-259.

Shutts, G. J., 1983: The propagation of eddies in diffluent jetstreams: Eddy vorticity forcing of "blocking" flow fields. *Q. J. R. Meteorol. Soc.,* **109**, 737-761.

----------, 1986: A case study of eddy forcing during an Altantic blocking episode. *Adv. Geophys.,* **29**, 135-161.

Shukla, J. and K. C. Mo, 1983 : Seasonal and geographical variation of blocking. *Mon. Wea. Rev.,* **41**, 3-21.

Stern, M. E., 1975: Minimal properties of planetary eddies. *J. Mar. Res.,* **33**, 1-13.

Swaters, G. E., 1985: Ekman layer dissipation in an eastward traveling modon. *J. Phys. Oceangr.,* **15**, 1212-16.

----------, 1986a: Stability conditions and a priori estimate for equivalent-barotropic modons. *Phys. Fluids,* **29**, 1419-1422.

----------, 1986b: Barotropic modon propagation over slowly varying topography. *Geophys. Astrophys. Fluid Dynamics,* **36**, 85-113.

----------, and G. R. Flierl, 1988: Ekman dissipation of barotropic modon. Mesoscale/Synoptic coherent structures in geophysical turbulence. ed. J. C. J. Nihoul, Elsevier, .

----------,1988: Propagation of two-dimensional solitary drift-vortices in viscous rotating fliud or plasma, to appear in Continuum Mechanics and its Application, edited by G. A. C. Graham and S. Malik, Springer-Verlag.

Swenson, M., 1986a: Equivalent modons in simple shear. *J. Atmos. Sci.,* **43**, 3177-3185.

----------, 1986b: Instability of equivalent barotropic riders . *J. Phys. Oceangr.,* **17**, 492-506.

Trenberth, K. E. and K. C. Mo, 1985: Blocking in the southern hemisphere. *Mon. Wea. Rev.,* **113**, 3-21.

Tribbia, J., 1984: Modons in spherical geometry. *Geophys. Astrophys. Fluid Dym.,* **30**, 131-168.

Tung, K. K., and R. S. Lindzen, 1979: A theory of stationary long waves. I: A simple theory of blocking. *Mon. Wea. Rev.,* **107**, 714-734.

Varley, E., and J. Dunwoody, 1965: The effect of nonlinearity at an acceleration wave. *J.*

Mech. Phys. Solids, **13**, 17-28.

---------, and E. Cumberbatch, 1965: Nonlinear theory of wave-front propagation. *J. Inst. Maths. Appl.,* **1**, 101-112.

---------, 1965: Acceleration fronts in viscoelastic materials . *Arch. Rational Mech. Anal.,* **19**, 215-225.

Verkley, W., 1984: The construction of barotropic modons on a sphere. *J. Atmos. Sci.,* **41**, 2592-2504.

Verkley, W. T. M., 1987: Stationary barotropic modons in westerly background flows.. *J. Atmos. Sci.,* **44**, 2383-2398.

Whitham, G. B., 1974: Linear and nonlinear waves. *Wiley, New York,* 636pp.

Appendix: Derivation of the nonlinear hyperbolic equation (A.6)

We begin by expanding (3.5), (4.14a) and (4.15a) in the following way:

$$l_T + cl_X + lc_X = 0, \tag{A.1}$$

$$l_T a^2c^2E_1 + 2laa_Tc^2E_1 + 2la^2cc_TE_1 + la^2c^2E_{1T} + l_Xa^2c^3E_1 + 2laa_Xc^3E_1 + 3la^2c^2c_XE_1 + la^2c^3E_{1X} = -la^2c^3E_1H_X/H - 2\tau la^2c^2E_1H, \tag{A.2}$$

$$l_Tc^2E_2 + 2lcc_TE_2 + lc^2E_{2T} + l_Xc^3E_2 + 3lc^2c_XE_2 + lc^3E_{2X} = lc^3E_2H_X/H - 2\tau lc^2E_2/H, \tag{A.3}$$

where

$$E_1 \equiv \frac{\gamma^2}{4\nu^2}(\gamma^2 + \nu^2)(1 + \frac{4R}{\gamma}),$$

$$E_2 \equiv \frac{\gamma^2}{2}(\gamma^2 + \nu^2)R^2.$$

If we use the following identities:

$$\gamma_T = \gamma(\frac{a_T}{a} - \frac{c_T}{2c}),$$

$$\gamma_X = \gamma(\frac{a_X}{a} - \frac{c_X}{2c}),$$

$$\nu_T = \nu(\frac{\kappa_T}{\kappa} + \frac{a_T}{a}),$$

$$\nu_X = \nu(\frac{\kappa_X}{\kappa} + \frac{a_X}{a}), \tag{A.4}$$

$$(\frac{\kappa_T}{\kappa} + \frac{a_T}{a}) = (1 + M)(\frac{a_T}{a} - \frac{c_T}{2c}),$$

$$(\frac{\kappa_X}{\kappa} + \frac{a_X}{a}) = (1 + M)(\frac{a_X}{a} - \frac{c_X}{2c}),$$

where $M \equiv -R(\gamma^2 + \nu^2)/(4\gamma + \gamma^2/R + R\nu^2)$ and $R \equiv K_2(\gamma)/K_1(\gamma)$, it is possible to

rewrite (A.1), (A.2) and (A.3) in the form

$$\mathbf{E}\,\underline{\mathbf{u}}_T + \mathbf{F}\,\underline{\mathbf{u}}_X = \mathbf{D}, \tag{A.5a}$$

where

$$\underline{\mathbf{u}} = \begin{bmatrix} l \\ a \\ c \end{bmatrix} \tag{A.5b}$$

$$\mathbf{E} = \begin{bmatrix} 1, & 0, & 0 \\ 0, & E_{22}, & E_{23} \\ 0, & E_{32}, & E_{33} \end{bmatrix} \tag{A.5c}$$

$$\mathbf{F} = \begin{bmatrix} c, & 0, & l \\ 0, & c\mathbf{E}_{22}, & cE_{23} \\ 0, & cE_{32}, & cE_{33} \end{bmatrix} \tag{A.5d}$$

$$\mathbf{D} = \begin{bmatrix} 0 \\ D_2 \\ D_3 \end{bmatrix} \tag{A.5e}$$

where

$$E_{22} = lac^2[2E_1 + E_{1_\gamma}\gamma + E_{1_\nu}\nu\,(M+1)],$$

$$E_{23} = la^2c[2E_1 - (E_{1_\gamma}\gamma + E_{1_\nu}\nu\,(M+1))/2],$$

$$E_{32} = lc^2[E_{2_\gamma}\gamma + E_{2_\nu}\nu\,(M+1)]/a,$$

$$E_{33} = lc[2E_2 - (E_{2_\gamma}\gamma + E_{2_\nu}\nu\,(M+1))/2],$$

and

$$D_2 = -la^2c^3E_1H_X/H - 2\tau la^2c^2E_1H,$$

$$D_3 = lc^3E_2H_X/H - 2\tau lc^2E_2/H.$$

If we left-multiply (A.5a) by the inverse of $\mathbf{E}$ (denoted $\mathbf{E}^{-1}$), we obtain

$$\underline{\mathbf{u}}_T + \mathbf{A}\underline{\mathbf{u}}_X + \mathbf{B} = 0, \tag{A.6a}$$

where

$$\mathbf{A} = \begin{bmatrix} c, & 0, & l \\ 0, & c, & 0 \\ 0, & 0, & c \end{bmatrix} = \mathbf{E}^{-1}\mathbf{F} \tag{A.6b}$$

$$\mathbf{B} = \begin{bmatrix} 0 \\ B_2 \\ B_3 \end{bmatrix} = -\mathbf{E}^{-1}\mathbf{D} \tag{A.6c}$$

with

$$B_2 = \frac{E_{23}D_3 - E_{33}D_2}{\mathrm{DET}},$$

$$B_3 = \frac{E_{32}D_2 - E_{22}D_3}{\mathrm{DET}},$$

and

$$\mathrm{DET} = E_{22}E_{33} - E_{23}E_{32}.$$

It follows immediately that (A.6a) is hyperbolic with a single eigenvalue given by $c(X,T)$ with multiplicity three.

B45924